LOS ALAMOS SCIENTIFIC LABORATORY
LOS ALAMOS ═══ of the ═══ NEW MEXICO
University of California

NUMERICAL FLUID DYNAMICS

USING THE PARTICLE-AND-FORCE METHOD

UNITED STATES
ATOMIC ENERGY COMMISSION
CONTRACT W-7405-ENG. 36

SEP 10 '65

This report expresses the opinions of the author or authors and does not necessarily reflect the opinions or views of the Los Alamos Scientific Laboratory.

LOS ALAMOS SCIENTIFIC LABORATORY
LOS ALAMOS ▬▬▬ of the ▬▬▬ NEW MEXICO
University of California

NUMERICAL FLUID DYNAMICS
USING THE PARTICLE-AND-FORCE METHOD

PART I

THE METHOD AND ITS APPLICATIONS

by

Bart J. Daly, Francis H. Harlow, and James E. Welch

Appendixes B, C, and D by Edward N. Wilson

PART II

SOME BASIC PROPERTIES OF PARTICLE DYNAMICS

by

Francis H. Harlow and Everett E. Sanmann

ABSTRACT

Since its original proposal in 1961, the Particle-and-Force (PAF) method for numerical fluid dynamic studies has been improved considerably and tested in a variety of new circumstances. This report, consisting of two parts, discusses at length a number of properties of the method from conceptual, practical, and experimental points of view.

Part I is directly concerned with the methodology, giving in detail the procedure as it is now applied. It also includes the results of experimental calculations, the conclusions, and a discussion of extensions now being developed. Part II delves more deeply into the meaning of the particle representation of fluid dynamics through a close examination of some pertinent idealized computer experiments.

TABLE OF CONTENTS

TABLES

FIGURES

PART II

SOME BASIC PROPERTIES OF PARTICLE DYNAMICS

PART I

THE METHOD AND ITS APPLICATIONS

INTRODUCTION

The Particle-and-Force method was first described in a report [I-1] written in 1961. The discussions given in that report are, to a great extent, still pertinent. Principal exceptions include the method of neighbor choice (page 12) and the manner in which the force function is derived (pages 16-19). Some of the more important parts of that paper are repeated in Part I here; others are omitted or merely summarized.

In the Introduction to the above mentioned report, a discussion is given of the various techniques which have commonly been used for computer studies of time-dependent fluid dynamics in several space dimensions. The principal conclusion from that discussion is that no method exists which is universally applicable; each method has limitations. This means that the method must be chosen in each case to fit the requirements at hand. There remain, however, many situations which still cannot be computed by any one technique, or in many cases even by an appropriate combination. The situation is shown in general terms in Table I-1.

A second PAF-method report [I-2] shows by statistical analysis how

TABLE I-1

A COMPARISON OF METHODS FOR CALCULATING TIME DEPENDENT FLUID DYNAMICS

Methods and References	Some Advantages	Some Disadvantages
Pure Lagrangian [I-3, I-4]	1. Follows material interfaces. 2. Allows fine resolution areas to move with fluid. 3. Is translationally, rotationally invariant. 4. Requires mesh of cells only where needed.	1. Tends to break down with large distortions. 2. Does not allow internal slip except along a priori known lines. 3. Does not allow for formation or closure of arbitrary internal cavities.
Pure Eulerian [I-5, I-6]	1. Calculates large distortions well. 2. Allows spontaneous generation of internal slip lines.	1. Produces diffusion of material interfaces. 2. Requires mesh of cells at all points where fluid will be, whether or not needed at some instant. 3. Does not allow for localized resolution. 4. Is not translationally or rotationally invariant.
PIC [I-7, I-8]	L-1,[a] E-1, E-2-plus handle cavitation easily.	E-2, E-3, E-4-plus require exceptionally large amount of storage.
PAF	L-1, L-2, L-3, L-4, E-1, E-2-plus handle cavitation easily.	None of above, but may need bigger and faster machine, since calculations are somewhat time consuming and require a large amount of storage.

[a]L and E, respectively, refer to the Lagrangian and Eulerian topics described above in the table.

the PAF interparticle force can be made to correspond to the form of the equation of state. These results have been extended and generalized in this report.

In any practical PAF-method calculations, it is essential to use a large, high-speed electronic computer. The examples presented in this report were obtained with an IBM-7094 computer, and configurational output was processed through a Stromberg-Carlson SC-4020 Microfilm Recorder.

Chapter 1 presents a detailed discussion of all aspects of the PAF methodology from both conceptual and practical points of view. Some actual tests of the computing technique are described in Chapter 2, while Chapter 3 contains some discussion of future plans for development, generalization, and extension of the PAF technique. Five Appendixes have been included; they contain a number of additional topics supplementing the remarks in the body of the report.

CHAPTER 1

DESCRIPTION OF THE METHOD

A. DIFFERENTIAL THEORY

The particles whose dynamics we follow are to represent the elements of a fluid. Insofar as possible, we have used the classical particle-dynamics theory to aid in the formulation of the method. At some point, however, a divergence from the classical theory will be necessary so that the dissipative effects in a real fluid can be represented. Our particles are not molecules whose internal energy is carried by velocity fluctuations; indeed, we expect that the velocity of a particle is to represent the mean velocity of the finite mass of fluid it represents. The macroscopic kinetic energy of the fluid is to be exactly the kinetic energy of all the particles, so the internal energy must be represented by an additional variable. If this variable is expressed as a function of particle positions alone, then only adiabatic motion can be represented. Compression and subsequent expansion would then return the set of particles to exactly their initial configuration with no dissipation. Thus a special prescription is needed to describe variations of particle internal energy.

We consider the dynamics of a set of particles described by the following nomenclature:

$i, j \equiv$ indexes describing the particle number,

$m_j \equiv$ mass of particle #j,

$\vec{r}_j \equiv$ space coordinate of particle #j,

$\vec{u}_j \equiv$ velocity of particle #j,

$\vec{F}_{ij} \equiv$ force exerted by particle #i onto particle #j,

$\vec{r}_{ij} \equiv \vec{r}_j - \vec{r}_i$,

$r_{ij} \equiv |\vec{r}_{ij}|$,

$\vec{s}_{ij} \equiv \vec{r}_{ij}/r_{ij}$ (a unit vector pointing from particle #i to particle #j),

$\vec{M}_j \equiv m_j \vec{u}_j \equiv$ momentum of particle #j,

$K_j \equiv \frac{1}{2} m_j \vec{u}_j \cdot \vec{u}_j \equiv$ kinetic energy of particle #j,

$J_j \equiv$ internal energy of particle #j.

Additional nomenclature will be introduced as required.

We commence by assuming that the particles are governed by the equations of motion

$$m_j \frac{d\vec{u}_j}{dt} = \sum_i{}^* \vec{F}_{ij}, \qquad (I-1)$$

$$\frac{d\vec{r}_j}{dt} = \vec{u}_j. \qquad (I-2)$$

The summation over i modified by the presence of * does not include the term i = j, and is further restricted to include only certain

neighbors of j as discussed later. Summation without * includes all particles in the system.

Next, we assume that the force function can be divided into two parts,

$$\vec{F}_{ij} = \vec{s}_{ij} f_{ij} + \vec{g}_{ij},$$ (I-3)

where

$$f_{ij} \equiv f(r_{ij}, J_i, J_j).$$

The first term in the force is to be associated in form with the equation of state of the fluid; the second term is introduced to achieve dissipation in the same manner as the "artificial viscosity" of Von Neumann and Richtmyer [I-9], or for the purpose of including real viscous effects.

1. Correspondence with Fluid Mechanics

The correspondence with fluid mechanics comes through an examination of the conservation laws in forms appropriate to the nature of the continum to be represented. In this discussion, the coordinate system is Cartesian; cylindrical coordinates are considered later in this chapter.

a. Conservation of mass. This is automatic. Each particle has constant mass, m_j, so that the total does not change with time. Likewise the change of mass in any fixed volume exactly equals the amount flowing over the bounding surface.

b. Conservation of momentum. To satisfy this requirement, the restriction is the same as in classical particle dynamics, namely $\vec{F}_{ij} \equiv -\vec{F}_{ji}$. To demonstrate this, consider the momentum change rate of a particular subset of all the particles

$$\frac{d\vec{M}}{dt} = \sum_{j(\text{subset})} m_j \frac{d\vec{u}_j}{dt} = \sum_{j(\text{subset})} \sum_i^* \vec{F}_{ij}.$$

We break the sum over i into two parts and write

$$\frac{d\vec{M}}{dt} = \sum_{i(\text{inside})}^* \sum_{j(\text{subset})} \vec{F}_{ij} + \sum_{i(\text{outside})} \sum_{j(\text{subset})} \vec{F}_{ij},$$

where inside and outside refer to inclusion or exclusion from the subset. In the first double sum, each pair of particles enters twice, so that the total contribution to the sum from a particular pair is $\vec{F}_{ij} + \vec{F}_{ji}$. Since there must be no contribution to momentum change from particles within the subset, the sum of the two terms must vanish. The second double sum does not thereby vanish, since each pair enters only once. Thus with $\vec{F}_{ij} = -\vec{F}_{ji}$, the momentum change of any subset of particles arises only through external forces, as required.

The restriction also means that

$$f_{ij} \equiv f_{ji},$$

$$\vec{g}_{ij} \equiv -\vec{g}_{ji}.$$

(I-4)

c. Conservation of energy. Here we must make a break from the usual procedure in particle mechanics. In devising a reasonable approach, we will be able to establish some of the crucial parts of the technique. The basis for the energy discussion is that the rate of change of energy of a particle should be given by the rate that the other particles do work

on it. This work rate is in turn given by the product of force by velocity. (To be properly symmetric, the velocity through which the work flux is carried from one particle to another must be the mean value of the two velocities.) Thus we write

$$\frac{d}{dt}(K_j + J_j) = \sum_i^* \vec{F}_{ij} \cdot \left(\frac{\vec{u}_i + \vec{u}_j}{2}\right).$$ (I-5)

It follows that the total energy of an isolated system is conserved,

$$\frac{dE}{dt} \equiv \frac{d}{dt} \sum_j (K_j + J_j) = \frac{1}{2} \sum_j \sum_i^* \vec{F}_{ij} \cdot (\vec{u}_i + \vec{u}_j) = 0,$$

where equality to zero follows from separate vanishing of the sum of contributions from each pair. Likewise the energy of the particles in any subset changes only through work done on them by external particles.

Now, we already know that

$$\frac{dK_j}{dt} = m_j \vec{u}_j \cdot \frac{d\vec{u}_j}{dt}$$

$$= \vec{u}_j \cdot \sum_i^* \vec{F}_{ij}.$$

Combination of this with Eq. (I-5) can be arranged to give

$$\frac{dJ_j}{dt} = \frac{1}{2} \sum_i^* \vec{F}_{ij} \cdot (\vec{u}_i - \vec{u}_j),$$ (I-6)

or

$$\frac{dJ_j}{dt} = -\frac{1}{2} \sum_i{}^* f_{ij} \frac{dr_{ij}}{dt} + \frac{1}{2} \sum_i{}^* \vec{g}_{ij} \cdot (\vec{u}_i - \vec{u}_j). \qquad (I-7)$$

B. FINITE TIME INTERVALS

In practice, the numerical computations must proceed through a sequence of finite time advancements whose steps are of duration δt. This is accomplished through a replacement of Eqs. (I-1), (I-2), and (I-6) by

$$m_j \frac{\vec{u}_j^{n+1} - \vec{u}_j^n}{\delta t} = \sum_i{}^* \vec{F}_{ij}^n , \qquad (I-8)$$

$$\frac{\vec{r}_j^{n+1} - \vec{r}_j^n}{\delta t} = \vec{u}_j^{n+1} , \qquad (I-9)$$

$$\frac{J_j^{n+1} - J_j^n}{\delta t} = \frac{1}{2} \sum_i{}^* \vec{F}_{ij}^n \left(\vec{u}_i^{n+\frac{1}{2}} - \vec{u}_j^{n+\frac{1}{2}} \right), \qquad (I-10)$$

where

$$\vec{u}^{n+\frac{1}{2}} \equiv \frac{1}{2} \left(\vec{u}^n + \vec{u}^{n+1} \right).$$

This shows how the variables for cycle #n+1 are obtained algebraically from those of cycle #n. The choice of time-centering of the equations is justified as follows:

Equation (I-8) — At the beginning of the calculations for advancement through a cycle, the only information available for the force calculation is that which pertains to the beginning of cycle #n. The force is thus labeled with index n.

Equation (I-9) — After calculation of the new velocity by Eq. (I-8), there is some arbitrariness as to what velocity should be used to

determine the new coordinate. It was shown on page 18 of Ref. I-1 that the newly calculated velocity is preferred to that which the particle had at the beginning of the cycle. The argument is based upon requirements of computational stability.

Equation (I-10) — The right side contains the average of the old and new velocities, a combination which is introduced to assure rigorous energy conservation in the time-difference form of the equations. (Mass and momentum have likewise been conserved; proof of this is the same as that for the differential equations.) To demonstrate energy conservation we start from the identity

$$\frac{1}{2}\left[\left(\vec{u}_j^{\,n+1}\right)^2 - \left(\vec{u}_j^{\,n}\right)^2\right] \equiv \vec{u}_j^{\,n+\frac{1}{2}} \cdot \left(\vec{u}_j^{\,n+1} - \vec{u}_j^{\,n}\right).$$

Thus, from Eq. (I-8), the change in kinetic energy of a particle is

$$K_j^{n+1} - K_j^n = \delta t \sum_i {}^* \vec{F}_{ij}^{\,n} \cdot \vec{u}_j^{\,n+\frac{1}{2}}.$$

Combination of this with Eq. (I-10) gives for the change in total particle energy, E_j,

$$E_j^{n+1} - E_j^n = \frac{1}{2} \sum_i {}^* \vec{F}_{ij} \cdot \left(\vec{u}_i^{\,n+\frac{1}{2}} + \vec{u}_j^{\,n+\frac{1}{2}}\right). \tag{I-11}$$

Since $\vec{F}_{ij} \equiv -\vec{F}_{ji}$, this result shows that the energy transferred from particle #i to particle #j is equal in magnitude to but opposite in sign from that transferred from #j to #i, thus proving the contention of conservation.

C. DISSIPATION

There is at least one other form alternative to Eq. (I-10) which could be considered for the internal energy calculation. The total energy difference could be calculated in a form analogous to Eq. (I-11), but without any time-centering of the right side. The result would still be conservative as long as the proper reciprocal symmetries were preserved.

-18-

From the new total energy of the cell, the new kinetic energy could then be subtracted, giving the new internal energy.

The reason for the specific choice of the form of Eq. (I-10) follows from the requirement of monotonic dissipation. The use of Eq. (I-10) (with the proper choice of the $\vec{g}_{ij}$ forces) can never result (at least to lowest order in δt) in decreased entropy, while most of the alternative forms can produce such decreases under certain circumstances.

D. NEIGHBORS

The manner in which a particle's neighbors are chosen has evolved partly from the demands of the method and partly through experiment. We already have mentioned some basic considerations of the method which place two primary restrictions on the choice of neighbors:

1. Particles shall interact only with adjacent particles.

2. A particle's effect on its neighbor must be reciprocated, i.e., if i is a neighbor of j, then j must also be one of i's neighbors.

The first condition is necessary for the representation of a fluid in which interactions are only with adjacent elements, while the second is required for rigorous momentum and energy conservation.

The neighbor search technique which will be described here satisfies both of these criteria and, in addition, is particularly suited to efficient memory storage assignment. A search radius, R, and a maximum number of neighbors, N^*, are predetermined for each problem. Among all of the particles in the system which lie within the search radius of particle #j, the N^* closest particles are tentatively chosen to be neighbors. Any of

these which do not similarly find j as one of their N^* closest neighbors are then subtracted from the list, thereby insuring reciprocity. Good results have been attained by choosing N^* equal to twice the number of dimensions of the problem.

By restricting neighbors to only the N^* closest particles, this procedure reduces the danger of interactions with nonadjacent particles in highly compressed regions, where numerous particles lie within the search radius. At the same time, however, the search radius restriction allows an interaction cutoff, which also can be useful. For instance, if one wishes to drive a shock through a fluid at rest, R can be chosen less than the interparticle spacing in the undisturbed material, so that this material will remain undisturbed until the shock reaches it. Also, when a particle becomes detached from the main body of the fluid, it will cease to accelerate or to change its internal energy. This would not be true if there were no limit on R. In that case, the particle would continue to cool until its internal energy became negative and its force attractive. This meaningless local occurrence could play havoc with the rest of the calculation.

An alternative method of achieving neighbor reciprocity would be to add rather than subtract neighbors, but the subtractive method has the distinct advantage for the programmer that he can place an upper limit on the storage requirements for interparticle relationships. Tests indicate that the two methods produce equally good results.

The success of the PAF method depends to such a large extent upon

the proper statistical averaging of interparticle fluctuations that it seems necessary to search for neighbors every time cycle. It would be preferable to avoid this, because it is by far the most time-consuming phase of the calculation, requiring 50 percent or more of the calculation time. Therefore, experiments are being performed to see under what circumstances the neighbor search can be conducted less often. In addition, an attempt has been made to speed up this part of the calculation as much as possible.

1. The Neighbor Search Technique

The first step in the current neighbor search technique is to overlay the computational system with a grid of square cells, each cell having a side of length R, the search radius. The particles are then classified according to the cells in which they fall and the actual search for neighbors begins. For any given particle j, the distances to all other particles within its own or a neighboring cell are computed and compared with R. If any such distance, r_{ij}, is less than R, then i is listed as a neighbor of j and j is listed as a neighbor of i, unless either i or j already has a full quota of neighbors. Then r_{ij} would be compared to the distances to the other neighbors, and the most distant particle would be dropped as a neighbor.

In order to achieve the greatest possible speed with this method, it is imperative to choose R as small as accuracy will permit. The customary choice is about one and a half times the anticipated particle separation in the least compressed region.

If one starts at the lower left-hand corner of the cell mesh and works from left to right and upward through the cells, it is possible to restrict somewhat the number of cells which must be searched for neighbors of any given particle. For example, if particle j lies in cell (k, ℓ), then it is necessary to search only through cells (k, ℓ), $(k, \ell + 1)$, $(k + 1, \ell - 1)$, $(k + 1, \ell)$, and $(k + 1, \ell + 1)$ for neighbors of j. If j had additional neighbors in other cells bordering (k, ℓ), this fact would have already been determined in searching for neighbors of those particles.

After these tentative neighbor determinations have been made, a second pass is made through the particles, dropping neighbors as necessary for reciprocity.

E. FORCES

A theory of correspondence between fluid dynamics and the PAF model has been worked out [I-2] which makes use of the methods of statistical mechanics. The conclusion is that if the method can be developed in such a manner that each particle follows closely the local mean of motion without extreme fluctuations, and if the force functions are chosen according to a prescribed format, then the results should satistically represent the fluid dynamics as desired.

1. Equation of State Force

The correspondence analysis [I-2] indicates that the nondissipative part of the force function, $f_{ij}(r_{ij}, J_i, J_j)$, should be associated with the equation of state of the fluid through an integral equation which in two-dimensional Cartesian space has the form

$$p(m\rho, I) = \frac{\pi \rho^2}{2} \int_0^\infty x^2 \sigma(\rho x^2) f(x, I) \, dx, \qquad \text{(I-12)}$$

where

       m = particle density (assumed constant),

       ρ = particle density (particles per unit area),

       I = specific internal energy,

       p = pressure (force per unit distance),

       $x = r_{ij}$,

       σ = a radial function describing the density of neighbors,
as defined in the previous section. The exact form of
σ is not uniquely determined, the only restriction
being that it satisfy

$$\pi \int_0^\infty \sigma(\xi) \, d\xi = N^*. \qquad \text{(I-13)}$$

In Ref. I-2, Eq. (I-12) is solved for the case in which σ is approximated by a step function. This formulation has proven satisfactory when applied to a polytropic equation of state,[*] but for more complicated equations of state it may lead to a force function that does not vanish at normal density and zero internal energy. This difficulty can be avoided by choosing a form of σ which is consistent with these requirements. We now describe a method for determining such a form.

Assume that the equation of state can be expanded in powers of the compression minus one:

---

[*]It can, in fact, be shown that every form of σ which satisfies Eq. (I-13) will produce the same force function for a polytropic equation of state.

$$p(m\rho, I) = \sum_k A_k(I) \left(\frac{m\rho}{\rho_0} - 1\right)^k.$$

The nondissipative part of the force function will then have a similar appearance

$$f(x, I) = x^\alpha \sum_k B_k(I) \left(\frac{m}{\rho_0 x^2} - 1\right)^k,$$

and the right-hand side of Eq. (I-12) will consist of a series of integrals, one for each value of k. Since

$$p(\rho_0, I) = A_0(I),$$

σ must be of such a form that each such integral vanishes when $m\rho = \rho_0$, except the one for which $k = 0$.

Consider a typical term from the series,

$$\psi_k(m\rho, I) = \frac{\pi\rho^2}{2} B_k(I) \int_0^\infty x^{\alpha+2} \left(\frac{m}{\rho_0 x^2} - 1\right)^k \sigma(\rho x^2)\, dx.$$

Let $\xi = \rho x^2$, to obtain

$$\psi_k(m\rho, I) = \frac{\pi}{4} \rho^{(1-\alpha)/2} B_k(I) \int_0^\infty \xi^{(\alpha+1)/2} \left(\frac{m\rho}{\rho_0 \xi} - 1\right)^k \sigma(\xi)\, d\xi,$$

$$= \frac{\pi}{4} \rho^{(1-\alpha)/2} B_k(I) \sum_{n=0}^k \frac{(-1)^{n+k} k! \left(\frac{m\rho}{\rho_0}\right)^n}{(k-n)! n!} \int_0^\infty \xi^{[(\alpha+1)/2]-n} \sigma(\xi)\, d\xi.$$

If the integrand is independent of n, then $\psi(\rho_0, I) = 0$, as it should. This suggests that

$$\sigma(\xi) = (\text{constant})\, \delta(\xi - 1),$$

where δ signifies the usual Dirac function. Equation (I-13) may be used to evaluate the constant and we obtain

$$\sigma(\xi) = \frac{N^*}{\pi}\, \delta(\xi - 1).$$

With this form of σ, the correspondence equation becomes

$$p(m\rho, I) = \frac{1}{2}\, N^* \rho^2 \int_0^\infty x^2 f(x, I)\, \delta(\rho x^2 - 1)\, dx.$$

Again, let $\xi = \rho x^2$,

$$p(m\rho, I) = \frac{1}{4}\, N^* \rho^{\frac{1}{2}} \int_0^\infty \xi^{\frac{1}{2}} f\left(\sqrt{\frac{\xi}{\rho}}, I\right) \delta(\xi - 1)\, d\xi$$

$$= \frac{1}{4}\, N^* \rho^{\frac{1}{2}} f\left(\sqrt{\frac{1}{\rho}}, I\right).$$

In plane coordinates, $\rho = 1/r_{ij}^2$, so we can finally write the correspondence between the equation-of-state pressure and the nondissipative part of the force as

$$f(r_{ij}, I) = \frac{4 r_{ij}}{N^*}\, p\left(\frac{m}{r_{ij}^2}, I\right). \qquad (I\text{-}14)$$

Applying this formula to a polytropic equation of state, $p = (\gamma - 1)m\rho I$, gives

$$f(r_{ij}, I) = \frac{4 r_{ij}}{N^*} (\gamma - 1) \frac{m}{r_{ij}^2} I$$

$$= \frac{4(\gamma - 1)\, mI}{N^* r_{ij}},$$

which, as indicated, is the same expression one would get using any form of σ which satisfies Eq. (I-13). When we use Eq. (I-14) for a "stiffened" gas equation of state, $p = (\gamma - 1)m\rho I + a(m\rho - \rho_0)$, we obtain

$$f(r_{ij}, I) = \frac{4(\gamma - 1)mI}{N^* r_{ij}} + \frac{4ma}{N^* r_{ij}} \left[1 - \frac{\rho_0 r_{ij}^2}{m} \right] . \qquad (I\text{-}15)$$

Notice that the bracket term vanishes at normal density. Using for σ the step function employed in Ref. I-2, one arrives at the same expression as in Eq. (I-15), except that the bracket term is

$$\left[1 - \frac{\pi \rho_0 r_{ij}^2}{3m} \right] ,$$

which does not vanish at normal density.

The same correspondence result is derived by a virial approach in Appendix A, and it is also shown there why the number of neighbors per particle must be twice the number of space dimensions.

2. Dissipative Force

Reference I-2 also provides a correlation between the dissipative force and "true" viscosity,[*] so that theoretically one could include real viscous effects in the calculation. As a practical matter, however, the main requirement of a dissipative mechanism in PAF is, as in all finite difference methods which are not inherently stable, to prevent the growth of instabilities. In all of the experiments reported here only the minimum amount of this "artificial" viscosity required for stability has been employed.

_____

[*]The theory of correspondence for dissipative forces is discussed in Appendix B.

Dissipation is only required in those portions of the fluid which are undergoing comparison; hence the dissipative force, $\vec{g}_{ij}$, between particles i and j is nonzero only when $\vec{s}_{ij} \cdot (\vec{u}_i - \vec{u}_j) > 0$. In a previous report on the PAF technique [I-1], a dissipative force of the type

$$\vec{g}_{ij} = m\omega(\vec{u}_i - \vec{u}_j) \tag{I-16}$$

was proposed, where ω was a constant with dimensions of reciprocal time. But, in Appendix II of Ref. I-1, it was demonstrated that this form of the dissipative force did not rigorously conserve angular momentum; therefore, an alternative of the form

$$\vec{g}_{ij} = m\omega\vec{s}_{ij}[\vec{s}_{ij} \cdot (\vec{u}_i - \vec{u}_j)] \tag{I-17a}$$

was suggested. Not only does a force of the type Eq. (I-17a) conserve angular momentum, but it also gives a measure of the compression between particles i and j. [Note that Eq.(I-17a) represents the component of Eq. (I-16) lying along the line of particle centers.] Thus Eq. (I-17a) is consistent with the one-dimensional stability analysis which assumes that all compression is head-on; it is less likely to lead to interpenetration than is Eq. (I-16) for a large (but theoretically stable) value of ω.

The two forms, however, share the drawback of being independent of the interparticle spacing. Thus the dissipative force is the same when the particles are a search radius apart as when they almost coincide. This situation has been corrected in subsequent work by employing one or the other of the following modifications of the type Eq. (I-17a) force,

$$\vec{g}_{ij} = \frac{m\omega \sqrt{\left|\frac{J_i + J_j}{2m}\right|} \left[\vec{s}_{ij} \cdot (\vec{u}_i - \vec{u}_j)\right]}{r_{ij}} \vec{s}_{ij}, \qquad \text{(I-17b)}$$

$$\vec{g}_{ij} = \frac{m\omega u_0 \left[\vec{s}_{ij} \cdot (\vec{u}_i - \vec{u}_j)\right]}{r_{ij}} \vec{s}_{ij} \qquad \text{(I-17c)}$$

where ω is now dimensionless and u_0 is chosen equal to a typical sound speed for the problem. The first of these two forms has been in the most common usage; the second one is reserved mainly for problems whose initial conditions require the material to be cold. The force Eq. (I-17b) is patterned after a form suggested by Landshoff [I-10]; the square-root factor is simply proportional to local sound speed in a polytropic gas and closely related to it for many other materials.

F. CYLINDRICAL COORDINATES

Many fluid dynamics problems deal with flows which possess an angular symmetry about some axis through the flow field. To allow the PAF method to take advantage of this symmetry requires certain modifications of its concepts. The particles now become rings about the axis of symmetry and, since rings at different radii occupy different volumes, it has been convenient to make the mass of a particle proportional to its initial distance from the axis if the density throughout the fluid is constant.

At the present time, no correlation theory such as that given in Ref. I-2 exists for cylindrical coordinates. (Some newly derived results are given in Appendix C.) Therefore, in order to arrive at a force function appropriate to these rings about the axis, it was necessary to resort

to the equations of motion themselves. This approach lacks the unambiguity of the theoretical correlation method, so there were, as might be expected, several false starts. We review the major one of these in order to demonstrate some of the rather subtle difficulties which can arise with PAF and to show how these were eventually avoided.

1. A Preliminary Cylindrical Coordinate Force

In flows possessing cylindrical symmetry, a cylindrical shell of fluid is seen to have a radial acceleration which is independent of exterior forces and depends only upon the pressures that exist within the shell (for example, see pages 33 and 34 of Ref. I-11). The average radial acceleration of such a shell is given by

$$m \frac{du_r}{dt} = (pA)_{inside} - (pA)_{outside} + 2\pi L \int_{r_1}^{r_2} p \, dr, \qquad (I-18)$$

where A refers to the surface area (inside or outside) of the shell of thickness $r_2 - r_1$ and length L. If we consider the PAF particles to be arranged in a rectangular array (as in the accompanying figure), then, since each particle actually represents a toroidal shell of fluid about the cylindrical axis, Eq. (I-18) might be suitable for the derivation of the radial nondissipative forces felt by a particle. Assuming a polytropic equation of state, $p = (\gamma - 1)\rho I$, Eq. (I-18) can be rewritten
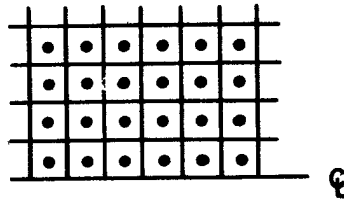
$$m \frac{dv}{dt} = (\gamma - 1) \left[\left(\frac{J}{\delta r}\right)_{inside} - \left(\frac{J}{\delta r}\right)_{outside} + \left(\frac{J}{r}\right)_{particle} \right],$$

where $v \ (= u_r)$ is the radial component of velocity and L is taken to be the interparticle spacing in the Z direction. Since the treatment in the Z direction is entirely unchanged from that of plane coordinates, it would seem that the nondissipative portion of the force felt by particle j could be written

$$\vec{F}_j = \sum_i^* \left[\left(\frac{\gamma - 1}{2}\right) \left(\frac{J_i + J_j}{r_{ij}}\right) \vec{s}_{ij} \right] + \frac{(\gamma - 1)J_j}{r_j} \hat{r}, \qquad (I-19)$$

where $\hat{r}$ is a unit radial vector.

The self-administered force, the second term on the right in Eq. (I-19), is the force exerted on the particle by the rest of its own ring. It is positive for positive J and can be thought of as a self-expanding force, tending to carry the particle away from the axis of symmetry.

Extending this same meaning to the dissipative part of the force, one can view the self-administered part as the compressive force which results whenever the radius of the ring decreases. The force is in the positive r direction, so we could think of it as the force exerted by the image of the particle through the axis of symmetry. Therefore, the self-administered part of the dissipative force should be obtainable from the normal dissipative force with the velocity of the neighbor, $\vec{u}_i$, replaced by $-\vec{u}_j$. At the time that these forces were derived for cylindrical

coordinates, a dissipative force which was the sum of the expressions in Eqs. (I-16) and (I-17a) was being used. Hence, the self-administered dissipative force was taken as

$$\vec{g}_j = \begin{cases} -2m_j(\omega_1 + \omega_2)v_j\hat{r} & \text{when } v_j \leq 0 \\ 0 & \text{when } v_j \geq 0, \end{cases}$$

and the entire force exerted on particle j was

$$\vec{F}_j = \sum_i^* \left\{ \left(\frac{\gamma-1}{2}\right) \frac{(J_i + J_j)}{r_{ij}} \vec{s}_{ij} + m_{ij}\omega_1 (\vec{u}_i - \vec{u}_j) + m_{ij}\omega_2[\vec{s}_{ij}\cdot(\vec{u}_i - \vec{u}_j)]\vec{s}_{ij} \right\}$$

$$+ \left[\frac{(\gamma-1)J_j}{r_j} - 2m_j(\omega_1 + \omega_2)v_j\right]\hat{r}, \qquad (I\text{-}20)$$

for a polytropic equation of state. Here, $m_{ij} = 1/2 \, (m_i + m_j)$.

Several problems were run using this force function. When applied to a problem involving flow past a cone, it was discovered that the shock reflected from the face of the cone did not take the form expected, but became elongated with time in the radial direction. This difficulty was traced to the fact that the self-expanding force was producing an excessive mass flux away from the axis of symmetry.

As a result of this discovery, the derivation of Eq. (I-20) was reexamined. It was realized then that a cylindrical shell of fluid bounded by free surfaces would expand both inward and outward at escape velocity, and that the net increase in outward momentum was simply a result of the fact that more mass was exposed to the outer surface. The nonnegative

self-expanding force was therefore clearly wrong. What was needed was a force function which would allow an unconfined fluid to expand in all directions in a manner that was consistent with the equations of motion in cylindrical coordinates.

Very often in the derivation of finite difference formulas it is found that equivalent differential expressions can give rise to difference equations with markedly different properties. Such is the case here; for if we return to the momentum equation with cylindrical symmetry,

$$\rho \frac{d\vec{u}}{dt} = - \frac{\partial p}{\partial r} \hat{r} - \frac{\partial p}{\partial z} \hat{z}, \tag{I-21}$$

from which Eq. (I-18) was obtained, we can derive force expressions which do not give rise to these large mass fluxes.

2. The Present Cylindrical Coordinate Force Function

Once again, let us consider the particles to be in rectangular array and examine the effect of the r component of Eq. (I-21) along a radial line in this array. By referring to the particles along this line by an index number, k (which increases with radius), we can write

$$\frac{m_k}{\tau_k} \frac{dv_k}{dt} = \frac{1}{\delta r} \left(p_{k-\frac{1}{2}} + q_{k-\frac{1}{2}} - p_{k+\frac{1}{2}} - q_{k+\frac{1}{2}} \right), \tag{I-22}$$

where we have added artificial viscosity terms, q, in the form of pressure modifications. Assume that

$$p_{k\pm\frac{1}{2}} = (\gamma - 1)\rho_{k\pm\frac{1}{2}} I_{k\pm\frac{1}{2}} = \frac{(\gamma - 1)}{\tau_{k\pm\frac{1}{2}}} \left(\frac{J_k + J_{k\pm1}}{2} \right),$$

$$q_{k\pm\frac{1}{2}} = \begin{cases} \mp \,\omega\, \rho_{k\pm\frac{1}{2}} \bar{u}_{k\pm\frac{1}{2}} (v_{k\pm1} - v_k) & \text{if} > 0 \\ 0 & \text{otherwise,} \end{cases}$$

where the $\bar{u}_{k\pm\frac{1}{2}}$ is some as yet undesignated quantity having the dimension of a velocity. Then we can rewrite Eq. (I-22) as

$$\frac{m_k}{\tau_k} \frac{dv_k}{dt} = \frac{(\gamma - 1)}{2} \left[\frac{J_k + J_{k-1}}{\tau_{k-\frac{1}{2}}(r_k - r_{k-1})} - \frac{J_{k+1} + J_k}{\tau_{k+\frac{1}{2}}(r_{k+1} - r_k)} \right]$$

$$+ \;\omega \left[\left(\frac{m_k + m_{k-1}}{2} \right) \frac{(v_{k-1} - v_k)\bar{u}_{k-\frac{1}{2}}}{\tau_{k-\frac{1}{2}}(r_k - r_{k-1})} - \left(\frac{m_{k+1} + m_k}{2} \right) \frac{(v_k - v_{k+1})\bar{u}_{k+\frac{1}{2}}}{\tau_{k+\frac{1}{2}}(r_{k+1} - r_k)} \right].$$

If, as in Eq. (I-17b), we choose

$$\bar{u}_{k\pm\frac{1}{2}} = \sqrt{\frac{|J_{k\pm1} + J_k|}{m_{k\pm1} + m_k}} \,,$$

and make the substitution

$$\frac{\tau_k}{\tau_{k\pm\frac{1}{2}}} = \frac{2r_k}{r_{k\pm1} + r_k} \,,$$

this equation can be expressed as

$$m_k \frac{dv_k}{dt} = (\gamma - 1)r_k \left[\frac{J_k + J_{k-1}}{(r_k + r_{k-1})(r_k - r_{k-1})} - \frac{J_{k+1} + J_k}{(r_{k+1} + r_k)(r_{k+1} - r_k)} \right]$$

$$+ \;\omega r_k \left[\frac{(v_{k-1} - v_k)\sqrt{|J_k + J_{k-1}|(m_k + m_{k-1})}}{(r_k + r_{k-1})(r_k - r_{k-1})} \right.$$

$$\left. - \frac{(v_k - v_{k+1})\sqrt{|J_{k+1} + J_k|(m_{k+1} + m_k)}}{(r_{k+1} + r_k)(r_{k+1} - r_k)} \right].$$

Thus, generalizing to any random array of particles, we obtain for the r component of the interparticle force the expression

$$F_{ij}(r) = \frac{(r_j - r_i)r_j}{(r_j + r_i)r_{ij}^2}$$

$$\times \left[(\gamma - 1)(J_i + J_j) + \omega \vec{s}_{ij} \cdot (\vec{u}_i - \vec{u}_j) \sqrt{|J_i + J_j|(m_i + m_j)} \right], \qquad (\text{I-23a})$$

where the term with ω in it is set to zero if not positive. The z component of the force carries over directly from plane coordinates,

$$F_{ij}(z) = \frac{z_j - z_i}{2r_{ij}^2}$$

$$\times \left[(\gamma - 1)(J_i + J_j) + \omega \vec{s}_{ij} \cdot (\vec{u}_i - \vec{u}_j) \sqrt{|J_i + J_j|(m_i + m_j)} \right]. \qquad (\text{I-23b})$$

Notice that this choice of $\bar{u}_{k \pm \frac{1}{2}}$ produced a $\vec{g}_{ij}$ force of the type Eq. (I-17b). If we had chosen $\bar{u}_{k \pm \frac{1}{2}} \equiv$ constant, we would have obtained a force of the type Eq. (I-17c).

A study of the function expressed in Eqs. (I-23) confirms that it does satisfy the requirements demanded of a force function for calculation in cylindrical coordinates. First of all, having been derived from the equations of motion in that coordinate system, it is consistent with them to at least first order.

The other quality which we demanded of a cylindrical coordinate force function was that it allow an unconfined fluid of uniform density and internal energy to have the same rate of expansion in the positive

and negative radial directions. The force function expressed in Eqs. (I-23) does have this property. To see this, consider a system in which all particles have specific internal energy, I_0. The radial acceleration imparted to particle #j by its neighbor, #i, is

$$\frac{F_{ij}(r)}{m_j} = \frac{r_j(m_i + m_j)}{(r_i + r_j)m_j} \left\{ \left(\frac{r_j - r_i}{r_{ij}^2} \right) \left[(\gamma - 1)I_0 + \omega \vec{s}_{ij} \cdot (\vec{u}_i - \vec{u}_j)\sqrt{I_0} \right] \right\}.$$

In this uniform density fluid, particles are equally spaced and have masses proportional to their radii. All particles, therefore, experience the same acceleration, so rarefactions move into the fluid from the interior and exterior boundaries at the same velocity.

Conservation of energy in a cylindrical coordinate system requires, as it did in the plane coordinate case, that the rate of change of the energy of particle j be given by the rate that other particles do work on it. This work rate is in turn given by the product of interparticle forces times appropriate velocities less the portion of this product which is attributable to self-expanding forces. Since the total energy of the system must be conserved, we have

$$\frac{dE}{dt} = \sum_j \left\{ \sum_i^* \left[\vec{F}_{ij} \cdot \left(\frac{\vec{u}_i + \vec{u}_j}{2} \right) \right] - \frac{d}{dt} \text{(Energy of Self-Expansion)} \right\} = 0.$$

Thus the rate of change of the energy of self-expansion is given by

$$\sum_j \sum_i^* \left[\vec{F}_{ij} \cdot \left(\frac{\vec{u}_i + \vec{u}_j}{2} \right) \right] = \frac{1}{2} \sum_{\text{pairs}} \left\{ \frac{(r_j - r_i)^2}{(r_j + r_i)r_{ij}^2} \left[\quad \right]_{ij} (v_i + v_j) \right\},$$

where $[\quad]_{ij}$ represents the bracket term in Eqs. (I-23);

so we can write the equation for the rate of change of internal energy in cylindrical coordinates as

$$\frac{dJ_j}{dt} = \frac{dE_j}{dt} - \frac{dK_j}{dt}$$

$$= \sum_i{}^{*}\left[\vec{F}_{ij}\cdot\left(\frac{\vec{u}_i + \vec{u}_j}{2}\right)\right] - \frac{1}{4}\sum_i{}^{*}\left\{\frac{(r_j - r_i)^2}{(r_j + r_i)r_{ij}^2}\left[\quad\right]_{ij}(v_i + v_j)\right\} - \vec{u}_j\cdot\sum_i{}^{*}\vec{F}_{ij}$$

$$= \sum_i{}^{*}\left\{\vec{F}_{ij}\cdot\left(\frac{\vec{u}_i - \vec{u}_j}{2}\right) - \frac{(r_j - r_i)^2}{4(r_j + r_i)r_{ij}^2}\left[\quad\right]_{ij}(v_i + v_j)\right\}. \qquad \text{(I-24)}$$

In the finite time-difference approximation to Eq. (I-24), the velocities must be time-centered for energy conservation, as was the case in plane coordinates.

By extending the procedure used to derive the polytropic equation of state force, Eqs. (I-23), to the "stiffened" gas equation of state, one can derive the analogue of Eq. (I-15) in cylindrical coordinates,

$$F_{ij}(r) = \frac{(r_j - r_i)r_j}{(r_j + r_i)r_{ij}^2}\left\{(\gamma - 1)(J_i + J_j) + a(m_i + m_j)\left[1 - \frac{2\pi(r_i + r_j)r_{ij}^2\rho_0}{(m_i + m_j)}\right]\right.$$

$$\left. + \omega\vec{s}_{ij}\cdot(\vec{u}_i - \vec{u}_j)\sqrt{|J_i + J_j|(m_i + m_j)}\right\} \qquad \text{(I-25a)}$$

$$F_{ij}(z) = \frac{(z_j - z_i)}{2r_{ij}^2}\left\{(\gamma - 1)(J_i + J_j) + a(m_i + m_j)\left[1 - \frac{2\pi(r_i + r_j)r_{ij}^2\rho_0}{(m_i + m_j)}\right]\right.$$

$$\left. + \omega\vec{s}_{ij}\cdot(\vec{u}_i - \vec{u}_j)\sqrt{|J_i + J_j|(m_i + m_j)}\right\}. \qquad \text{(I-25b)}$$

This force function has been applied successfully to several problems, one of which is described in Chapter 2.

G. BOUNDARY CONDITIONS

From a computational standpoint it would be perfectly reasonable to perform a PAF calculation without boundary constraints, since the method is not tied to a fixed mesh system. But for the practical reasons of efficient neighbor searching, taking advantage of flow symmetries and the logical presentation of results, the fluid is usually bounded. In many physical circumstances, of course, such bounding also exists.

Two types of boundary conditions have been used (sometimes in combination): prescribed input, continuative output conditions for flow into and out of a channel, and reflection from rigid walls.

1. Prescribed Input, Continuative Output

In the case of flow through a channel, particles are periodically created at the input boundary with the proper mass, velocity, internal energy, and interparticle spacing to represent the required state of the incoming fluid. At the output boundary, particles are destroyed and their mass and energy are subtracted from the totals for the system. The memory storage which had been used by the destroyed particle is then made available for new particles, so the problem can be run indefinitely.

Particle creation and destruction actually occurs at a distance of approximately the search radius outside the input and output boundaries, respectively. During the time that these particles exist outside the system, they exert a force on their neighbors inside, but they themselves

are not so influenced. They therefore do work on the interior particles, so it is necessary (for the purpose of checking energy conservation) to calculate the change in the energy of the system which stems from their influence. In plane coordinates, the change in energy which results from particle #j outside the system exerting a force on its neighbors i inside the system is

$$\delta E = \delta t \sum_{i}^{*} \left[\vec{F}_{ji} \cdot \frac{(\vec{u}_i + \vec{u}_j)}{2} \right].$$ (I-26)

But in cylindrical coordinates a portion of the interparticle reaction is attributable to the self-expanding force of a particle. This is not actually work done by an external body on the system, so the energy change in Eq. (I-26) must be reduced by this amount. The self-expanding energy attributable to each of the neighbors, i, above, is given by one-half the amount by which

$$\delta t \left[(\vec{F}_{ji} + \vec{F}_{ij}) \cdot \frac{(\vec{u}_i + \vec{u}_j)}{2} \right]$$

fails to reduce to zero. Hence, by making use of the fact that in cylindrical coordinates

$$r_j F_{ji}(r) = -r_i F_{ij}(r), \qquad F_{ji}(z) = -F_{ij}(z),$$

we can write the cylindrical coordinate analogue of Eq. (I-26) as

$$\delta E = \delta t \sum_{i}^{*} \left\{ \left[\vec{F}_{ji} \cdot \frac{(\vec{u}_i + \vec{u}_j)}{2} \right] - \frac{1}{2} \left(\frac{r_i - r_j}{r_i} \right) F_{ji}(r) \left(\frac{v_i + v_j}{2} \right) \right\}.$$ (I-27)

The velocities in Eqs. (I-26) and (I-27) must be time-centered in the finite time-difference form, as was required in the previous sections on energy conservation.

2. Rigid Walls

The problem of devising boundary conditions which accurately describe the interaction of a fluid with a rigid wall is one which has received extensive study. We have experimented with many different boundary treatments, almost all of which work quite well in plane coordinates or in unobstructed flow parallel to the axis of symmetry in cylindrical coordinates. The most difficult problem for all such methods involves flow past a cylindrically symmetric obstacle in a channel.

The difficulty arises from the fact that the boundary conditions at the obstacle cause rather large fluctuations in what should be a stagnant region adjacent to it. These fluctuations are compounded in cylindrical coordinates by the presence of both very light and heavy particles at the face of the obstacle. A light particle caught between the wall and several heavy neighbors may begin to oscillate at such a rapid rate that it becomes drained of internal energy and develops a negative (attractive) force. In time, this particle's neighbors will also develop negative forces and the results will soon become meaningless.

We have attempted to alleviate this tendency by developing boundary conditions which damp particle fluctuations near the wall, but in some cases more drastic action is required. For example, calculations of flow past a cylindrically symmetric cone were attempted using each of the

-39-

boundary conditions described in the next two sections of this report, and in no case could the problem be run long enough to achieve steady state. As light particles moved up the face of the cone and encountered massive neighbors, boundary instabilities invariably developed. One way of avoiding this difficulty is to destroy the light particle before the instability fluctuations damage the calculations.

Any particle whose mass is less than some fraction, k, of the average mass of its neighbors is destroyed, and its mass, momentum, and energy are distributed among its neighbors. Values of k from 0.2 to 0.4 have been suitable for this purpose.

The mass of the destroyed particle is distributed among its neighbors on the basis of interparticle distance. That is, a particular neighbor, #1, of the light particle, #j, gets some fraction,

$$\kappa_i = \frac{r_{ij}}{\sum\limits_i^* r_{ij}},$$

of j's mass. The new mass of particle #1 is then

$$m_i = \tilde{m}_i + \kappa_i \tilde{m}_j,$$

where the tilde indicates the quantity before distribution.

The total momentum and energy of the group of particles will then be conserved if we compute each neighbor's new velocity and internal energy from the formulas

$$u_i = \frac{\tilde{m}_i \tilde{u}_i + \kappa_i \tilde{m}_j \tilde{u}_j}{\tilde{m}_i + \kappa_i \tilde{m}_j},$$

$$v_i = \frac{\tilde{m}_i \tilde{v}_i + \kappa_i \tilde{m}_j \tilde{v}_j}{\tilde{m}_i + \kappa_i \tilde{m}_j},$$

$$J_i = \frac{\tilde{m}_i}{2} \left[(\tilde{u}_i)^2 + (\tilde{v}_i)^2 \right] + \tilde{J}_i + \kappa_i \left\{ \frac{\tilde{m}_i}{2} \left[(\tilde{u}_j)^2 + (\tilde{v}_j)^2 \right] + \tilde{J}_j \right\}$$

$$- \frac{m_i}{2} \left[(u_i)^2 + (v_i)^2 \right].$$

Another procedure, described in Appendix E, makes use of a mass flux from heavy to light particles.

3. Mechanical Reflection from a Wall

Two general classifications of boundary conditions, along with many variations, have been employed: mechanical reflection of particles from the wall and reflection by means of image particles on the opposite side of the wall. The simplest type of mechanical reflection (from a pro- grammer's standpoint) is to allow the particle to cross the wall, calcu- late its interparticle forces, its velocity, and its internal energy in the usual manner, and then, for the purpose of moving the particle, re- verse its component of velocity normal to the wall. Energy is conserved by this process and, since the particle will be accelerating as it crosses the boundary, it will re-enter the system within one time cycle. But, rather than having a dissipative effect on the fluctuations of adjacent particles, this manner of treatment increases those fluctua- tions by returning the particle to the system with a higher velocity

-41-

than that with which it left. To alleviate this situation, an attempt
was made to allow the wall to exert a force on nearby particles within
the system, thereby slowing them down before they crossed the boundary.
This, however, had the disadvantage of subjecting particles near the
boundary to continual compression, thereby raising their internal energy
to abnormally high levels.

An alternative approach toward reducing fluctuations near an obstacle
wall is to set to zero the normal component of the velocity of any par-
ticle which strikes the wall. The particle is therefore constrained to
move in the plane of the wall until it reaches the top of the obstacle.
The physical basis for this boundary condition is the fact that the nor-
mal component of velocity of a continuous fluid impinging on a rigid
wall would be zero.

But, while this approach damps out fluctuations normal to the wall,
it leads to severe tangential fluctuations. Since the particles at the
wall are very hot (the lost kinetic energy is transformed to internal
energy) and highly concentrated (since none can escape from the wall),
their interparticle forces become extremely large. The great accelera-
tions which result will cause particle interpenetrations unless the time
step is made very small.

The most successful form of mechanical reflection of particles from
a wall has been specular reflection. At the instant that a particle
strikes a wall its velocity component normal to the wall is reversed.
Therefore, there is no time lag in returning a particle to the system,

as there was with the treatment by which a particle actually penetrated the wall before being reflected. This greatly reduces the fluctuations in the vicinity of the wall. Particles tend to stick to the wall with this method, as they did in the case where the normal velocity component was set to zero. Now, however, this is not so serious a problem, since the particles on the wall are neither especially hot nor highly concentrated, as they were in that case.

4. Images

All of the forms of mechanical reflection from a wall share one important defect: they affect particles in a way that is entirely unrelated to the interparticle relationships which exist in other parts of the computational system. Granted that rigid walls must, by definition, present an abrupt obstruction to the flow, it is usually preferable in a computational scheme to make this treatment an extension of the calculational method in the interior of the system. This can be accomplished with PAF by the use of self-images for particles near the boundary.

An image particle is created (see the following diagram) for every

NO IMAGE

$\frac{R}{2}$

ONE IMAGE

TWO IMAGES
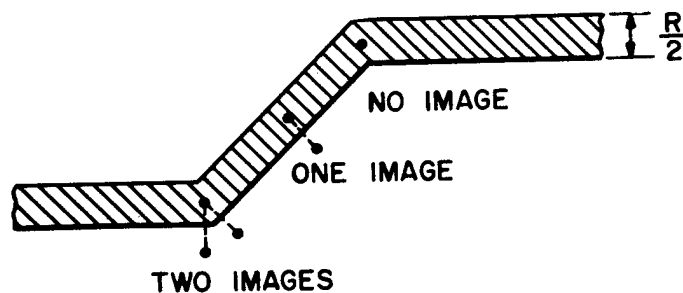
particle in the system which lies within a distance of one-half the search radius of a rigid boundary and from which a normal to that boundary can be constructed. Notice that with this definition, it is possible for a particle within the required distance of a wall to have no, one, or two images. A particle at a concave boundary corner would require two images so that it would be aware of both boundaries. At a convex boundary corner it would be possible to create an image which is a reflection of the particle through the point of intersection of the two boundary lines. This was not done for the problems described in this report, but subsequent experimentation indicates that it is desirable.

The image particle is given the reflected properties of the corresponding particle within the system. If particle i is the image of a particle j within the system, these properties can be described as follows. Coordinates: Particle i is given the coordinates of a point which is the same distance from the wall as j and lies on the same normal to the wall. These coordinates can be written:

$$x_i = \frac{(1 - \zeta^2)x_j + 2\zeta y_j + 2\zeta^2 x_w}{1 + \zeta^2} ,$$

$$y_i = \frac{2\zeta x_j + (\zeta^2 - 1)y_j - 2\zeta x_w}{1 + \zeta^2} ,$$

where ζ is the slope of the wall and x_w is its intercept with the x axis. Velocities: Particle i has the same component of velocity tangential to the wall as does j, but it has a normal component which is the negative

of j's. Relative to the coordinate axes these can be written:

$$u_i = \frac{(1 - \zeta^2)u_j + 2\zeta v_j}{1 + \zeta^2},$$

$$v_i = \frac{2\zeta u_j + (\zeta^2 - 1)v_j}{1 + \zeta^2}.$$

Mass: $m_i = m_j$.

Internal energy: $J_i = J_j$.

Of course, these properties apply only to straight boundaries. To devise boundary conditions that are appropriate to curved boundaries will require additional thought and experimentation.

Images are created only when needed and are destroyed after each cycle of calculation. The fact that a particle is sufficiently close to a rigid wall to have an image does not necessarily mean that the image will be one of the particle's neighbors. If the particle should find N^* closer neighbors, then its image will have no effect. On the other hand, it would be possible to include among a particle's neighbors the images of other particles. In this case we would have to require (for energy conservation) that an additional principle of reciprocity be adhered to, i.e., if i finds j's image as a neighbor, then j must have i's image as one of its neighbors. None of the problems described in this report involve such multiple image neighbors.

5. Conservation of Energy

Images have as their sole purpose for existence the influence of

other particles; hence, we neither calculate changes in their properties not include their mass and energy in the totals for the system. Nevertheless, they behave in every way as conventional particles and, for the purpose of confirming the presence of energy conservation near a wall, it is convenient to consider them as such.

To demonstrate that the image method requires no special treatment to insure conservation, let us consider a specific example. The accompanying figure shows two particles, 1 and 2, and their respective images, 1' and 2', across a wall in either plane or cylindrical coordinates. Since the wall itself has no effect on any of the calculations, we are free to look on these four particles as an isolated region of the fluid and allow them to interact only with one another. Total energy is conserved among these four particles, as it would be among any isolated subset of particles, i.e.,
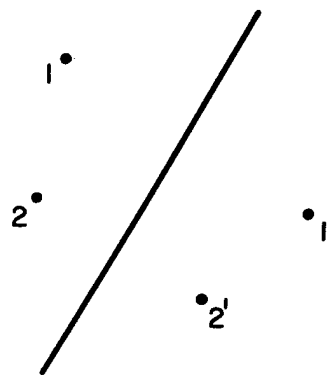
$$\delta E_1 + \delta E_2 + \delta E_{1'} + \delta E_{2'} = 0.$$

Furthermore, by symmetry, the work done on any one of the particles during a time cycle (which equals the change in its energy during that cycle) is equivalent to that experienced by its image; hence

$$\delta E_1 + \delta E_2 = \delta E_{1'} + \delta E_{2'}.$$

To be consistent, the above equations require that

$$\delta E_1 + \delta E_2 = 0,$$

i.e., that the energy of the interior particles be conserved.

Because of the asymmetry of the r component of the force function in cylindrical coordinates, it might seem that the work done on the particle and its image would not be the same in that coordinate system. But, in cylindrical coordinates, the actual work which a particle i does on its neighbor j is defined (for the PAF method) to be the plane coordinate work rate,

$$\vec{F}_{ij} \cdot \left(\frac{\vec{u}_i + \vec{u}_j}{2} \right),$$

less the portion

$$\frac{1}{2} (\vec{F}_{ij} + \vec{F}_{ji}) \cdot \left(\frac{\vec{u}_i + \vec{u}_j}{2} \right)$$

which is attributable to the work the ring j does on itself. Thus the actual work rate is

$$\frac{1}{2} (\vec{F}_{ij} - \vec{F}_{ji}) \cdot \left(\frac{\vec{u}_i + \vec{u}_j}{2} \right),$$

and this is a symmetric function.

H. PARTICLE CONFIGURATIONS

A problem was run rather early in the development of the two-dimensional PAF technique in order to determine the equilibrium configuration of a box of particles. The box was initially filled with a random arrangement of warm particles at rest. These particles then

began to interact and it was observed that when the initial large fluctuations had subsided the particles had attained a hexagonal configuration.

This same hexagonal array of particles (see accompanying figure) was observed in every problem in which a rectangular (or near rectangular) configuration was subjected to some type of deforming process. For example, as a shock moves through a rectangular array of particles at rest, such a configuration is attained within two or three particle spacings behind the shock. If the particles at rest are initially slightly displaced in some random manner, the hexagonal array is assumed immediately behind the shock. In this case the shock is observed to move at more nearly the theoretically predicted speed than in the case where the particles are not subjected to a random displacement.

The primary advantage of random particle displacement is that it allows systems of particles to become deformed rather easily. When a disturbance moves through a system of rectangularly arranged particles in a direction parallel to their rows, the two-dimensional effects of the disturbance are resisted because the particles can exert forces on one another only along a line connecting their centers. Therefore, in almost all two-dimensional problems it is preferable to stagger particles
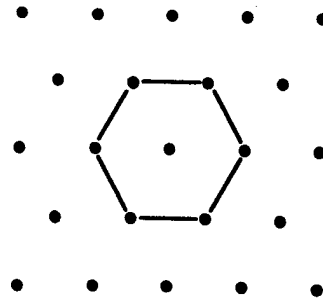
slightly from a purely rectangular array. The only noteworthy exception
to this rule occurs when, for illustrative purposes, one wishes to see
where the first slight two-dimensional effects become apparent (as in de-
fining the bow wave in flow past an obstacle).

Particles are generally offset as much as one-fourth the inter-
particle spacing in each of the coordinate directions. Two random numbers
between -1 and +1 are generated for each particle and the particle is then
displaced from its rectangular position by these fractions of the maximum
displacement in each of the coordinate directions.

CHAPTER 2

TESTS OF THE METHOD

A previous report on the PAF method [I-1] included descriptions of several tests of the method. These were simple fluid flow problems for which analytic solutions existed. The calculations were in good agreement with these analytic solutions.

We now describe some more complicated tests of the calculational technique, for which analytic solutions are not available. The results of most of these are checked against experimental results from shock tube and wind tunnel tests, and one is compared with the results obtained by another numerical method. Several other problems, for which there are no comparisons, are used to illustrate some of the properties and capabilities of PAF calculations. The computations were performed on IBM Electronic Data Processing Machines types 7090 and 7094.

A. FLOW PAST A WEDGE

This is a study of the rate of growth of a detached bow wave produced by the passage of a shock over a two-dimensional wedge suspended in air. Time zero corresponds to the time of arrival of the shock at the

apex of the wedge; we therefore begin the PAF problem with particles in a shocked state on the left of a vertical line through that point and in an ambient state on the right of that line. Particles move from left to right past the wedge and exit through the continuative right-hand boundary. New particles, in a shocked state, enter the system through the left-hand boundary.

For this problem the Mach number of the flow is 1.35 and the apex angle of the wedge is 90°. We use a polytropic equation of state for the air, with specific heat ratio $\gamma = 1.4$. Other input data are listed below, where subscript 1 signifies shocked air and subscript o is ambient air.

x component of velocity (cm/μsec)	$u_1 = 0.0755$	$u_0 = 0$
y component of velocity (cm/μsec)	$v_1 = 0$	$v_0 = 0$
particle internal energy (10^{-2} joule)	$J_1 = 1.0403$	$J_0 = 0.3932$
particle spacing in the x direction (cm)	$\delta x_1 = 0.0635$	$\delta x_0 = 0.1243$
particle spacing in the y direction (cm)	$\delta y_1 = 0.0635$	$\delta y_0 = 0.1243$
particle mass (gm)	$m = 1.861 \times 10^{-5}$	
time step (μsec)	$\delta t = 0.1$	
artificial viscosity coefficient (type I-17a force)	$\omega = 0.07$	

The locations of the detached bow wave at times of 18 and 46 μsec after impact are compared in Fig. I-1 with those observed by Griffith [I-12] in a shock tube experiment. The PAF results are indicated by the dashed lines in the figure, while the solid lines show the location of Griffith's detached shock fronts at the two times.

The shapes of the two curves are somewhat different at the first observation time, but are essentially the same at the second time, except for the reflection on the PAF curve which was caused by interaction with the top reflective boundary. Griffith reports, however, that his measured shock strength of 1.35 may be in error by as much as 5%, so the qualitative agreement between the two curves is as much as could be expected. This in itself is important, for it demonstrates (at least qualitatively) that PAF calculates early bow wave development correctly.
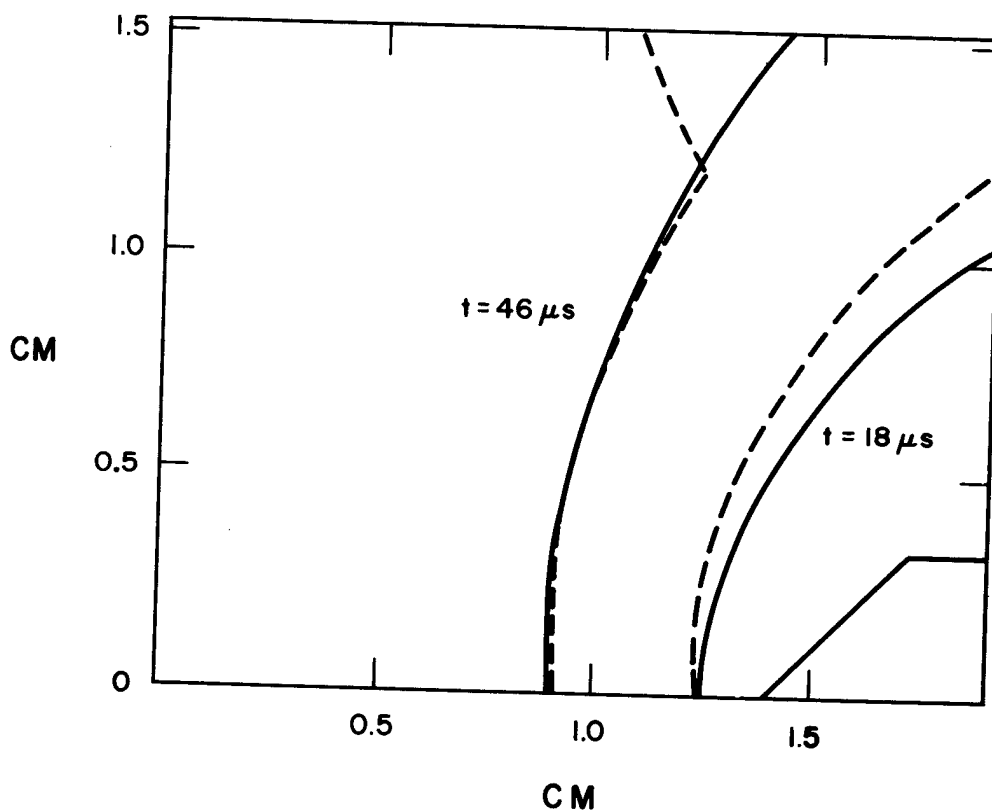
Fig. I-1. A comparison of the PAF detached bow wave positions (dashed lines) at 18 and 46 μsec after impact with those observed in a shock tube experiment involving a Mach 1.35 flow past a wedge.

The Griffith report shows subsequent bow front positions at times up to and including steady state, which is attained at about 500 μsec. Unfortunately, computer memory limitations restrict the PAF run to about 90 μsec.

B. FLOW PAST A BLUNT CYLINDER

In contrast to the previous problem, in which we were concerned with the ability of PAF to resolve the initial characteristics of flow past an obstacle, we now consider a test of its steady-state predictions.

This is the study of a Mach 1.58 air flow ($\gamma = 1.4$) past a blunt axially symmetric cylinder in cylindrical coordinates. We are not concerned with the time dependency of the flow in this case; hence we can state the free-stream conditions without specifying their units. Those conditions are:

z component of velocity	$u_o = 1.58$
r component of velocity	$v_o = 0$
sound speed	$c_o = 1.0$
particle spacing in the z direction	$\delta z_o = 1.0$
particle spacing in the r direction	$\delta r_o = 1.0$
particle mass	$m = $ initial radius
time step	$\delta t = 0.1$
artificial viscosity coefficient (type I-17b force)	$\omega = 0.5$

The first test of the calculations is a comparison of the PAF steady-state stagnation pressure with the theoretical value. The theoretical

value can be determined by making use of Bernoulli's law, which states that along a streamline in steady flow, the quantity

$$\frac{1}{2} (u^2 + v^2) + \frac{\gamma}{\gamma - 1} \frac{p}{\rho}$$

is constant. We can therefore relate conditions at the stagnation point $(u \equiv 0, v \equiv 0)$, which is located at the center of the cylinder face, to conditions at a point immediately behind the detached shock on the axis of symmetry, because these two points lie on the streamline. Referring to values at the stagnation point with subscript s and to the shocked quantities with a prime, we can write this relationship as

$$\frac{\gamma}{\gamma - 1} \frac{p_s}{\rho_s} = \frac{1}{2} (u'^2 + v'^2) + \frac{\gamma}{\gamma - 1} \frac{p'}{\rho'} .$$

The stagnation density can be eliminated by means of the adiabatic equation of state.

$$\frac{p_s}{\rho_s^\gamma} = \frac{p'}{\rho'^\gamma} ,$$

to obtain an expression for the stagnation pressure in terms of the conditions behind the detached shock,

$$p_s = \left\{ \left[\left(\frac{\gamma - 1}{2\gamma} \right) (u'^2 + v'^2) + \frac{p'}{\rho'} \right] \frac{\rho'}{(p')^{1/\gamma}} \right\}^{\gamma/\gamma-1} . \tag{I-28}$$

The shock conditions can, in turn, be related to our input quantities by means of the Rankine-Hugoniot relations. The theoretical value

of the stagnation pressure, Eq. (I-28), for the present problem is $p_s = 0.426$. In Fig. I-2 the PAF pressures are compared with this value for times 15 through 37.

Although the PAF pressures fluctuate a great deal, the average of these fluctuations is in good agreement with the theoretical stagnation pressure.

The reason for these fluctuations is that the pressure at any instant of time is obtained by summing the forces exerted by image particles across a small disk at the center of the cylinder at that time and dividing this sum by the area of the disk. The number of particle interactions sampled at a particular time is small, so the total force varies considerably with time.

Another check on the PAF steady-state predictions can be obtained by comparing the final PAF bow wave position with that obtained by Marschner [I-13] for this same problem in a wind tunnel experiment. Figure I-3 shows a steady-state PAF particle plot on which has been super-imposed Marschner's steady-state detached shock position. Good agreement is evident near the axis of symmetry where the shock is strong. In order to provide a basis for comparison in the weak shock region away from the axis, the PAF particles were constrained to enter the system through the left boundary in a linear fashion (in contrast to their usual staggered arrangement). The point at which these lines of particles become de-flected from their horizontal trajectories is the point of intersection with the PAF shock front. One may verify that this shock front agrees
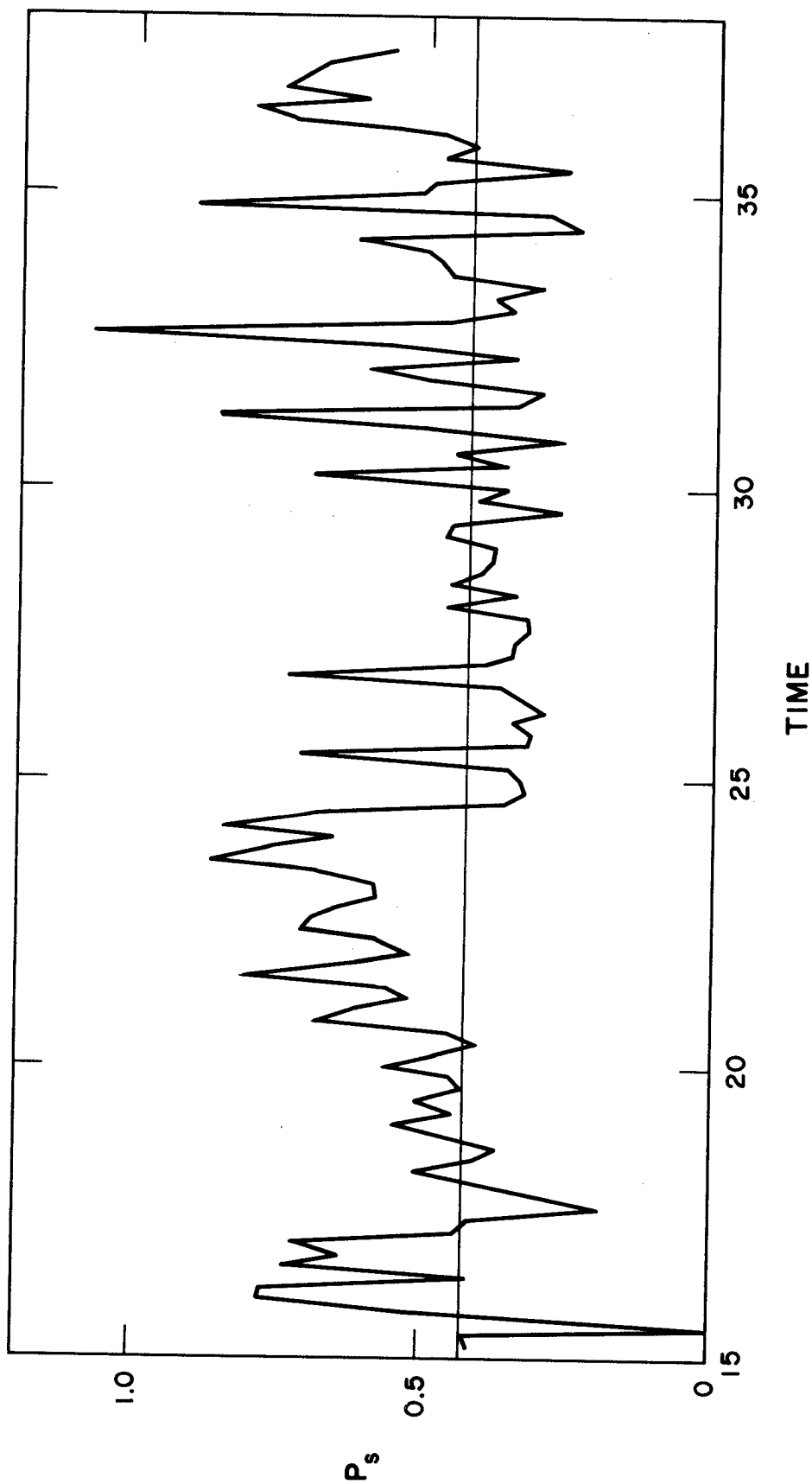
Fig. I-2. A plot of steady-state stagnation pressure observed in a PAF calculation of a Mach 1.58 flow past a blunt, axially symmetric cylinder. The theoretical stagnation pressure of 0.426 is indicated by the light line in the figure.
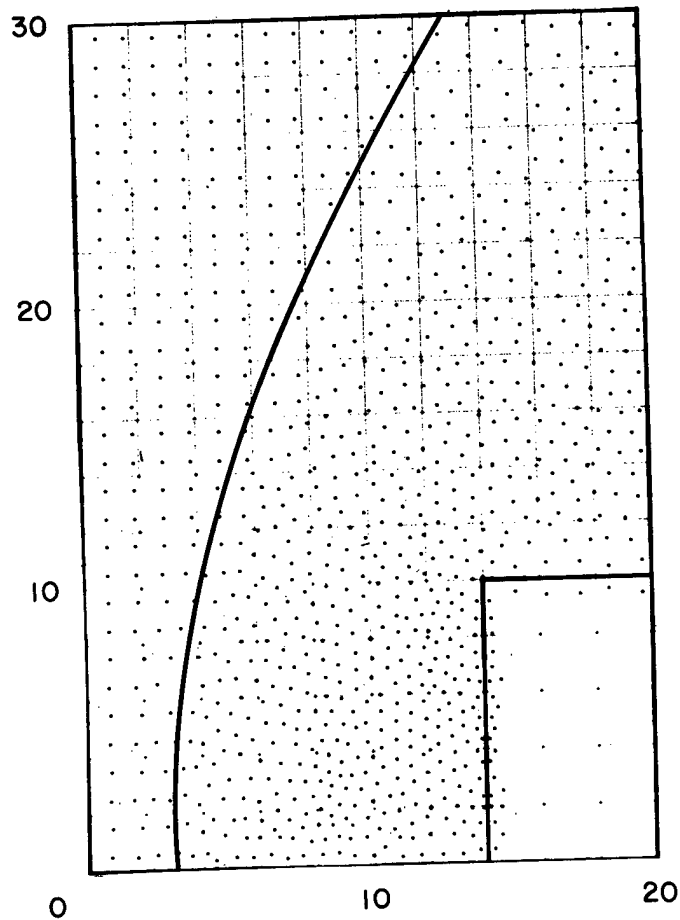
Fig. I-3. The steady-state detached shock front position observed
experimentally in a Mach 1.58 flow past a blunt, axially
symmetric cylinder is plotted on a late-time PAF particle
configuration from the calculation of the same problem.

nicely with Marschner's bow wave. Because of the weakness of the shock in the vicinity of the reflective boundaries, there is no visible evidence of shock reflection as there was in the previous problem involving flow past a wedge.

C. FLOW PAST A CONE

The third and last example involving flow past an obstacle is concerned with the passage of a Mach 1.41 air shock over a 75° cone. We compare the steady-state pressure along the obstacle face and the final bow wave shape with those observed experimentally by Marschner [I-13].

The free stream conditions for this problem are:

z component of velocity	$u_o = 1.41$
r component of velocity	$v_o = 0$
sound speed	$c_o = 1.0$
particle spacing in the z direction	$\delta z_o = 0.1$
particle spacing in the r direction	$\delta r_o = 0.1$
particle mass	$m =$ initial radius
time step	$\delta t = 0.01$
artificial viscosity coefficient (type I-17b force)	$\omega = 1.0$

Figure I-4 shows a comparison of the PAF pressures along the face of the cone (the dots) with those observed by Marschner (the line). The location on the cone face is plotted in the nondimensional form x/s, where x is the distance along the face of the cone measured from the nose
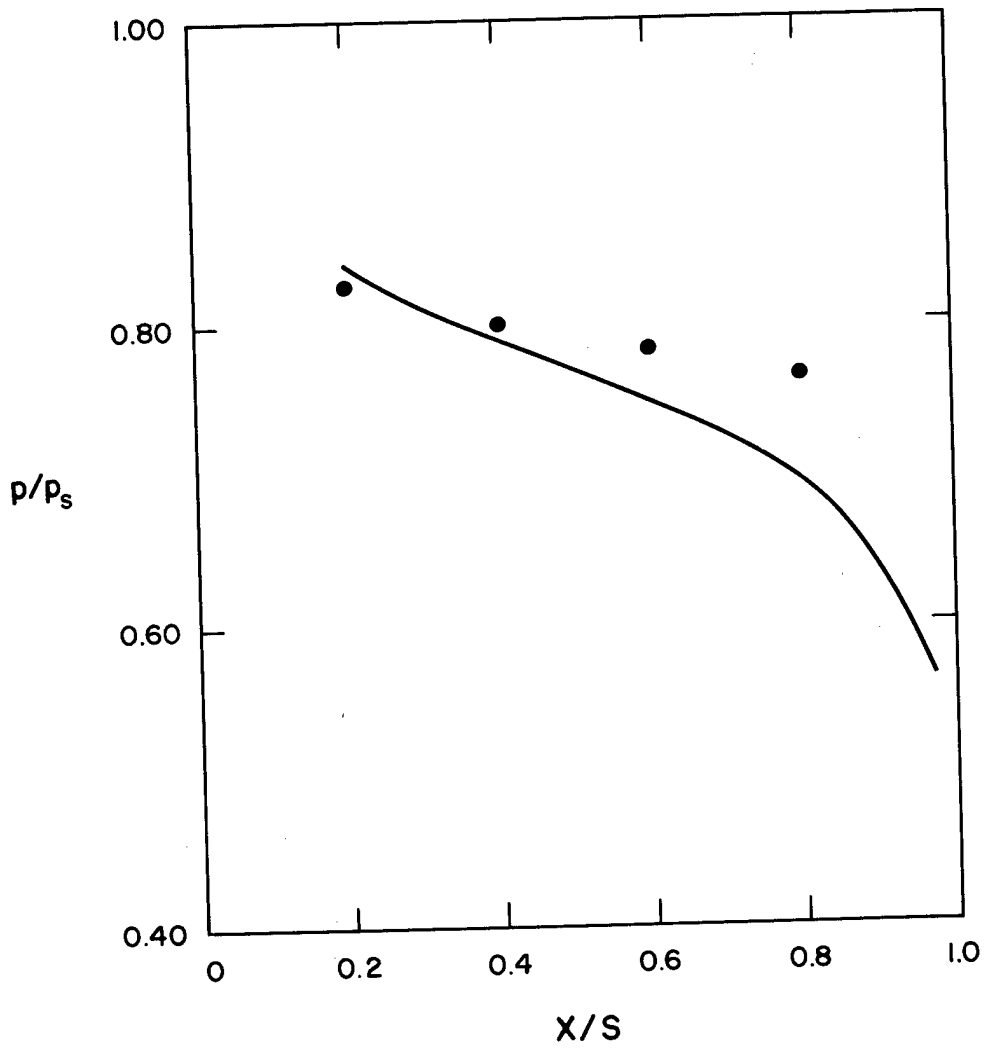
Fig. I-4. A comparison of steady-state PAF pressures (the dots) along the cone face with experimental values observed in a Mach 1.41 flow past a 75° cone.

and s is the slant length of the cone from nose to shoulder. The pressures are also plotted in a nondimensional form p/p_s, where p is the observed pressure at the point and p_s is the theoretical stagnation pressure which develops on a blunt cylinder subject to these free stream conditions. The stagnation pressure used by Marschner is an observed value, whereas that used to reduce the PAF data was calculated from Eq. (I-28).

The PAF pressures were obtained in a manner similar to those plotted in Fig. I-2. The z components of the forces exerted by image particles across a punctured disk of radii $x/s \pm 0.1$ were summed, averaged over time, and divided by the area of the punctured disk (this is equivalent to dividing the total force across a segment of the cone face by the area of the segment).

Agreement with Marschner's curve is considered to be good, although there is less variation in PAF pressures across the cone face than was observed in the wind tunnel experiments. Perhaps this can be attributed to the PAF strategy (described in the discussion of boundary conditions) of destroying light particles as they move up the cone face and distributing their mass, momentum, and energy among their heavier neighbors. As a result one obtains poorer resolution, and perhaps poorer agreement with experiment, in the vicinity of the shoulder of the cone than in the region near the nose. The good agreement near the nose conforms with the results obtained in the two previous examples of flow past an obstacle.

Figure I-5 shows a particle plot at a late time on which has been superimposed Marschner's steady-state bow wave position. Because of the
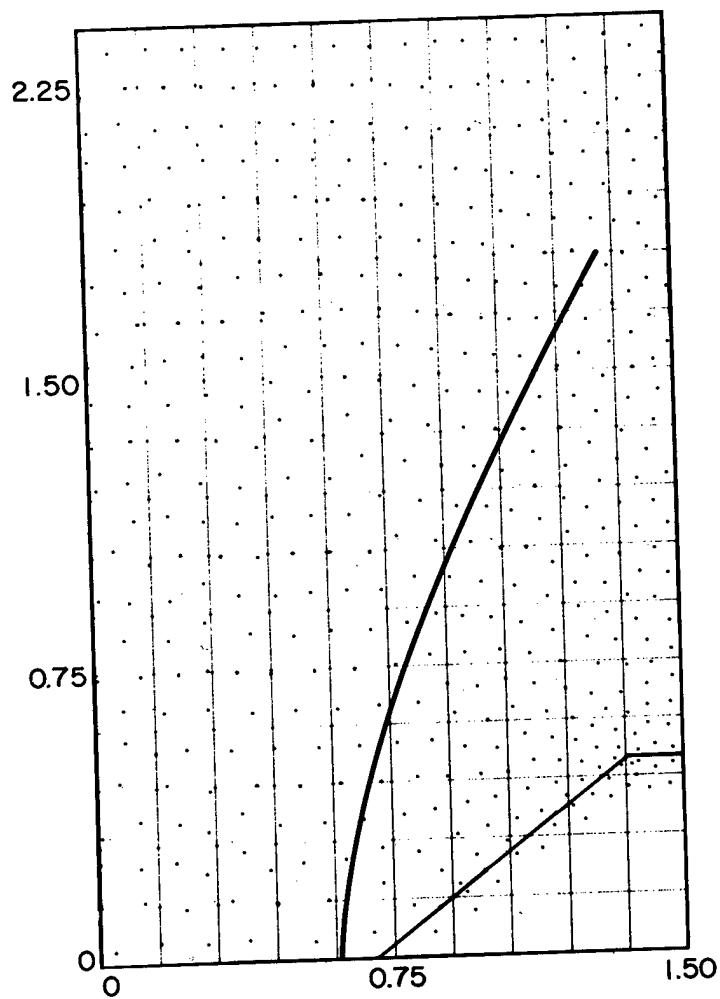
Fig. I-5. A late-time PAF particle plot on which has been super-
imposed Marschner's steady-state bow wave position for
the same experiment described in the caption for Fig. I-4.

weakness of the shock it is difficult to pinpoint the PAF shock front, but it seems to agree quite well with Marschner's, at least in the bottom half of the mesh. The method of locating the shock front in the weak shock region by observing the deflection of horizontal lines of particles, as was done in the case of flow past a blunt cylinder, could not be used here. We have not as yet been able to avoid boundary instabilities when calculating flow past a cone with unstaggered particles.

D. FLOW THROUGH A BENT CHANNEL

The three previous examples have dealt with flow past a symmetric obstacle in a straight channel. In each such case a single detached shock developed and moved upstream from the obstacle, eventually reaching a steady-state bow wave position.

We now consider the more complicated flow through a channel which contains two 90° bends. A plane shock enters the channel and interacts with the channel walls, producing numerous reflected shocks. The problem is to calculate correctly the flow through the channel while a uniform inflow is sustained at the mouth.

These experiments were prompted by shock tube studies performed by H. Reichenbach and his associates at the Ernst-Mach Institute, Freiburg, Germany. In Fig. I-6 a series of 12 photographs trace the flow through the channel for one such shock tube experiment. The very complicated structure of the flow is evident from these pictures which are spaced at 40 μsec intervals. We are grateful to Dr. Reichenbach for his permission to use both these pictures and his detailed measurements, with which we compare our results.
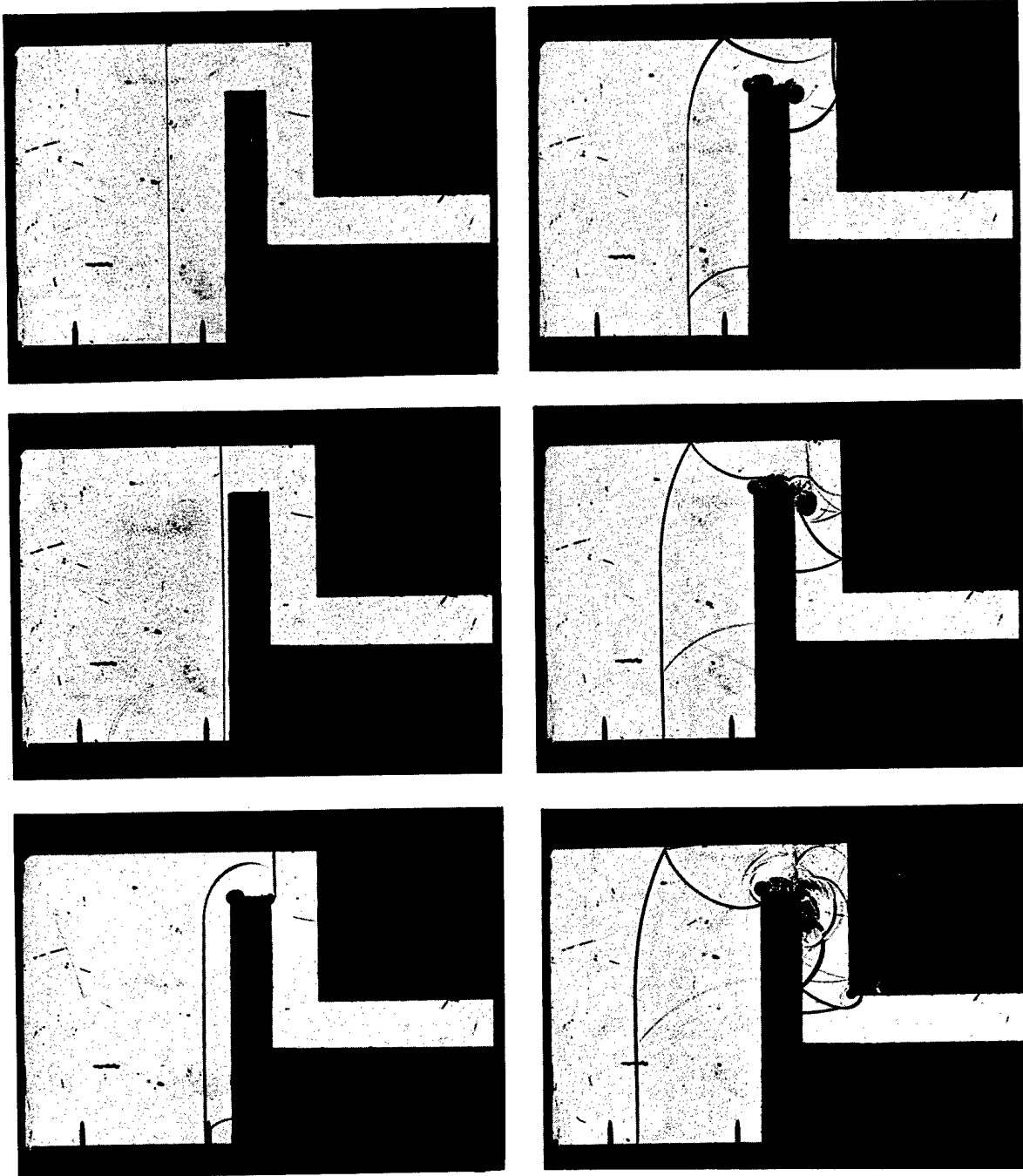
Fig. I-6.   This series of photographs, spaced at 40 μsec intervals, traces the flow observed in a channel when a uniform inflow is sustained at the mouth. The pictures were obtained from a shock tube experiment performed at the Ernst-Mach Institute.
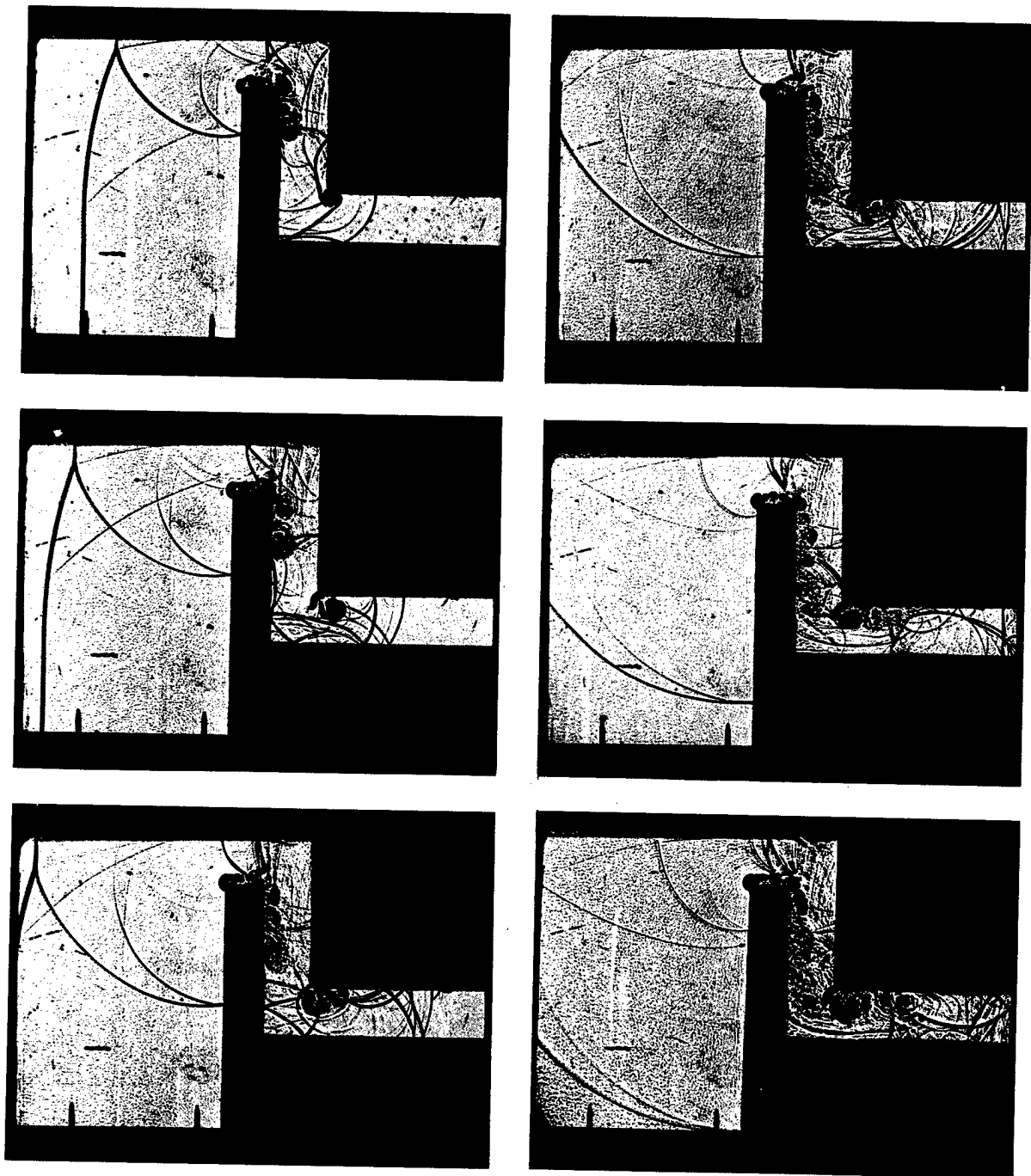
Fig. I-6. (continued)

The experiment with which we will compare was performed in the same manner as that illustrated in Fig. I-6 except that a deposit plate was placed at the mouth of the channel (see accompanying diagram) in order to
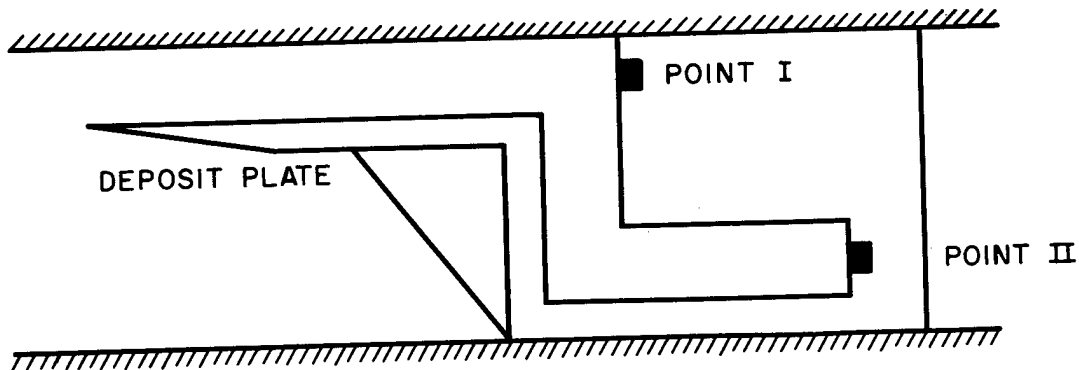
obtain a controlled uniform pulse. The incoming shock had an overpressure of 2.29 relative to the ambient air initially contained in the 2 cm wide channel. This fact can be translated into the following initial data for the PAF problem:

x component of velocity (cm/μsec)	$u_1 = 0.0218$	$u_0 = 0$
y component of velocity (cm/μsec)	$v_1 = 0$	$v_0 = 0$
particle internal energy (10^{-2} joule)	$J_1 = 3.6233$	$j_0 = 2.8133$
particle spacing in the x direction (cm)	$\delta x_1 = 0.25$	$\delta x_0 = 0.333$
particle spacing in the y direction (cm)	$\delta y_1 = 0.25$	$\delta y_0 = 0.333$
particle mass (gm)	$m = 1.339 \times 10^{-4}$	
time step (μsec)	$\delta t = 1.0$	
artificial viscosity coefficient (type I-17b force)	$\omega = 0.1$	

where, as before, subscript 1 is shocked air and subscript o is ambient air. The calculations are performed in a Cartesian coordinate system.

In Fig. I-7 a comparison is made between the PAF pressures recorded at the two observing points in the channel (shown in the diagram on the previous page) with average curves (the dashed lines) drawn through the experimental measurements at these two points. Dr. Reichenbach warns us that the relationship between his measurements and the pressure is not strictly linear, although he points out that the deviation from linearity is not very great. The comparison with the PAF pressures can therefore be evaluated only from a qualitative standpoint.

Nevertheless, the agreement between these resolutions of a very complicated flow structure is remarkable. The shock front arrival times at observing point II (at the end of the channel) are almost identical and the magnitudes of the pressure jumps at points I and II are in good agreement. Furthermore, the major fluctuations in pressure after the initial jumps compare quite nicely.

E. COLLAPSE OF A SPHERICAL SHELL

We do not attempt to justify the development of the PAF method on the basis of competition with the numerical methods already in existence. Several of these have been carried to a high degree of sophistication and, when applied to problems for which they are well suited, may give results superior to those which could be obtained with PAF.

Rather, the strength of the PAF technique lies in its ability to resolve problems which could not be handled by other methods or which
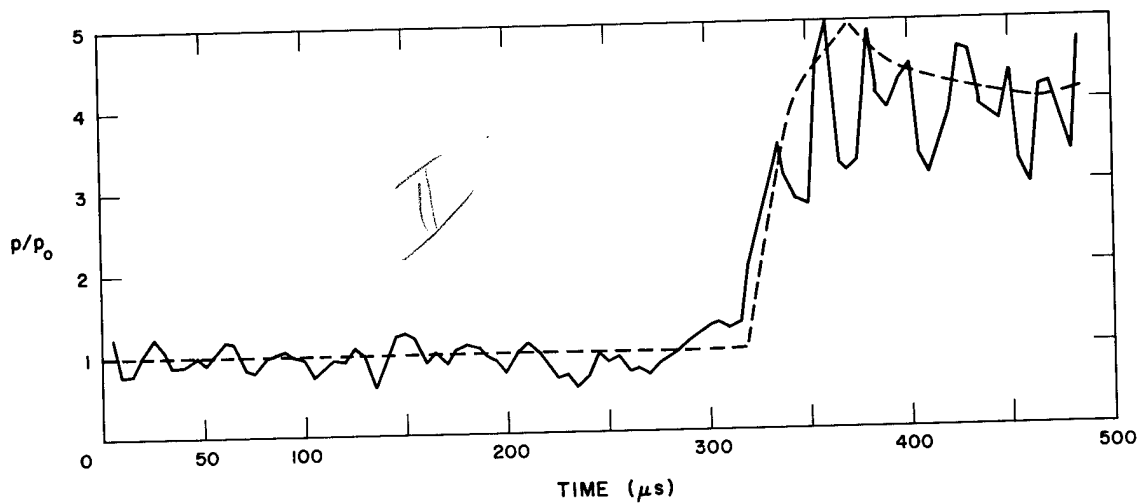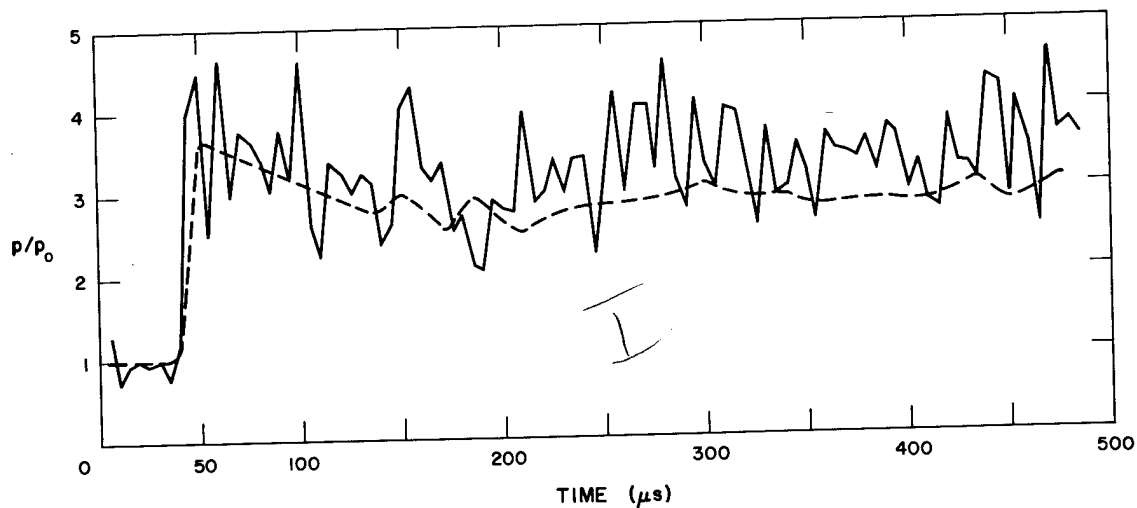
Fig. I-7. Two comparisons between PAF pressures (solid lines) and experimental measurements (dashed lines) from the problem involving flow through a bent channel. The top plot shows the comparison at measuring point I near the mouth and the bottom plot at measuring point II at the end of the channel.

could be attempted only with great difficulty. Such problems fall into two categories: those involving curved or otherwise complicated boundaries and those whose changing geometry hampers any type of mesh resolution. The previous example, involving flow through a bent channel, is one which would be extremely difficult to solve by most other numerical methods because of the complicated boundary. If the bends had been curved rather than at right angles, it is doubtful that any method other than PAF could be applied.

An example of the second category of problems is the calculation of the collapse of a thin spherical shell of material to the shape of a ball. This type of problem does not lend itself to easy solution for any type of calculational method which is tied to a mesh, whether the mesh is fixed in space or moves with the fluid. The primary difficulty encountered by the fixed cell schemes in calculating such a collpase is one of spatial resolution. To cover the entire region with a mesh that is fine enough to resolve all the details of the flow would require a storage capability which exceeds that of even the largest computers.

For the methods whose mesh moves with the fluid, this is no problem. Instead, the problem begins when the shell approaches the final stages of its collapse. Then, cells which were roughly square initially become so elongated and twisted that accurate calculations can no longer be made. The life of the problem can be prolonged by rezoning distorted regions of the mesh as needed, but in no way can the problem be carried to completion. To do this would require that there be interactions between cells which

form opposite sides of the shell and, in these methods, interactions are restricted to cells that were originally contiguous.

To evaluate the ability of PAF to calculate such a collapse, a rather simple test was prepared. A spherical shell of cold particles was given a velocity of uniform magnitude toward the center of the sphere. The material had a polytropic equation of state (with $\gamma = 4$) so, with zero internal energy, only dissipative forces were in effect initially. These, it was hoped, would remain small throughout the early stages of the problem so that the collapse could be maintained without the assistance of an external driving force (for which there was no provision in the code).

The problem was calculated in cylindrical coordinates in order to take advantage of the cylindrical symmetry of the shell, although polar coordinates were used in the initial arrangement of the particles. They were located along radial lines from the center of the sphere[*] and then displaced slightly from their original positions. Other details of the setup are listed below:

internal radius of the shell	$R_o = 20.0$
particle spacing in the R direction	$\delta R = 0.56$
particle spacing in the θ direction	$\delta\theta = 0.026 = \dfrac{\pi}{120}$
z component of velocity	$u = -\cos\theta$
r component of velocity	$v = -\sin\theta$

---

[*]To differentiate between radial distance as measured from the center of the sphere and that measured from the axis of cylindrical symmetry, we refer to the former as R, and to the latter as r.

particle mass	m = product of initial radii, rR
particle internal energy	J = 0
time step	δt = 0.1
artificial viscosity coefficient (type I-17c force)	ω = 1.0

The left-hand series of pictures in Fig. I-8 show particle configurations for this problem at two time unit intervals, from time zero until collapse. The calculation proceeded without difficulty, although it was necessary to reduce the time step from 0.1 to 0.0125 during the last part of the problem when the interparticle spacing was small.

The long black specks which appear in some of the last pictures represent particles whose internal energy has gone negative. They lie along the edges of the shell and have been cooled by the rarefactions which are working their way into the material. It is apparent that these particles do not attain large negative internal energies, for they do no damage to the calculations and in subsequent pictures are positive again.

The pictures seem to indicate that the shell retains its spherical symmetry very nicely throughout the collapse. This may be confirmed by a study of the kinetic energy history of the problem. In spherically symmetric shell motion the r and z components of kinetic energy can be expressed as

$$K_r = \int_0^\pi \int_{R_1}^{R_2} \left(\frac{u^2}{2} \sin^2 \theta \right) \left(2\pi R^2 \rho \sin \theta \, dr \, d\theta \right),$$
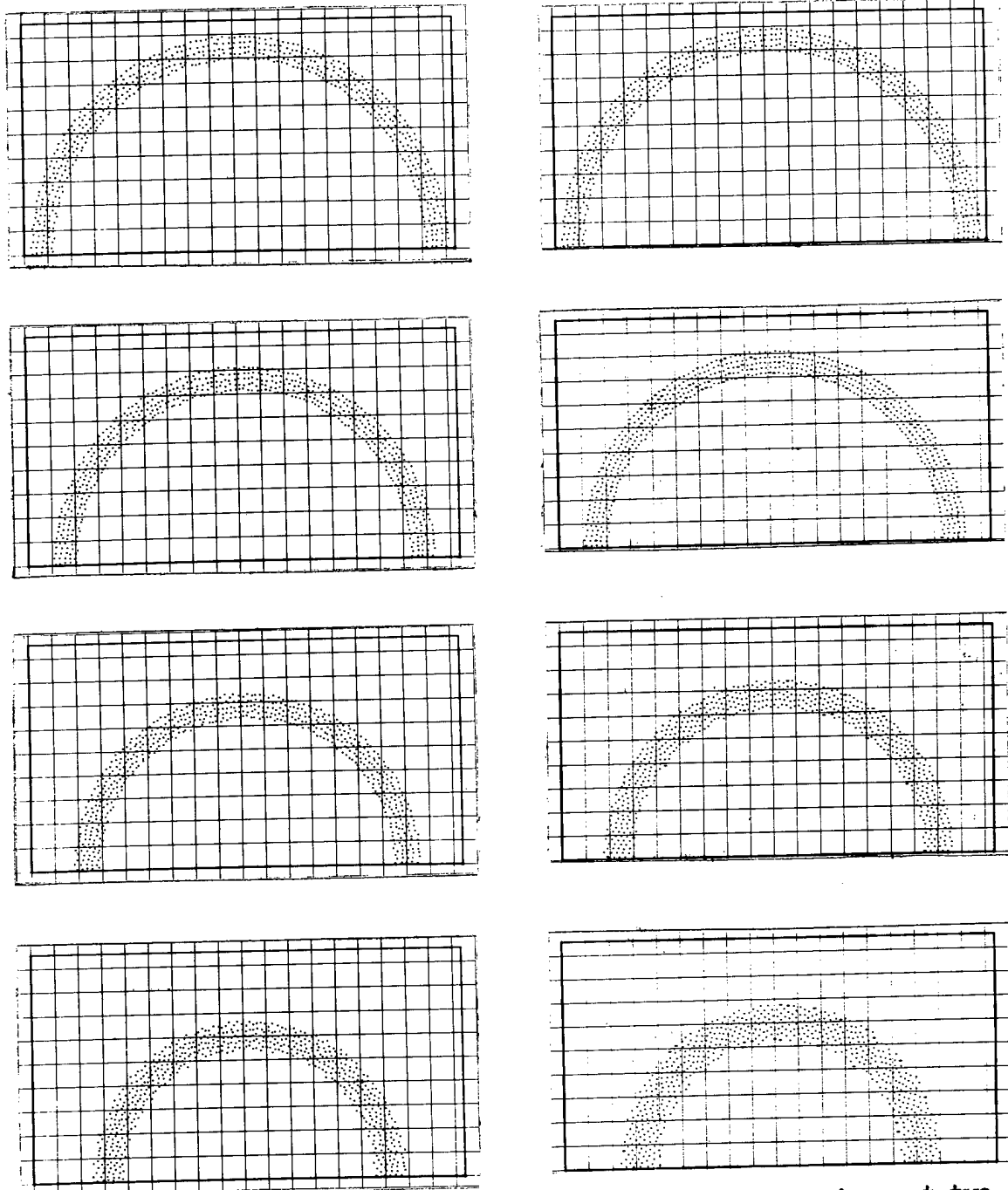
Fig. I-8. These two series of particle configurations, shown at two time unit intervals and beginning at time zero, trace the collapse of a thin spherical shell of material to a ball. The left-hand series was obtained from a problem in which a polytropic equation of state was used, and the right-hand series from one in which a "stiffened" gas equation of state was used.
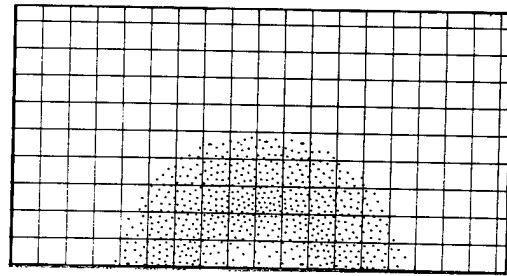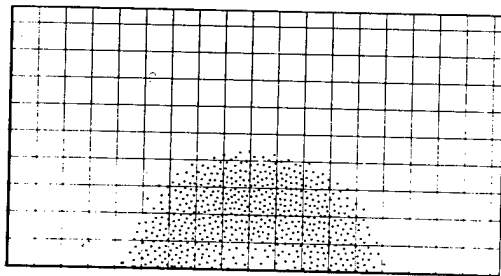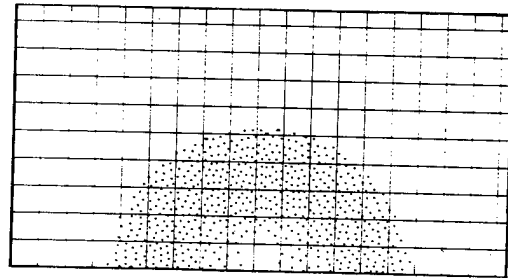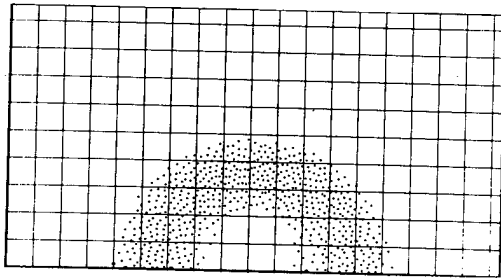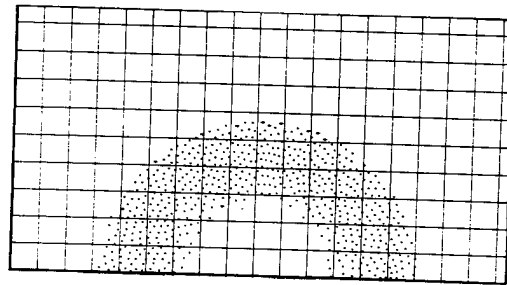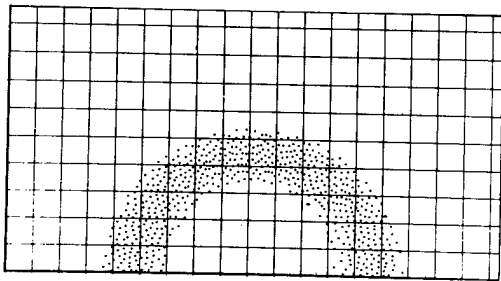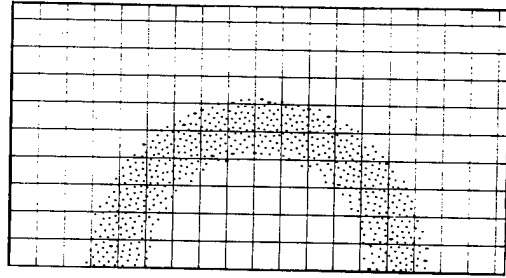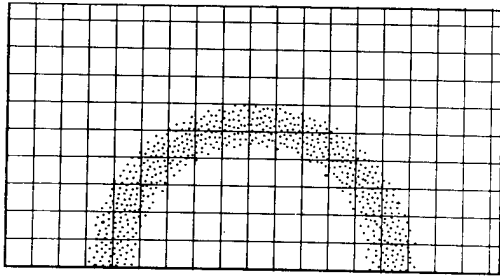
Fig. I-8. (Continued)

$$K_z = \int_0^\pi \int_{R_1}^{R_2} \left(\frac{u^2}{2} \cos^2 \theta\right) \left(2\pi R^2 \rho \sin \theta \, dr \, d\theta\right),$$

so that

$$\frac{K_r}{K_z} = \frac{\int_0^\pi \sin^3 \theta \, d\theta}{\int_0^\pi \cos^2 \theta \sin \theta \, d\theta} = 2.$$

One might therefore choose the function $(K_r - 2K_z)/(K_r + 2K_z)$ as an appropriate measure of the sphericity of the collapse; the more nearly this expression approaches zero, the greater the sphericity. These values are listed at two time unit intervals for this problem in the second column of Table I-2. Very good sphericity is maintained until a time of 12, at which time the decelerating force is starting to become important. This leads to increased fluctuation and, hence, decreased sphericity in the velocity field.

A logarithmic plot of the total internal energy of the system as a function of time can be seen in Fig. I-9.

The problem was also calculated by PAF using a force function derived from a "stiffened" gas equation of state [see Eqs. (I-25)]. Initial conditions were exactly the same as those used in the first problem, p. 69, except for the additional specifications of normal density and the coefficient of the "stiffening" term, which were

$$\rho_0 = 11.003,$$
$$a = 0.0676.$$

TABLE I-2

A MEASURE OF THE SPHERICITY OF TWO PROBLEMS
WHICH DEPICT THE COLLAPSE OF A SPHERICAL
SHELL OF MATERIAL

$$\text{Sphericity} \left(\frac{K_r - 2K_z}{K_r + 2K_z} \right)$$

Time	Equation of State Polytropic	Stiffened Gas
0	0	0
2	0.0009	0.0009
4	0.0018	0.0036
6	0.0018	0.0027
8	0	0.0018
10	-0.0028	-0.0056
12	-0.0134	-0.0203
14	0.0125	-0.2191
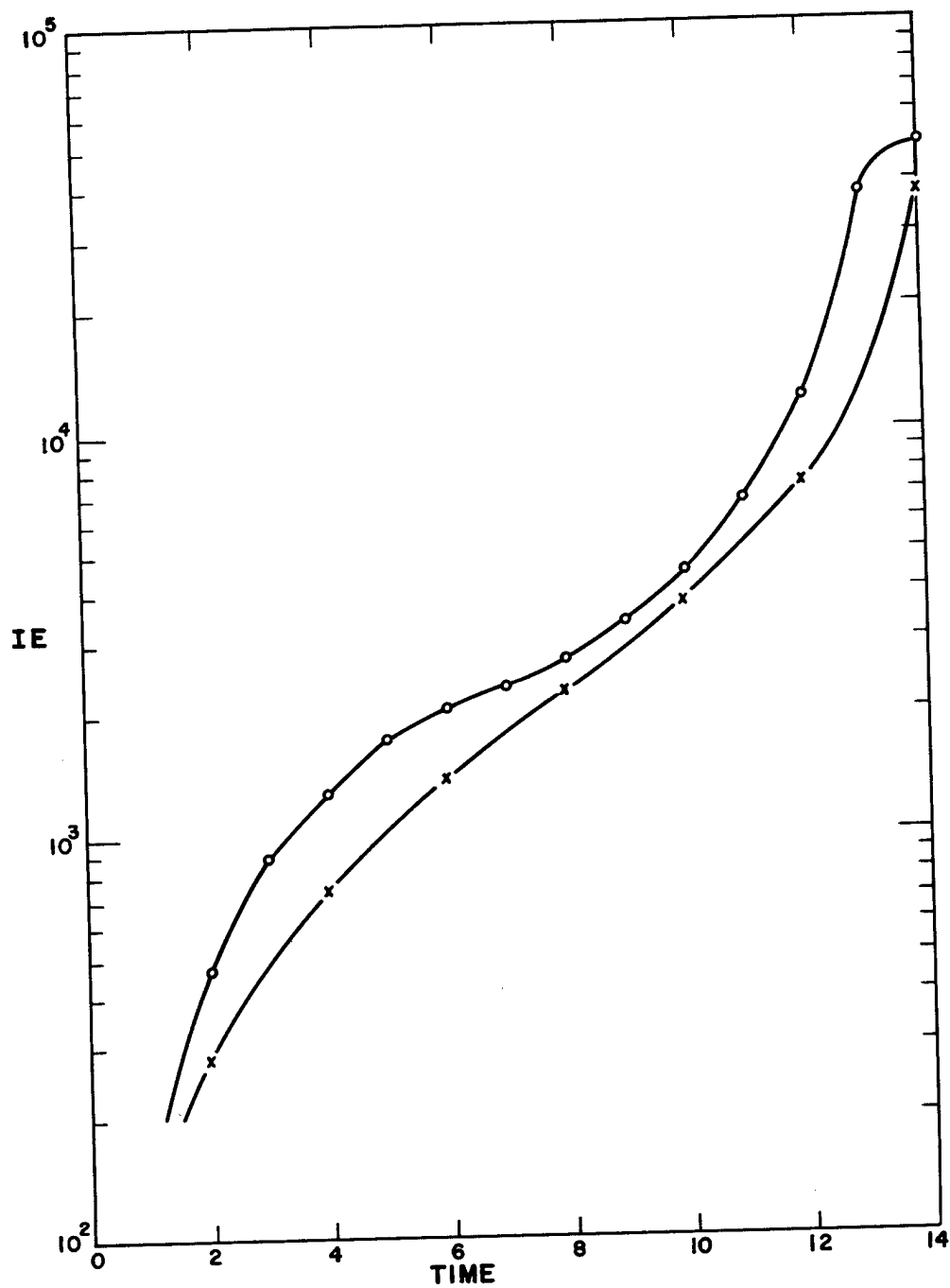
Fig. I-9. A logarithmic plot of total internal energy versus time for two collapsing shell problems, one for which the interparticle force function was derived from a polytropic equation of state (x) and the other for which it corresponds to a "stiffened" gas equation of state (o).

The normal density was chosen equal to the average initial density of the shell and is approximately that of silver. The coefficient, which is the square of the sound speed under normal conditions, is one which would be appropriate for a silver shell.

Before discussing the results of this run it would, perhaps, be instructive to point out one limitation of this force function. It is possible to have attractive interparticle forces with this equation of state whenever the interparticle spacing is greater than that appropriate for normal density material. While very small forces of this type would be acceptable for metals, they should be limited in magnitude by the tensile strength of the material. No such cutoff has as yet been included in our calculations so that the only limit on attractive forces in this problem is that provided by the maximum interparticle search radius.

A study of the particle configurations for this problem, which are shown in the right-hand series of Fig. I-8, and a comparison with the configurations from the previous problem on the left will demonstrate some noticeable differences which arise as a result of this added term in the force function. In the plot at time 2, several particles with negative internal energy are observed, where none are present in the left-hand plot. These negative internal energies develop when the cold, initially staggered particles rearrange themselves in an attempt to attain a more uniform interparticle spacing. Once this has been accomplished (about time 4), negative internal energies seem to be associated with only the rarefied regions along the edges of the shell, as they

were in the previous problem.

Another result of this early rearrangement of particles in the second problem is a much more rapid growth of interparticle dissipative forces than was observed in the first problem. This causes an accelerated growth in the internal energy of the system (as can be seen in Fig. I-9), which, in turn, leads to an increase in the nondissipative forces.

When one couples these increased interparticle forces with the resistance to compression offered by the stiffening term, it is not hard to understand the much greater thickening of the shell in the right-hand series of pictures than in the left-hand series. As a consequence of this thickening, the motion of the interior of the shell toward the center is accelerated, so that final collapse occurs about one time unit sooner. In the final picture in these series the shell on the right is beginning to expand while the one on the left has just reached final collapse.

Because the shell on the right is undergoing expansion at time 14, the sphericity of its velocity field has degenerated, as can be seen in Table I-2. Up to that time its sphericity was comparative to that of the shell with the polytropic equation of state, although slightly poorer as a result of increased interparticle activity.

One conclusion which can be drawn from these two collapsing shell examples is that such calculations can be made with PAF without appreciable difficulty. With the addition of an external drawing force to

the PAF calculations there would seem to be no reason why truly practical problems of this type could not be handled.

The second example also demonstrates that force functions other than those derived from a polytropic equation of state can be applied effectively with the PAF method. The particular function used, however, requires some modification to account for the limited tensile strength of the material.

F. IMPACT OF A BLUNT NOSED CYLINDER ON A THICK PLATE

In the examples of flow past a wedge and flow through a bent channel, we dealt with interactions between fluids in shocked and unshocked states. Satisfactory results were obtained, indicating that the PAF method encounters no serious difficulty in calculating interactions between particles with markedly different properties. In both of these cases, however, the shock strength was rather moderate. We now wish to consider a test of the method in which the material has been subjected to a shock of infinite strength.

A cylindrical projectile of cold material strikes a cold target plate, producing shocks which proceed into the projectile and the target at the same velocity relative to the interface. We wish to check the accuracy of the shock properties and also verify that no calculational difficulties arise at the interface.

Both materials are represented by a polytropic equation of state with $\gamma = 4$. The other starting data are summarized below, where subscript 1 signifies shocked material and subscript o unshocked material.

z component of velocity	$u_1 = 1$	$u_0 = 0$
r component of velocity	$v_1 = 0$	$v_0 = 0$
particle internal energy	$J_1 = 0$	$J_0 = 0$
particle spacing in the z direction	$\delta z_1 = 1$	$\delta z_0 = 1$
particle spacing in the r direction	$\delta r_1 = 1$	$\delta r_0 = 1$
particle mass		$m = $ initial radius
time step		$\delta t = 0.05$
artificial viscosity coefficient (type I-17c force)		$\omega = 1$

The initial particle configuration can be seen in the top plot in Fig. I-10.

At early times the two shocks produced by the impact are essentially one dimensional, so their properties can be calculated from simple shock theory. The magnitude of the shock velocity relative to the interface is given by

$$v_s = \left(\frac{\gamma + 1}{2}\right) (\text{velocity of interface})$$

$$= \frac{5}{4}.$$

The mass of material swept up by the shocks during one time unit is

$$M = 2\pi\rho(\text{projectile radius})^2 v_s$$

$$= 125.$$

The specific internal energy is

$$I = \frac{1}{2}(\text{interface velocity})^2,$$
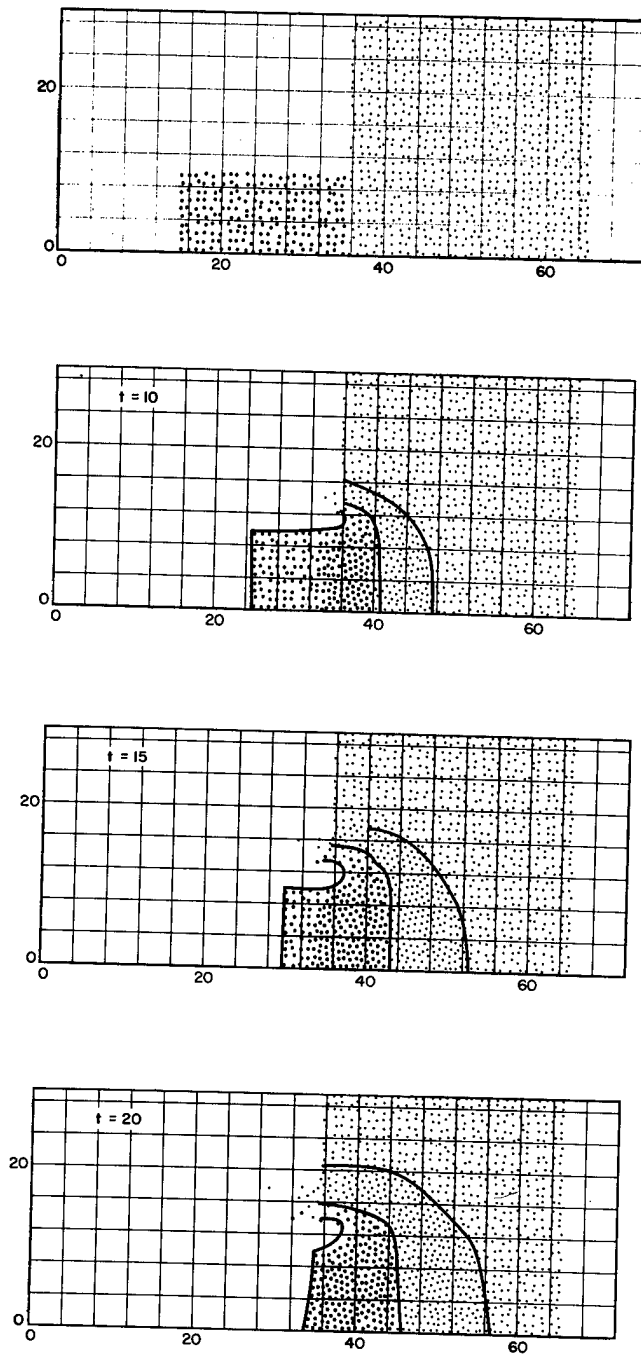
Fig. I-10. PAF particle configurations from the calculation of the
impact of a blunt cylinder on a thick plate at initial
time (top) and at times 10, 15, and 20. On the three
bottom plots there have been superimposed the shock
front, the material interface, and the cylinder outline
as calculated by PIC.

so that during the one-dimensional phase internal energy is produced at the rate

$$\frac{dJ}{dt} = MI = 15.625. \tag{I-29}$$

We merely state, without illustration, that the early time shock velocities from the PAF calculation are in very good agreement with the above prediction, and proceed with an evaluation of late time results.

In the two-dimensional flow regime we have no simple theory with which to make comparisons. Instead, we compare our results with those obtained using another numerical technique, the Particle-in-Cell (PIC) method [I-7]. Admittedly, this makes the evaluation of results somewhat less definitive than would be the case if we used an actual physical experiment for a standard. To the extent that the two methods agree, however, we may draw confidence and in regions of disagreement we can seek explanations.

The initial conditions for the PIC problem were the same as the PAF conditions, except that they were expressed in terms of the PIC model. A comparison between the late time geometries of the flow as produced by the two calculations can be seen in the bottom three plots of Fig. I-10. These show PAF particle configurations at times of 10, 15, and 20, on which have been superimposed the front of the shock which is proceeding into the target plate, the material interface, and the outline of the projectile as they were observed from the PIC particle plots.

The excellent agreement with regard to the position of the shock front indicates that both methods are probably calculating at least the

gross features of the discontinuity correctly. There is some disagreement in the position of the interface and there is reason to believe that part of the blame can be laid to each method. Because of the more random nature of the PAF particle movements, one expects (and sees) a less well defined interface from that method; this could probably be improved with increased resolution. On the other hand, a detailed examination of the PIC quantities indicates that there exist rather large fluctuations in density and internal energy in the vicinity of the interface which result from the manner in which internal energy is distributed in mixed cells. Some of the disagreement may be caused by this difficulty. The outline of the projectile agrees quite well, although there is a minor discrepancy in the low density crater region.

In Fig. I-11 we see a comparison between the internal energy histories of the PIC and the PAF versions. The figure also includes a plot of the one-dimensional internal energy rise rate, Eq. (I-29), with which they both agree nicely at early times. The two methods are in excellent agreement up to a time of about 10, after which they diverge; the PIC profile attains a more gentle slope, while the PAF method continues the rapid rise.

This disagreement is somewhat puzzling, in view of the fact that the outline of the shocked region agrees so nicely at late times. One might suppose that the depressed internal energy curve of the PIC method results from greater velocity fluctuations for that method, but this conclusion is not borne out by detailed studies of the data. A calculation
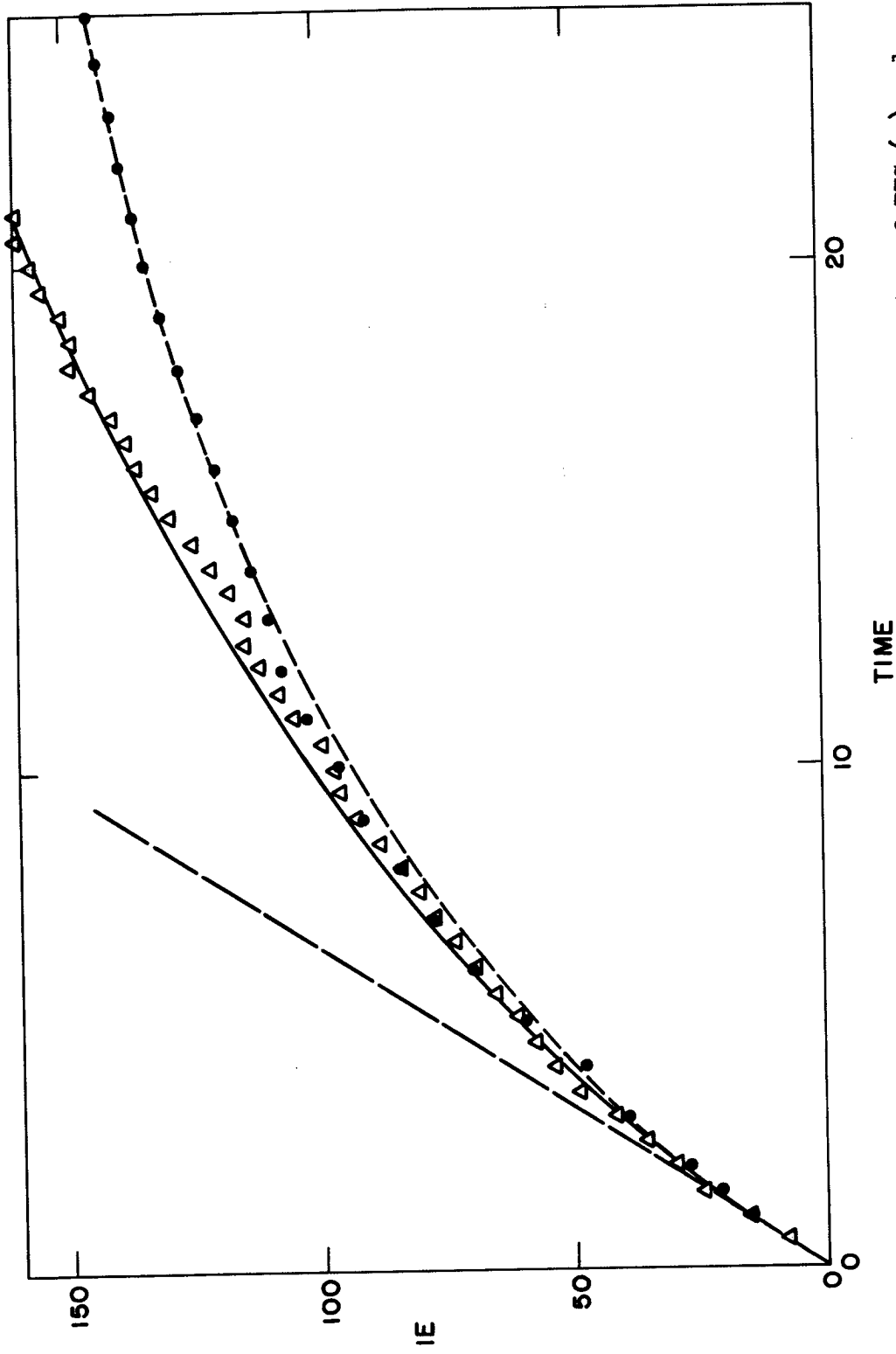
Fig. I-11. A comparison between the internal energy histories of PIC (●) and PAF (△) versions of a high velocity impact problem. The long dashed line is the theoretical one-dimensional internal energy rise rate.

of the variance of velocity magnitude for sample regions of the fluid indicates that the two methods experience about the same amount of velocity fluctuations.

The divergence of internal energy growth rates persists even when the problem is recalculated with different values for the time step or the viscosity coefficient or with increased resolution. This would indicate that the discrepancy represents an inherent difference between the two techniques, but which is more nearly correct is difficult to say.

CHAPTER 3

THE FUTURE DEVELOPMENT OF PAF

The development of a numerical model of a complicated physical
system generally proceeds through several distinct stages of evolution.
First, a computer code embracing the basic concepts of the method in the
simplest form in which they can be expressed (usually a one-dimensional
coordinate system, if applicable) is written and tested against uncompli-
cated problems for which easily verified solutions exist. This stage of
the development often involves a considerable amount of experimentation
with mesh geometries, boundary conditions, and the form of the difference
equations.

If the results justify it, the technique is then extended to a
more complicated frame of reference and applied to more difficult prob-
lems. Such an extension often introduces a host of new problems for the
representation and may even require some further refinements in the basic
formulation. Depending upon the amount of success attained in these more
difficult problems, an evaluation can be made of the range of applicability
for the method and the avenues in which further development might be
channeled.

Practical applications of the method to problems of immediate interest begin at this stage with the development of a working code which is designed for a specific class of problems. At the same time, developmental work continues, extending the method to more complicated calculational regimes.

The evolution of the PAF method has followed this pattern very closely. This report, in fact, marks the culmination of the second stage of development and we are in the process of writing a working code to be applied to several hydrodynamic problems for which the method seems ideally suited (see p. 66). Simultaneously, plans are being made to extend the method in order to include the calculation of the interaction between materials with different equations of state.

The remainder of this chapter is concerned with a discussion of our future plans.

A. THE NEW CODE

The PAF developmental work has often been severely hampered by insufficient particle resolution. For example, the problem of flow past a wedge, which is described in Chapter 2, was halted far short of steady state because there was no longer any machine storage available to accommodate new particles entering the system. Other problems, particularly those involving flow past blunt obstacles, were carried to completion only by employing the minimum of resolution.

The reason for this difficulty is that PAF requires a large amount of machine storage per particle. Not only must we store the quantities

needed to describe the state of each particle, such as mass, coordinate components, the present and advanced values of the velocity components, and the present and advanced values of the internal energy, but we must also keep track of the interparticle relationships. For each particle, space is set aside to list up to four neighbors and the interparticle forces with these neighbors. Also storage is required to accommodate the cellular mesh which is used in the neighbor search routine.

We have attempted to minimize this problem by the use of revolving storage whenever possible. Several quantities which are not being used during the same phase of the calculation and which must be recomputed each cycle share the same memory regions. Also, the storage required for interparticle forces is kept at the lowest possible level by storing only the kernel of the force function [the part which is common to $F_{ij}(x)$, $F_{ji}(x)$, $F_{ij}(y)$, and $F_{ji}(y)$] and by recomputing the additional factors whenever necessary. Even with these economies, however, a minimum of 15 memory words per particle is required for PAF calculations.

With this storage limitation it has become necessary to graduate to a calculating machine with a larger memory capacity in order to be able to apply the method accurately to a variety of problems. The new PAF code is being written for the IBM 7030 machine which has a fast memory capacity of 98,000 words. This added facility will permit us to calculate with as many as 5000 particles, which should be sufficient for the problems we now have in mind.

In addition to increased resolution, other improvements are

expected from the new code. The facilities for data presentation will certainly be expanded. One such addition will be streamline plots. These should not only be invaluable for illustrative purposes but also as a diagnostic tool. Other features which are under consideration include moving pictures of particle configurations, graphs of functionals, such as pressure, density, and internal energy, and listings of local variables, averaged over small regions of space. At the time of this writing, several of these have already been tested and found to be extremely useful.

B. A REVISED FORM OF THE ENERGY EQUATION

Another modification to be included in the new code, this time of a computational nature, has to do with the calculation of internal energy change. The equation which governs this change has been rewritten in a form which is designed to eliminate negative internal energies.

In some of the examples described in Chapter 2, a few particles have developed negative internal energies; usually these were particles that were located along the edge of an unconfined fluid. These negative values were tolerated because the particles were either isolated, and therefore had little or no effect on the rest of the system, or else they were only slightly (and temporarily) negative, and again had little effect on the total calculation. No physical defense for negative internal energy is tenable, however, and from a calculational standpoint it can do great harm because it leads to attractive interparticle forces for which there is no cutoff.

In the present code the change in internal energy which results from an interparticle encounter is shared equally by the two particles. (In cylindrical coordinates this is only approximately true.) The magnitude of the change is therefore the same for the two particles but the percentage change may be quite different. One particle's internal energy might even go from a positive to a negative value while its neighbor's was altered only slightly.

The method would be a better model of true physical changes if the variation of a particle's internal energy was more strongly dependent upon its magnitude. The purpose of the calculational change we now describe is to introduce this dependency into the energy equation.

To accomplish this in the plane coordinate version we rewrite Eq. (I-6) in the form

$$\frac{dJ_j}{dt} = J_j \sum_i^* \frac{1}{J_i + J_j} \left[\vec{F}_{ij} \cdot (\vec{u}_i - \vec{u}_j) \right]. \qquad \text{(I-30)}$$

A criterion for avoiding negative internal energies can quite easily be demonstrated for the case where $\vec{F}_{ij}$ is the interparticle force function associated with a polytropic equation of state. To see this we write Eq. (I-30) in difference form,

$$\frac{\delta J_j^n}{J_j^n} = \frac{(\gamma - 1)\delta t}{2} \sum_i^* \frac{1}{r_{ij}^n} \left[\vec{s}_{ij}^n \cdot \left(\vec{u}_i^{n+\frac{1}{2}} - \vec{u}_j^{n+\frac{1}{2}} \right) \right], \qquad \text{(I-31)}$$

where we have neglected the dissipative terms, whose only effect can be

to increase J_j^n.[*] A sufficient condition for insuring that $\delta J_j^n / J_j^n < 1$ is then

$$\frac{|\vec{u}|_{max} \, \delta t}{\delta r_{min}} < \frac{1}{(\gamma - 1)N^*} \, .$$

This criterion is not violently restrictive, but is comparable to restrictions already required for accuracy.

Energy conservation is not hampered by this modification of the internal energy equation. To demonstrate this we begin by summing Eq. (I-30) over all the particles in the system.

$$\sum_j \frac{dJ_j}{dt} = \sum_j \sum_i{}^* \frac{J_j}{J_i + J_j} \left[\vec{F}_{ij} \cdot (\vec{u}_i - \vec{u}_j) \right]. \qquad (I-32)$$

The sum is, of course, independent of the order of summation, so that we may rewrite the equation

$$\sum_j \frac{dJ_j}{dt} = \sum_i \sum_j{}^* \frac{J_j}{J_i + J_j} \left[\vec{F}_{ij} \cdot (\vec{u}_i - \vec{u}_j) \right],$$

$$= \sum_j \sum_i{}^* \frac{J_i}{J_i + J_j} \left[\vec{F}_{ji} \cdot (\vec{u}_j - \vec{u}_i) \right],$$

$$= \sum_j \sum_i{}^* \frac{J_i}{J_i + J_j} \left[\vec{F}_{ij} \cdot (\vec{u}_i - \vec{u}_j) \right],$$

_____

[*] The treatment of the dissipative term in the force function remains unchanged from Chapter 1. Because of this difference in treatment, the kernels of the dissipative and nondissipative parts of the force function must be stored separately.

where the last expression is possible because $\vec{F}_{ij} = -\vec{F}_{ji}$. Combining this expression with Eq. (I-32), we find that

$$\sum_j \frac{dJ_j}{dt} = \frac{1}{2} \sum_j \sum_i {}^* \vec{F}_{ij} \cdot (\vec{u}_i - \vec{u}_j),$$

in which form the summation is now identical with that obtained from our original conservative equation [see Eq. (I-6)]. Conservation is assured in the finite difference form of the equations if, as before, the velocities are evaluated at time $t = (n + \frac{1}{2}) \delta t$.

A similar treatment of the cylindrical coordinate equations does not, however, produce energy conservation. In that coordinate system the analogous equation for the change in internal energy would be

$$\frac{dJ_j}{dt} = J_j \sum_i {}^* \frac{1}{J_i + J_j} \left[\vec{F}_{ij} \cdot (\vec{u}_i - \vec{u}_j) + \frac{1}{2} \left(\frac{r_i - r_j}{r_j} \right) F_{ij}(r)(v_i + v_j) \right]. \quad (I-33)$$

When we sum this change over all of the particles in the system and add to it the total change in kinetic energy, we find, after considerable simplification, that the total energy change fails to equal zero by an amount

$$\frac{dE}{dt} = \frac{1}{4} \sum_j \sum_i {}^* \left[\left(\frac{r_i - r_j}{r_j} \right) \left(\frac{J_j - J_i}{J_i + J_j} \right) F_{ij}(r)(v_j - v_i) \right].$$

To correct for this discrepancy and insure conservation, we therefore rewrite Eq. (I-33) in the form

$$\frac{dJ_j}{dt} = \sum_i{}^* \left\{ \frac{J_j}{J_i + J_j} \left[\vec{F}_{ij} \cdot (\vec{u}_i - \vec{u}_j) + \frac{1}{2} \left(\frac{r_i - r_j}{r_j} \right) F_{ij}(r)(v_i + v_j) \right] \right.$$

$$\left. - \frac{1}{4} \left[\left(\frac{r_i - r_j}{r_j} \right) \left(\frac{J_j - J_i}{J_i + J_j} \right) F_{ij}(r)(v_j - v_i) \right] \right\}. \tag{I-34}$$

Once again, this conservation carries through to the difference equations if the velocities are time-centered.

At the time that this report was written several tests of the new code had been made and these preliminary results indicated that the revised internal energy calculation was performing satisfactorily. In comparison with runs performed with the earlier version of the code, it was apparent that the large scale features of the calculation were essentially unaltered, but the absence of negative internal energies where they had been present before testified to the effectiveness of the new technique. It remains to be seen whether this revised calculation will obviate the particle destruction procedure which had been necessary in order to avoid boundary instabilities in certain cylindrically symmetric flow problems (see pp. 41, 42).

C. MULTI-MATERIAL PAF

The new PAF code is a one-material program, as is the one described in this report. Plans exist, however, to extend the method to include interactions between materials with different equations of state.

Fundamental to these plans is the concept of a force function between particles of unlike kinds. In the absence of a correspondence theory

(such as that described in Ref. I-2) for this type of interaction, we derive the interparticle force function on the basis of preserving fluid equilibrium. In particular we require that the average pressure be constant on either side of a material interface in a fluid in equilibrium.

1. Plane Coordinates

For simplicity, let us assume that the particles which represent this fluid are arranged in a square array (see accompanying diagram) and that the coordinate system is Cartesian. The derived conditions should then be necessary, but perhaps not sufficient, for general equilibrium in a plane coordinate system.
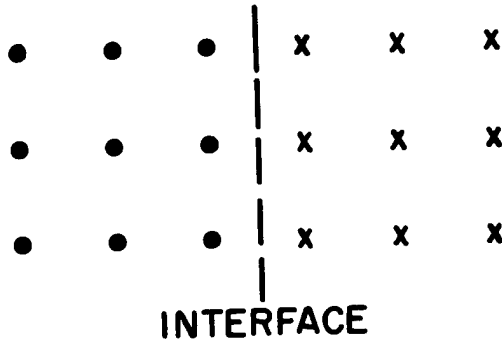
INTERFACE

The material to the left of the interface we shall call dot material and that on the right x material. The interparticle spacing is the same for both materials; hence, the dot and x particles must have different masses if their densities are to be different. Likewise there are two distinct interparticle force functions,

$$\vec{F}_{\cdot_{ij}} = \vec{s}_{ij} f_{\cdot}(r_{ij}, J_i, J_j),$$

$$\vec{F}_{x_{ij}} = \vec{s}_{ij} f_{x}(r_{ij}, J_i, J_j),$$

for the two fluids. At the interface, equilibrium requires that these two be equal:

-93-

$$f_{\bullet}(r_{ij}, J_i, J_j) \equiv f_x(r_{ij}, J_i, J_j) \equiv f_{\bullet x}(r_{ij}, J_i, J_j). \qquad \text{(I-35a)}$$

If the two fluids were polytropic, this equation would be written

$$\frac{(\gamma_\bullet - 1)J_\bullet}{r_{ij}} = \frac{(\gamma_x - 1)J_x}{r_{ij}} = f_{\bullet x}(r_{ij}, J_i, J_j). \qquad \text{(I-35b)}$$

For $f_{\bullet x}$ we try an expression of the form

$$f_{\bullet x}(r_{ij}, J_\bullet, J_x) = \lambda \left(\frac{J_\bullet + J_x}{2r_{ij}} \right),$$

and solve for a value of λ which is consistent with the equation above.
Thus

$$(\gamma_\bullet - 1)\, J_\bullet = \lambda \left[\frac{J_\bullet + \left(\dfrac{\gamma_\bullet - 1}{\gamma_x - 1} \right) J_\bullet}{2} \right],$$

$$\lambda = \frac{2(\gamma_\bullet - 1)(\gamma_x - 1)}{\gamma_\bullet + \gamma_x - 2}.$$

The interparticle force function between two fluids with polytropic equations of state can therefore be written

$$\vec{F}_{ij} = \vec{s}_{ij} \left[\frac{(\gamma_i - 1)(\gamma_j - 1)(J_i + J_j)}{(\gamma_i + \gamma_j - 2)r_{ij}} \right].$$

Notice that when i and j are the same material this expression reduces to the usual one-material force function.

If the two fluids had stiffened gas equations of state we could write Eqs. (I-35) as

$$\frac{(\gamma_. - 1)J_.}{r_{ij}} + \frac{m_. a_.}{r_{ij}}\left(1 - \frac{\rho_{o.} r_{ij}^2}{m_.}\right) = \frac{(\gamma_x - 1)J_x}{r_{ij}} + \frac{m_x a_x}{r_{ij}}\left(1 - \frac{\rho_{ox} r_{ij}^2}{m_x}\right)$$

$$= \lambda\left(\frac{J_. + J_x}{2r_{ij}}\right) + \frac{\Gamma}{\delta x} .$$

Using the same value of λ as was used for the polytropic equation of

state, we can reduce this equation to

$$m_. a_.\left(1 - \frac{\rho_{o.} r_{ij}^2}{m_.}\right) = m_x a_x\left(1 - \frac{\rho_{ox} r_{ij}^2}{m_x}\right) = \Gamma.$$

The only symmetric value for Γ is the average of the two terms

$$\Gamma = \frac{m_. a_. + m_x a_x}{2}\left[1 - \frac{(a_. \rho_{o.} + a_x \rho_{ox})r_{ij}^2}{m_. a_. + m_x a_x}\right].$$

The force function appropriate for two unlike stiffened gases can there-

fore be written as

$$\vec{F}_{ij} = \vec{s}_{ij}\left\{\left[\frac{(\gamma_i - 1)(\gamma_j - 1)(J_i + J_j)}{(\gamma_i + \gamma_j - 2)r_{ij}}\right]\right.$$

$$\left. + \left(\frac{m_i a_i + m_j a_j}{2r_{ij}}\right)\left[1 - \frac{(\rho_{oi} a_i + \rho_{oj} a_j)r_{ij}^2}{m_i a_i + m_j a_j}\right]\right\}.$$

2. Cylindrical Coordinates

Consider the problem of maintaining equilibrium among a square array

of particles in a cylindrical coordinate calculational system. If we

confine our attention to the z component of the interparticle

relationships, we see that the problem is entirely unchanged from the plane coordinate case. Therefore, the plane coordinate form of the interparticle force function will apply as well to the z component in cylindrical coordinates.

The r component of this interparticle force requires additional consideration, however, because of its asymmetry. We begin by recalling that the one-material form of this force was derived subject to the constraint that an unconfined fluid of uniform density and internal energy must have the same rate of expansion in the positive and negative radial directions. As a consequence of this demand, a confined fluid in equilibrium which is subject to the proper boundary conditions must remain forever in equilibrium. We wish now to extend this requirement to the case where more than one fluid is so confined. For simplicity of calculation we again specify that the particles be arranged in a square array.

Consider a radial line of these particles (see accompanying diagram), numbered 1, 2, 3, and 4, which crosses this interface. Particles 1 and 2 are dot material, 3 and 4 are x material. In the one-material case, when the density and specific internal energy were uniform, it turned out that the force on a particle from its neighbor above was exactly balanced by the force exerted by its neighbor below. We now require that this hold in the vicinity of an interface, so that
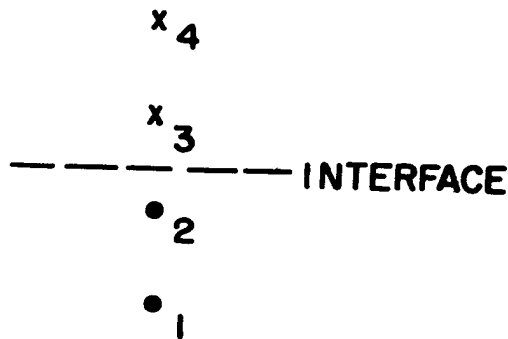
$$\vec{F}_{23} = -\vec{F}_{43}, \qquad \vec{F}_{32} = -\vec{F}_{12}. \tag{I-36}$$

The one-material analogy is carried even further with the requirement that

$$\vec{F}_{23} = -\frac{r_3}{r_2}\vec{F}_{32}. \tag{I-37}$$

If a force function can be discovered which satisfies conditions (I-36) and (I-37), then equilibrium will be assured, for the pressure will be uniform in the vicinity of the interface.

If the two fluids have polytropic equations of state, condition (I-36) can be expressed

$$\vec{F}_{23} = \frac{(\gamma_x - 1)r_3(J_3 + J_4)}{\delta r(r_3 + r_4)}\,\hat{r} = \frac{(\gamma_x - 1)r_3^m\, I_x}{\delta r}\,\hat{r},$$

$$\vec{F}_{32} = -\frac{(\gamma_. - 1)r_2^m\, I_.}{\delta r}\,\hat{r},$$

where we have made use of the fact that in a uniform density fluid the mass is proportional to the radius. We now use condition (I-37) to determine the form of the interparticle force function:

$$\vec{F}_{23} = \frac{(\gamma_x - 1)r_3^m\, I_x}{\delta r}\,\hat{r} = \frac{(\gamma_. - 1)r_3^m\, I_.}{\delta r}\,\hat{r} = \lambda r_3\left[\frac{J_2 + J_3}{\delta r(r_2 + r_3)}\right]\hat{r},$$

$$\lambda = \frac{(\gamma_. - 1)(\gamma_x - 1)(r_2 + r_3)}{r_3(\gamma_. - 1) + r_2(\gamma_x - 1)}.$$

Generalizing, now, to any array of particles we write the interparticle force function as

$$F_{ij}(r) = \frac{(r_j - r_i)}{r_{ij}} \left[\frac{(\gamma_i - 1)(\gamma_j - 1)r_j}{r_j(\gamma_i - 1) + r_i(\gamma_j - 1)} \right] \frac{(J_j + J_i)}{r_{ij}} \; ,$$

$$F_{ij}(z) = \frac{(z_j - z_i)}{r_{ij}} \left[\frac{(\gamma_i - 1)(\gamma_j - 1)}{\gamma_i + \gamma_j - 2} \right] \frac{(J_j + J_i)}{r_{ij}} \; .$$

The uniformity of pressure along the radial line may now be verified by applying either of the relations from conditions (I-36). For example,

$$\vec{F}_{23} = \left[\frac{(\gamma_. - 1)(\gamma_x - 1)r_3}{r_3(\gamma_. - 1) + r_2(\gamma_x - 1)} \right] \frac{(J_3 + J_2)}{\delta r} \hat{r} = \frac{(\gamma_x - 1)r_3 m_x I_x}{\delta r} \hat{r} = -\vec{F}_{43}$$

simplifies to

$$(\gamma_. - 1)m_. I_. = (\gamma_x - 1)m_x I_x ,$$

so the same pressure exists on either side of the interface.

Applying the same technique to two fluids with "stiffened" gas equations of state in cylindrical coordinates, one can obtain an interparticle force function with components

$$F_{ij}(r) = \frac{(r_j - r_i)}{r_{ij}} \left\{ \left[\frac{(\gamma_i - 1)(\gamma_j - 1)r_j}{r_j(\gamma_i - 1) + r_i(\gamma_j - 1)} \right] \left[\frac{(J_j + J_i)}{r_{ij}} \right] \right.$$

$$\left. + \left[\frac{(m_i a_i + m_j a_j)r_j}{(r_j + r_i)r_{ij}} \right] \left[1 - \frac{2\pi r_{ij}^2 (r_j \rho_{oj} a_j + r_i \rho_{oi} a_i)}{(m_i a_i + m_j a_j)} \right] \right\} ,$$

-98-

$$F_{ij}(z) = \frac{(z_j - z_i)}{r_{ij}} \left\{ \left[\frac{(\gamma_i - 1)(\gamma_j - 1)}{\gamma_i + \gamma_j - 2} \right] \left(\frac{J_j + J_i}{r_{ij}} \right) \right.$$

$$\left. + \left[\frac{(m_i a_i + m_j a_j)}{2r_{ij}} \right] \left[1 - \frac{2\pi r_{ij}^2 (r_j \rho_{oj} a_j + r_i \rho_{oi} a_i)}{(m_i a_i + m_j a_j)} \right] \right\} .$$

It can be verified that, when particles i and j have the same equation of state, these expressions are identical with Eqs. (I-25).

Notice that the kernels of these cylindrical coordinate multi-material force functions are not identical for the r and z components, as they were in the single material functions. As a result, the multi-material PAF code will require twice as much memory for the storage of interparticle forces as does the present code.

APPENDIX A

VIRIAL APPROACH TO CORRESPONDENCE THEORY

Neglecting the dissipative forces, we may write for the PAF particle dynamics the equations

$$m_j \frac{d\vec{u}_j}{dt} = \sum_i^* \vec{s}_{ij} f_{ij},$$

$$\frac{d\vec{x}_j}{dt} = \vec{u}_j.$$

From these can be derived

$$\frac{d}{dt}(m_j \vec{x}_j \cdot \vec{u}_j) - m_j \vec{u}_j^2 = \sum_i^* \vec{x}_j \cdot \vec{s}_{ij} f_{ij}.$$

Suppose that the particles are confined within a rigid circular (or spherical) region by means of images beyond a wall of radius R. The above equation can be summed over the particles within R and rearranged as follows:

$$\sum_{j,int} \frac{d}{dt}(m_j \vec{x}_j \cdot \vec{u}_j) - \sum_{j,int} m_j \vec{u}_j^2 = \frac{1}{2} \sum_{j,all} \sum_i^* (\vec{x}_j - \vec{x}_i) \cdot \vec{s}_{ij} f_{ij}$$

$$- \sum_{j,ext} \sum_i^* \vec{x}_j \cdot \vec{s}_{ij} f_{ij}.$$

The sum over j,int means the sum over particles within R, while the sum over j,ext means the sum over the exterior images only. Summing over j,all includes both.

Consider now the long time average of this equation. The first term vanishes, since $m_j \vec{x}_j \cdot \vec{u}_j$ is bounded for these confined particles. The second term vanishes because the PAF correspondence is supposed to force all particle kinetic energy to be macroscopic only. Thus, we obtain

$$\frac{1}{2} \sum_{j,all} < \sum_{i}^{*} r_{ij} f_{ij} > = \sum_{j,ext} < \sum_{i}^{*} \vec{x}_j \cdot \vec{s}_{ij} f_{ij} > \, ,$$

where $< \ >$ means the appropriate long time average. For the exterior particles, $\vec{x}_j \cdot \vec{s}_{ij} \equiv R + \epsilon_j$, where ϵ_j is the distance out to the image from the wall. In n dimensions, f_{ij}/s^{n-1} is the surface pressure, where s is the mean interparticle spacing. Thus, with the assumption of strong correlation, the virial equation becomes

$$\frac{1}{2} (N_i N^{*} + N_e) s f(s) = N_e (R + \frac{s}{2}) s^{n-1} p\left(\frac{m}{s^n}\right) \, ,$$

where N_i is the number of interior particles, N_e is the number of exterior images, N^{*} is the number of neighbors per particle, and $p(m\rho)$ is the pressure as a function of mass density. It can be shown that $N_e R = n N_i s$, so that

$$\left(1 + \frac{N_i N^{*}}{N_e}\right) f(s) = \left(1 + \frac{2n N_i}{N_e}\right) s^{n-1} p\left(\frac{m}{s^n}\right) \, .$$

Thus, in order to have a correspondence equation which is independent of N_i/N_e, it is necessary that $N^* = 2n$, proving, therefore, the contention that the number of neighbors per particle must be twice the number of space dimensions. We also obtain

$$f(s) = s^{n-1} p\left(\frac{m}{s^n}\right),$$

which is the same as the result obtained from the Liouville correspondence theory — see, for example, Eq. (I-14).

APPENDIX B

THEORY OF CORRESPONDENCE FOR CYLINDRICAL COORDINATES

We wish to extend the correspondence theory to show that three-dimensional problems with cylindrical symmetry can be approximated by a two-dimensional PAF model. In other words, we wish to use a two-dimensional array of particles and forces between them to represent a three-dimensional array of particles and corresponding forces.

One of the restrictions we should like to make is that the force between two particles be dependent only on the plane coordinates of the particles and the usual variables $\bar{\varphi}$ and $\vec{\bar{u}}$. (Notation throughout this appendix is the same as that in Ref. I-2.)

One possible scheme suggests itself immediately. We could consider each two-dimensional particle as the representative of a ring of particles. Then the force between two such representatives would be just the average of the actual force over the entire ring. Unfortunately such an association of the two-dimensional array of particles with rings also means that a "self-force" would be imposed on each member of the array because of the other particles in the ring it represents. This

self-force leads to considerable trouble, as will be seen below. However, if the initial distribution were such that this self-force could be ignored, this approach is partially successful.

A slight alteration of this technique is to assume that the initial distribution is such that, while it is not formed of rings, little error is involved in computing interparticle forces by means of an average. However, it seems difficult to justify this procedure on anything other than an intuitive basis.

It should be noted that it is necessary to assume that variables such as ρ_1, $\bar{\varphi}$ and $\vec{u}$ do not change with θ (where r, θ, and z are cylindrical coordinates and the z axis is the axis of symmetry). These assumptions are justified by cylindrical symmetry.

We begin with N particles in a three-dimensional array whose motion is governed by a distribution function $z_N(\vec{r}_j,\vec{u}_j,\varphi_j,t)$, where j runs from 1 to N and $\vec{r}_j$ is the ordinary three-dimensional position vector.

We first integrate out θ_j for each j to obtain a new distribution function

$$\zeta_N(\vec{R}_j,\vec{u}_j,\varphi_j,t) = r_1 \cdots r_N \int_0^{2\pi} \cdots \int_0^{2\pi} z_N \, d\theta_1 \cdots d\theta_N,$$

where $\vec{R}_j = (r_j,z_j)$ is the ordinary two-dimensional position vector.

This means, of course, that we are considering each particle only in terms of its r and z coordinates. As in the previous correspondence [I-2], we conclude that

$$0 = \frac{d}{dt} \int_V \zeta_N \, d\vec{R}_1 \cdots d\vec{R}_N \, d\vec{u}_1 \cdots d\vec{u}_N \, d\varphi_1 \cdots d\varphi_N$$

for a generalized volume V whose boundary is not crossed by particle trajectories. This leads to the Liouville equation

$$\frac{\partial \zeta_N}{\partial t} + \sum_{j=1}^{N} \left[\nabla_{\vec{R}_j} \cdot \left(\zeta_N \frac{d\vec{R}_j}{dt} \right) + \nabla_{\vec{u}_j} \cdot \left(\zeta_N \frac{d\vec{u}_j}{dt} \right) + \frac{\partial}{\partial \varphi_j} \left(\zeta_N \frac{d\varphi_j}{dt} \right) \right] = 0.$$

(B-1)

If $\omega_N = \dfrac{\zeta_N}{r_1 \cdots r_N}$, this means that

$$\frac{\partial \omega_N}{\partial t} + \sum_{j} \left[\nabla_{\vec{R}_j} \cdot \left(\omega_N \frac{d\vec{R}_j}{dt} \right) + \frac{\omega_N}{r_j} \frac{dr_j}{dt} + \nabla_{\vec{u}_j} \cdot \left(\omega_N \frac{d\vec{u}_j}{dt} \right) + \frac{\partial}{\partial \varphi_j} \left(\omega_N \frac{d\varphi_j}{dt} \right) \right] = 0.$$

(B-2)

Assuming that the particles are intrinsically identical (i.e., have no identifying property such as mass which they carry along in space), then the reduction shown on p. 13 of Ref. I-2 is valid and the result is

$$0 = \frac{\partial \omega_1}{\partial t} = \vec{u}_1 \cdot \nabla_{\vec{R}} \omega_1 + \frac{\omega_1}{r_1} \frac{dr_1}{dt}$$
$$+ \iiint \left\{ \nabla_{\vec{u}_1} \cdot \left(\frac{z_2}{m_1} \vec{F}_{21} \right) + \frac{\partial}{\partial \varphi_1} \left[\frac{\omega_2}{2 m T_1} [\vec{g}_{21} \cdot (\vec{u}_2 - \vec{u}_1) + \text{heat flux terms}] \right] \right\}$$

(B-3)

$$\times r_2 \, d\vec{R}_2 \, d\vec{u}_2 \, d\varphi_2.$$

As before, we assume that

$$z_2 = \rho(\vec{r}_2) \sigma(\vec{r}_2 - \vec{r}_1, \rho_{12}, \varphi_{12}) \, \delta(\vec{u}_2 - \vec{u}_1 - \vec{\alpha}_{12}) \, \delta(\varphi_2 - \varphi_1 - \beta_{12}) z_1 + z_2'.$$

Since $\partial z_1 / \partial \theta = 0$, this implies that $\omega_1 = 2\pi z_1$ and

$$\omega_2 = \frac{1}{r_1 r_2} \zeta_2 = \int_0^{2\pi} \int_0^{2\pi} z_2 \, d\theta_1 \, d\theta_2$$

$$= \rho(\vec{R}_2) \, \delta(\vec{u}_2 - \vec{u}_1 - \vec{\alpha}_{12}) \, \delta(\varphi_2 - \varphi_1 - \beta_{12}) \qquad \text{(B-4)}$$

$$\times \frac{\omega_1}{2\pi} \int_0^{2\pi} \int_0^{2\pi} \sigma(r_{12}, \vec{s}_{21}, \rho_{12}, \varphi_{12}) \, d\theta_1 \, d\theta_2 + \omega_2' \, .$$

Note that $\sigma(r_{12}, \rho_{12}, \varphi_{12})$ depends only on $\theta_2 - \theta_1$, since

$$r_{12}^2 = (z_2 - z_1)^2 + r_2^2 + r_1^2 - 2r_1 r_2 \cos(\theta_2 - \theta_1).$$

Since ρ_{12} and φ_{12} are independent of θ_1 and θ_2,

$$\int_0^{2\pi} \int_0^{2\pi} \sigma \, d\theta_1 \, d\theta_2 = \int_0^{2\pi} \left[\int_{-\theta_2}^{2\pi - \theta_2} \sigma(\theta_1 - \theta_2) \, d(\theta_1 - \theta_2) \right] d\theta_2$$

$$= 2\pi \int_0^{2\pi} \sigma(\theta) \, d(\theta) \equiv 2\pi\sigma',$$

so that

$$\omega_2 = \rho(\vec{R}_2) \, \delta(\vec{u}_2 - \vec{u}_1 - \vec{\alpha}_{12}) \, \delta(\varphi_2 - \varphi_1 - \beta_{12})\omega_1 \, \sigma'(\vec{R}_2 - \vec{R}_1, \rho_{12}, \varphi_{12}) + \omega_2' \, .$$

$$\text{(B-5)}$$

Substituting Eq. (B-5) into Eq. (B-3) and integrating with respect to $d\vec{u}_1 \, d\varphi_1$ gives

$$\frac{\rho}{r} \frac{dr}{dt} + \frac{\partial \rho}{\partial t} + \nabla_{\vec{R}} \cdot (\rho\vec{u}) = 0, \qquad \text{(B-6)}$$

where

$$\nabla_{\overrightarrow{R}} = \left(\frac{\partial}{\partial r}, \frac{\partial}{\partial z}\right) \cdot$$

This is just the equation of continuity in cylindrical coordinates.

In similar fashion, integration with respect to $\overrightarrow{u}\, d\overrightarrow{u}\, d\varphi$ and $\varphi\, d\overrightarrow{u}\, d\varphi$

yields the equations

$$\rho\, \frac{d\overrightarrow{\overline{u}}}{dt} + \rho(\overrightarrow{\overline{u}} \cdot \nabla_{\overrightarrow{R}})\overrightarrow{\overline{u}} = \rho\overrightarrow{P}, \qquad \text{(B-7)}$$

or

$$\frac{\partial}{\partial t}(\rho\overrightarrow{\overline{u}}) + \nabla_{\overrightarrow{R}} \cdot (\rho\overrightarrow{\overline{u}}\,\overrightarrow{\overline{u}}) + \rho\,\frac{\overline{u}_r}{r} = \rho\overrightarrow{P}$$

and

$$\frac{\partial\rho\overline{\varphi}}{\partial t} + \nabla_{\overrightarrow{R}} \cdot (\rho\overrightarrow{\overline{u}}\,\overline{\varphi}) + \rho\,\frac{\overline{\varphi}}{r}\,\overline{u}_r = \rho\overline{Q}, \qquad \text{(B-8)}$$

which are the expected momentum and entropy equations.

Note that one need not assume $R\, d\theta/dt = \overline{u}_\theta = 0$ in order to derive

these equations, as long as we have $(\partial/\partial\theta)\,\overline{u}_\theta = 0$.

The above is a straightforward adaptation of the previous theory.
We must now choose a form for the force function between two particles,
and then evaluate the expressions $\rho\overrightarrow{P}$ and $\rho\overline{Q}$.

In actual practice, the two-dimensional array of particles have
mass proportioned to their initial distance from the axis of symmetry.
For purposes of this correspondence, it seems much easier to assume that
all have the same mass (otherwise, the basic assumption that particles

are identical would be invalid). As noted above, if we assume that each particle is the representative of a ring of particles, a self-force must be taken into consideration. If one goes back to Eq. (B-3) and lets $\vec{F}_{21}$ contain a term $\vec{f}_{self}$ independent of particle 2, then it can be readily checked that the momentum equation will become

$$\frac{\partial(\rho\vec{u})}{\partial t} + \nabla\cdot(\rho\vec{u}\,\vec{u}) = \rho\vec{P} + \rho\vec{f}_{self}. \tag{B-9}$$

By symmetry this $\vec{f}_{self}$ is a radial force and will in general make it impossible to express the right-hand side of Eq. (B-9) as the gradient of a function.

In addition, this $\vec{f}_{self}$ is most reasonably expressed as an average over the hypothetical ring. In other words, if $\vec{f}_{21}$ is the usual force between particles, one expects the self-force to be something like

$$\frac{1}{2\pi} \int_{\substack{0 \\ r_2=r_1 \\ z_2=z_1}}^{2\pi} f_{21}\, d\theta_2,$$

and this may well diverge.

Therefore, we must discard the self-force concept. However, we wish to preserve the averaging technique. To do this, we appeal to cylindrical symmetry to argue that the averaging procedure is the best two-dimensional description of the actual three-dimensional force distribution. Hence, while each particle is not now regarded as the representative of a ring of particles, its θ coordinate is essentially arbitrary.

Therefore, we take as the force function between two particles in our two-dimensional array the quantity

$$\vec{f}_{21} \equiv \frac{1}{2\pi} \int_0^{2\pi} f(r_{12}, \varphi_{12}) \vec{s}_{21} \, d\theta_2$$

$$= - \left[\frac{1}{2\pi} \int_0^{2\pi} f(r_{12}, \varphi_{12}) \frac{1}{r_{12}} (r_2 \cos \theta_2 - r_1) \, d\theta \right] \hat{r}$$

$$- \left[\frac{1}{2\pi} \int_0^{2\pi} f(r_{12}, \varphi_{12}) \frac{1}{r_{12}} (z_2 - z_1) \, d\theta \right] \hat{z}$$

$$= f_{21,r} \, \hat{r} + f_{21,z} \, \hat{z},$$

where $f\vec{s}_{21}$ is the usual interparticle function between three-dimensional particles (for convenience, only nondissipative forces are discussed here — dissipative forces will be discussed below). Therefore,

$$(\rho \vec{P})_z = \frac{\rho}{m} \int\int \rho(\vec{R}_2) \sigma' \, f_{21,z} r_2 \, dr_2 \, dz_2, \qquad \text{(B-10)}$$

and

$$(\rho \vec{P})_r = \frac{\rho}{m} \int\int \rho(\vec{R}_2) \sigma' f_{21,r} r_2 \, dr_2 \, dz_2. \qquad \text{(B-11)}$$

One now makes the usual first order approximations and applies symmetry considerations to obtain

$$(\rho \vec{P})_z = - \frac{\partial}{\partial z} \left[\frac{\rho^2}{m} \int\int \sigma' f_{21,z} (z_2 - z_1) r_2 \, dr_2 \, dz_2 \right], \qquad \text{(B-12)}$$

$$(\rho \vec{P})_r = - \frac{\partial}{\partial r} \left[\frac{\rho^2}{m} \int\int \sigma' f_{21,r} (r_2 - r_1) r_2 \, dr_2 \, dz_2 \right]. \qquad \text{(B-13)}$$

This would be fine if the two quantities in brackets were in fact equal. The bracketed quantity in Eq. (B-12) can be expressed

$$\frac{\rho^2}{m} \int \sigma' \frac{f}{r_{12}} (z_2 - z_1)^2 \, d\tau,$$

where $d\tau = r_2 \, dr_2 \, dz_2 \, d\theta_2$ is the three-dimensional volume element. However its counterpart in Eq. (B-13) is

$$\frac{\rho^2}{m} \int \sigma' \frac{f}{r_{12}} (r_2 \cos \theta_2 - \theta_1)(r_2 - r_1) \, d\tau.$$

In general, these expressions will not be equal, since σ' can be a complicated expression in r_2 and z_2.

The problem is that we have lost a good deal of symmetry in these expressions by integrating σ and f separately over θ. Initially, σ is a cutoff function symmetric in all three directions, which allows one to make general first-order expansions. However, σ' is a nonsymmetric cutoff function in two directions which allows one to make first-order expansions only in r and z.

Hence, this simple averaging technique for interparticle forces is not valid either. Instead we must take a weighted average in order to introduce symmetry into the appropriate integrals. Therefore, we now define

$$\vec{f}_{21} = \frac{1}{\int_0^{2\pi} \sigma \, d\theta_2} \int_0^{2\pi} \sigma f(r_{12}, \varphi_{12}) \vec{s}_{21} \, d\theta_2$$

so that Eqs. (B-10) and (B-11) are replaced by

$$(\vec{P})_r = \frac{\rho}{m} \int \int \rho(\vec{r}_2) \sigma' f_{21,r} r_2 \, dr_2 \, dz_2,$$

$$= -\frac{\rho}{m} \int \rho(\vec{r}_2) \sigma \frac{f}{r_{12}} (r_2 \cos \theta_2 - r_1) \, d\tau,$$

and

$$(\vec{P})_z = -\frac{\rho}{m} \int \rho(\vec{r}_2) \frac{f}{r_{12}} (z_2 - z_1) \sigma \, d\tau.$$

Now we can make three-dimensional expansions, using the fact that σ is a symmetric cutoff function, and the result will be

$$(\vec{P})_r = -\frac{\partial}{\partial r} \left[\frac{\rho^2}{m} \int \frac{f}{r_{12}} (r_2 \cos \theta_2 - r_1)^2 \, d\tau \right], \qquad \text{(B-14)}$$

$$(\vec{P})_z = -\frac{\partial}{\partial z} \left[\frac{\rho^2}{m} \int \frac{f}{r_{12}} (z_2 - z_1)^2 \, d\tau \right], \qquad \text{(B-15)}$$

which are equal by symmetry. Hence we make the association

$$p = -\frac{\rho^2}{m} \int \frac{f}{r_{12}} (z_2 - z_1)^2 \, d\tau,$$

where p is the pressure. Exactly the same symmetry considerations enter with regard to dissipative forces. If $\vec{g}_{21}$ is the usual dissipative force between three-dimensional particles, one takes as the dissipative force between particles in the two-dimensional array

$$\vec{g}_{21}' = \frac{1}{\int_0^{2\pi} \sigma \, d\theta_2} \int_0^{2\pi} \sigma \vec{g}_{21} \, d\theta_2,$$

and the resulting integrals $\rho\vec{\vec{P}}$ and $\rho\vec{Q}$ will be analogous to those evaluated in the previous correspondence theory and in Appendixes C and D. Hence, one will get derivatives of a quantity interpreted as the stress tensor in $\rho\vec{\vec{P}}$ and the heat conduction term $\nabla\cdot(\kappa\vec{\nabla T})$ in $\rho\vec{Q}$.

To conclude, it has been shown that correspondence can be achieved for problems with cylindrical symmetry when all masses are assumed equal. Attempts were made to relate this approach to that actually used in calculations by coalescing particles in order to approximate a distribution with mass proportional to distance from the axis of symmetry. Thus far, such attempts have not been successful.

APPENDIX C

VISCOUS CORRESPONDENCE FOR PAF

As on p. 20 of Ref. I-2, we wish to find a formula for dissipative forces between PAF particles for which angular integration gives us a term to be associated with the derivative $\partial\sigma_{ik}/\partial x_k$ of a stress tensor

$$\sigma_{ik} = \eta\left(\frac{\partial u_i}{\partial x_k} + \frac{\partial u_k}{\partial x_i} - \frac{2}{3}\delta_{ik}\frac{\partial u_\ell}{\partial x_\ell}\right) + \zeta\,\delta_{ik}\frac{\partial u_\ell}{\partial x_\ell}\,.$$

If $\rho(\vec{r})$ is constant in space, then Eq. (24) of Ref. I-2 is in such a form. However, in general, there is no reason for ρ to be constant; in fact, in almost all problems studied, it can vary considerably. Therefore, it is necessary to look for new terms to put in Eq. (22), Ref. I-2.

Actually, several terms were omitted in the derivation of Eq. (24) of Ref. I-2, and, before looking for new forces, we will discover the correct expression for the forces used in Eq. (22)

The expression

$$\int \rho(\vec{r}_2)\sigma(\rho_{12},r_{12})\vec{g}_{21}(r_{12},\vec{s}_{12},\vec{\varphi}+\tfrac{1}{2}\beta_{12},\vec{\alpha}_{12})\,d\vec{r}_2$$

can be expanded to

$$\int \left[\rho(\vec{r}_1) + (\vec{r}_2 - \vec{r}_1) \cdot \vec{\nabla}_\rho \right] \left\{ \sigma[\rho(\vec{r}_1), r_{12}] + \frac{\partial \sigma}{\partial \rho} (\vec{r}_2 - \vec{r}_1) \cdot \vec{\nabla}_\rho \right\}$$

$$\left[(\vec{\alpha}_{12} \cdot \vec{\nabla}_{\vec{\alpha}_{12}}) \vec{g}_{21}(r_{12}, \vec{s}_{12}, \bar{\varphi}, 0) + \frac{\beta_{12}}{2} \frac{\partial}{\partial \varphi} (\vec{\alpha}_{12} \cdot \vec{\nabla}_{\vec{\alpha}_{12}}) \vec{g}_{21}(r_{12}, \vec{s}_{12}, \bar{\varphi}, 0) \right.$$

$$\left. + \frac{1}{2}(\vec{\alpha}_{12} \cdot \vec{\nabla}_{\vec{\alpha}_{12}})^2 \, \vec{g}_{21}(r_{12}, \vec{s}_{21}, \bar{\varphi}, 0) \right] d\vec{r}_2,$$

where use has been made of the fact that $\vec{g}$ and $\partial\vec{g}/\partial\varphi$ are expected to vanish for $\alpha = 0$. We have also assumed that σ was independent of φ. Removal of this assumption changes none of the results presented here, but merely adds complication.

If α is expanded to second order, we get one first-order term and five second-order terms. In the event that $\vec{g}$ is linear in α [so that the term in $(\vec{\alpha} \cdot \nabla)^2 \, \vec{g}$ vanishes] and that the first-order term vanishes, there will be four second-order terms to account for rather than one, as is shown on p. 20 of Ref. I-2.

With $\vec{g} = A(r_{12}, \varphi_{12})\vec{\alpha}_{21} + B(r_{12}, \varphi_{12})\vec{s}_{21}(\vec{s}_{21} \cdot \vec{\alpha}_{21})$, the first-order term does indeed vanish and $(\vec{\alpha} \cdot \nabla_{\vec{\alpha}})\vec{g} = \vec{g}$.

First consider $A(r_{12}, \varphi_{12})\vec{\alpha}_{21}$. With

$$\vec{\alpha}_{21} = [(\vec{r}_2 - \vec{r}_1) \cdot \nabla]\vec{u} + \frac{1}{2}[(\vec{r}_2 - \vec{r}_1) \cdot \nabla]^2 \vec{u},$$

the following are all second-order terms:

(1) $\quad \rho \int \sigma A(r_{12}, \bar{\varphi}) \, \frac{1}{2} \, [(\vec{r}_2 - \vec{r}_1) \cdot \nabla]^2 \, \vec{u} \, d\vec{r}$

$$= \frac{1}{2} \, \rho \int \sigma A x_j x_k \, \frac{\partial^2 \bar{u}_i}{\partial x_j \partial x_k} \, d\vec{r}$$

$$= \frac{\rho}{2} \int \sigma A r^2 x_k^2 \, \frac{\partial^2 \bar{u}_i}{\partial x_k^2} \, \sin \theta \, dr \, d\theta \, d\varphi$$

$$= \frac{2\pi\rho}{3} \left(\int_0^\infty \sigma A r^4 \, dr \right) \frac{\partial^2 \bar{u}_i}{\partial x_k^2} \, .$$

[Here, as in the following, i denotes the vector index (no summation) and sums are always taken over indexes j, k, ℓ, m, etc., whenever repeated. x_j means $(\vec{r}_2 - \vec{r}_1)_j$, and all derivatives of $\vec{u}$ are at $\vec{r}_1$.]

(2) $\quad \frac{1}{2} \int \rho A \, \frac{\partial \sigma}{\partial \rho} \, (\vec{r}_2 - \vec{r}_1) \cdot \vec{\nabla}_r \rho [(\vec{r}_2 - \vec{r}_1) \cdot \nabla] \bar{\vec{u}}$

$$= \frac{\rho}{2} \int A \, \frac{\partial \sigma}{\partial \rho} \, x_j \, \frac{\partial \rho}{\partial x_j} \, x_k \, \frac{\partial \bar{u}_i}{\partial x_k}$$

$$= \frac{\rho}{2} \int A \, \frac{\partial \sigma}{\partial \rho} \, x_k^2 \, \frac{\partial \rho}{\partial x_k} \, \frac{\partial \bar{u}_i}{\partial x_k}$$

$$= \frac{2\pi\rho}{3} \left(\int_0^\infty A \, \frac{\partial \sigma}{\partial \rho} \, r^4 \, dr \right) \frac{\partial \rho}{\partial x_k} \, \frac{\partial \bar{u}_i}{\partial x_k} \, .$$

(3) $\quad \int \sigma A (\vec{r}_2 - \vec{r}_1) \cdot \vec{\nabla}_r \, \rho [(\vec{r}_2 - \vec{r}_1) \cdot \nabla_r] \bar{\vec{u}}$

$$= \frac{4\pi}{3} \left(\int_0^\infty \sigma A r^4 \right) \frac{\partial \rho}{\partial x_k} \, \frac{\partial \bar{u}_i}{\partial x_k} \, .$$

(4)
$$\frac{\rho}{2} \int \sigma \frac{\partial A}{\partial \varphi} (\vec{r}_2 - \vec{r}_1) \cdot \nabla_r \vec{\varphi} \, [(\vec{r}_2 - \vec{r}_1) \cdot \nabla_r] \vec{\bar{u}}$$

$$= \frac{2\pi\rho}{3} \left(\int_0^\infty \sigma \frac{\partial A}{\partial \varphi} r^4 \, dr \right) \frac{\partial \bar{\varphi}}{\partial x_k} \frac{\partial \bar{u}_i}{\partial x_k} .$$

Hence, using these terms in the expression for $\rho \vec{P}$ gives

$$\frac{\partial}{\partial x_k} \left(\rho^2 \, \nu \, \frac{\partial u_i}{\partial x_k} \right)$$

with

$$\nu = \frac{2\pi}{3} \int_0^\infty A\sigma r^4 \, dr,$$

which is not of the desired form.

Next consider the term

$$B(r_{12}, \varphi_{12}) \vec{s}_{21} (\vec{\alpha}_{21} \cdot \vec{s}_{21}).$$

Again there are four second-order terms, and the final result is

$$\rho^2 \mu \frac{\partial}{\partial x_k} \left(\frac{\partial \bar{u}_i}{\partial x_k} + \frac{\partial \bar{u}_k}{\partial x_j} + \delta_{ik} \frac{\partial \bar{u}_\ell}{\partial x_\ell} \right)$$

$$+ 2\rho \frac{\partial \rho}{\partial x_k} \mu \left(\frac{\partial \bar{u}_i}{\partial x_k} + \frac{\partial \bar{u}_k}{\partial x_i} + \delta_{ik} \frac{\partial u_\ell}{\partial x_\ell} \right)$$

$$+ \rho^2 \frac{\partial \mu}{\partial x_k} \left(\frac{\partial \bar{u}_j}{\partial x_k} + \frac{\partial \bar{u}_k}{\partial x_i} + \delta_{ik} \frac{\partial u_\ell}{\partial x_\ell} \right)$$

$$= \frac{\partial}{\partial x_k} \left[\rho^2 \mu \left(\frac{\partial \bar{u}_i}{\partial x_k} + \frac{\partial \bar{u}_k}{\partial x_i} + \delta_{ik} \frac{\partial \bar{u}_\ell}{\partial x_\ell} \right) \right],$$

where

$$\mu = \frac{2\pi}{15m} \left(\int_0^\infty \sigma B r^4 \, dr \right).$$

Since this means only one of the independent coefficients η, ζ has been determined, the problem is to find another expression to be added to $\vec{g}$ whose integral can also be associated with the derivative of a stress tensor. We hoped to find another expression linear in $\vec{\alpha}$; however, none was found to be suitable.

Hence, attention was turned to other expressions in the values $\vec{\vec{u}}(\vec{r}_1)$. We first observe that

$$\frac{1}{2} [(\nabla \cdot \vec{\vec{u}})(\vec{r}_1) + (\nabla \cdot \vec{\vec{u}})(\vec{r}_2)] = (\nabla \cdot \vec{\vec{u}}) \left(\frac{\vec{r}_1 + \vec{r}_2}{2} \right)$$

$$= (\nabla \cdot \vec{\vec{u}})(\vec{r}_1) + \frac{1}{2} [(\vec{r}_2 - \vec{r}_1) \cdot \nabla](\nabla \cdot \vec{\vec{u}})(\vec{r}_1)$$

to first order. If we suppose that

$$H(r_{12}, \varphi_{12}) \ (\nabla \cdot \vec{\vec{u}}) \left(\frac{\vec{r}_1 + \vec{r}_2}{2} \right)$$

were part of the $\vec{g}_{21}$ force, then it can be checked that the usual integration and multiplication would yield an additional term

$$\frac{\partial}{\partial x_k} \left(\rho^2 v_1 \delta_{ik} \frac{\partial \bar{u}_l}{\partial x_l} \right),$$

with

$$v_1 \frac{2\pi}{3m} \left(\int_0^\infty x^4 \sigma H \, dx \right).$$

Similarly, the term

$$G(r_{12}, \varphi_{12}) \left\{ \frac{\partial \vec{u}}{\partial x_i} \left(\frac{\vec{r}_1 + \vec{r}_2}{2} \right) \cdot (\vec{r}_2 - \vec{r}_1) \hat{i} + [(\vec{r}_2 - \vec{r}_1) \cdot \nabla] \vec{u} \left(\frac{\vec{r}_1 + \vec{r}_2}{2} \right) \right\}$$

$$= G(r_{12}, \varphi_{12}) \left(\left\{ \frac{\partial \vec{u}}{\partial x_i} (\vec{r}_1) \hat{i} + \left[\frac{1}{2} (\vec{r}_2 - \vec{r}_1) \cdot \nabla \right] \frac{\partial \vec{u}}{\partial x_i} (r_1) \right\} \cdot (\vec{r}_2 - \vec{r}_1) \hat{i} + \vec{\alpha}_{12} \right)$$

yields the expression

$$\frac{\partial}{\partial x_k} \left[\rho^2 \nu_2 \left(\frac{\partial \bar{u}_i}{\partial x_k} + \frac{\partial \bar{u}_k}{\partial x_i} \right) \right],$$

where

$$\nu_2 = \frac{2\pi}{3m} \left(\int_0^\infty \sigma G x^4 \, dx \right).$$

We note that both of these terms are of the desired form, and if $\vec{g}$ were equal to their sum, we would have

$$\left(\rho \vec{P} \right)_i = \frac{\partial}{\partial x_k} \left[\rho^2 \nu_2 \left(\frac{\partial \bar{u}_i}{\partial x_k} + \frac{\partial \bar{u}_k}{\partial k_i} \right) + \rho^2 \nu_1 \, \delta_{ik} \frac{\partial \bar{u}_\ell}{\partial x_\ell} \right]$$

as desired.

However, neither $(\nabla \cdot \vec{u}) \left(\frac{\vec{r}_1 + \vec{r}_2}{2} \right)$ nor $\frac{\partial u_j}{\partial x_i} \left(\frac{\vec{r}_1 + \vec{r}_2}{2} \right)$ can (in general) be approximated to first order by the values $\vec{u}(r_i)$.

Hence, we abandon the restriction that dissipative forces be of a two-particle nature and look for analogous expressions involving a particle and its neighbors, in the hopes that these more general expressions can be approximated by $\vec{u}(r_i)$.

The natural candidates are, of course, expressions in

$$(\nabla \cdot \vec{u}) \left(\frac{\vec{r}_1 + \ldots + \vec{r}_{N^*+1}}{N^* + 1} \right)$$

(where $\vec{r}_2 \ldots \vec{r}_{N^*+1}$ are the positions of the N^* neighbors of $\vec{r}_1$) and

$$\frac{\partial \bar{u}_j}{\partial x_i} \left(\frac{\vec{r}_1 + \ldots + \vec{r}_{N^*+1}}{N^* + 1} \right) .$$

In both cases, we are interested to see if derivatives of the vector field $\vec{\bar{u}}$ at the midpoint of $N^* + 1$ particles can be approximated by the values $\vec{\bar{u}}(\vec{r}_i)$ to first order.

We first observe that approximations of the form

$$\vec{\bar{u}}(\vec{r}_i) + \vec{\bar{u}}(\vec{r}_j) = 2\vec{\bar{u}} \left(\frac{\vec{r}_i + \vec{r}_j}{2} \right)$$

are only good to first order. Hence, the natural procedure of using such estimates for $\vec{\bar{u}}$ at hypothetical middle points is not valid, since the result can only be a zeroth-order approximation for a derivative. However, the approximation

$$\vec{\bar{u}}(\vec{r}_i) - \vec{\bar{u}}(\vec{r}_j) = \left[(\vec{r}_i - \vec{r}_j) \cdot \nabla \right] \vec{\bar{u}} \left(\frac{\vec{r}_i + \vec{r}_j}{2} \right)$$

is good to first order in the derivative, so we can assume that such directional derivatives at the midpoint of any line segment are known. Also to first order in derivatives of $\vec{\bar{u}}$ we can approximate

$$\frac{\partial \vec{\bar{u}}}{\partial x_k} \left(\frac{\vec{r}_1 + \vec{r}_2 + \vec{r}_3}{3} \right) = \frac{1}{3} \left[\frac{\partial \vec{\bar{u}}}{\partial x_k} \left(\frac{\vec{r}_1 + \vec{r}_2}{3} \right) + \frac{\partial \vec{\bar{u}}}{\partial x_k} \left(\frac{\vec{r}_1 + \vec{r}_3}{2} \right) + \frac{\partial \vec{\bar{u}}}{\partial x_k} \left(\frac{\vec{r}_2 + \vec{r}_3}{2} \right), \text{etc.} \right];$$

therefore, if we can find equations giving us the quantities

$$\frac{\partial \vec{\bar{u}}}{\partial x_k} \left(\frac{\vec{r}_1 + \vec{r}_j}{2} \right)$$

from the known directional derivatives at the points $\dfrac{\vec{r}_i + \vec{r}_j}{2}$, then we will indeed be able to approximate derivatives at the midpoint. In one dimension this is trivial, since all derivatives are in the same direction.

In two dimensions, first consider four particles at $\vec{r}_1$, $\vec{r}_2$, $\vec{r}_3$, and $\vec{r}_4$. Unknown are the 12 quantities:

$$\frac{\partial \vec{u}}{\partial x}\left(\frac{\vec{r}_i + \vec{r}_j}{2}\right) \equiv \vec{x}_{ij}$$

and

$$\frac{\partial \vec{u}}{\partial y}\left(\frac{\vec{r}_i + \vec{r}_j}{2}\right) \equiv \vec{y}_{ij}$$

for $i, j = 1, \cdots, 4$; $i < j$. If we denote

$$\vec{u}(\vec{r}_i) - \vec{u}(\vec{r}_j) \text{ by } \vec{c}_{ij} \ (= -\vec{c}_{ji}),$$

$$(\vec{r}_i - \vec{r}_j)_x \text{ by } a_{ij},$$

and

$$(\vec{r}_i - \vec{r}_j)_y \text{ by } b_{ij},$$

then we have the six equations

$$\vec{c}_{ij} = a_{ij}\vec{x}_{ij} + b_{ij}\vec{y}_{ij}.$$

Also both $\vec{x}_{ij}$ and $\vec{y}_{ij}$ satisfy the equations

$$\vec{z}_{12} + \vec{z}_{34} = \vec{z}_{14} + \vec{z}_{23},$$

and

$$\vec{z}_{12} + \vec{z}_{34} = \vec{z}_{13} + \vec{z}_{24}.$$

But this seems to exhaust our knowledge of the system and we have only 10 equations in 12 unknowns, so of course there is in general no solution.

We now go on to five particles in two dimensions, using the same notation as above. It can be checked that both $\vec{x}_{ij}$ and $\vec{y}_{ij}$ must satisfy the five independent equations

$$\vec{z}_{12} + \vec{z}_{34} = \vec{z}_{13} + \vec{z}_{24}$$
$$= \vec{z}_{14} + \vec{z}_{23},$$
$$\vec{z}_{15} + \vec{z}_{23} = \vec{z}_{15} + \vec{z}_{13}$$
$$= \vec{z}_{12} + \vec{z}_{35},$$

and

$$\vec{z}_{13} + \vec{z}_{45} = \vec{z}_{15} + \vec{z}_{34}.$$

These 10 equations together with the 10 equations

$$\vec{c}_{ij} = a_{ij}\vec{x}_{ij} + b_{ij}\vec{y}_{ij}$$

allow one to solve for the 20 unknowns $\vec{x}_{ij}$ and $\vec{y}_{ij}$ and thus to obtain the desired derivatives. This system of equations can be easily simplified to the problem of inverting a 5×5 matrix, but beyond this point further simplification seems difficult.

The analysis is quite similar in three dimensions. Here we write

$$\vec{u}(r_i) - \vec{u}(r_j) = (\vec{r_i} - \vec{r_j})_x \frac{\partial \vec{u}}{\partial x}\left(\frac{\vec{r_i} + \vec{r_j}}{2}\right) + (\vec{r_i} - \vec{r_j})_y \frac{\partial \vec{u}}{\partial y}\left(\frac{\vec{r_i} + \vec{r_j}}{2}\right)$$

$$+ (\vec{r_i} - \vec{r_j})_z \frac{\partial \vec{u}}{\partial z}\left(\frac{\vec{r_i} + \vec{r_j}}{2}\right),$$

or

$$\vec{K}_{ij} = a_{ij}\vec{x}_{ij} + b_{ij}\vec{y}_{ij} + c_{ij}\vec{z}_{ij}.$$

As with four particles in two dimensions, the use of six (or fewer) particles in three dimensions does not provide enough information for a general solution. However, with seven particles, the $\vec{x}_{ij}$, $\vec{y}_{ij}$, and $\vec{z}_{ij}$ must all satisfy 14 independent equations of the type

$$\vec{w}_{12} + \vec{w}_{34} = \vec{w}_{13} + \vec{w}_{24}$$
$$= \vec{w}_{14} + \vec{w}_{23}.$$

This gives 42 equations which, together with the 21 equations $\vec{K}_{ij} = a_{ij}\vec{x}_{ij} + b_{ij}\vec{y}_{ij} + c_{ij}\vec{z}_{ij}$, give 63 equations in the 63 unknowns. Solution of this system of equations can easily be reduced to the problem of inverting a 21 × 21 matrix, but further reduction seems difficult. Hence, in principle, one may always approximate (to first order) derivations of a vector field at the midpoint of $N^* + 1$ particles only from knowledge of the field itself at these points as long as $N^* \geq 2n$ (n is the dimension under consideration).

In practice, one would never invert such complicated matrixes as those above, but just use n sets of two particles whose midpoint was nearest the general midpoint, approximate directional derivatives at the general midpoint by directional derivatives at such two-particle midpoints. and use the resulting n × n matrixes to calculate the fixed derivatives.

We must now show that the generalized $\vec{g}$ force above can indeed be fitted into a correspondence between fluid dynamics and PAF. We retreat to the generalized Liouville equation on p. 12 of Ref. I-2

$$\frac{\partial z_N}{\partial t} - \sum_{j=1}^{N} \nabla_{\vec{r}_j} \cdot \left(z_N \frac{d\vec{r}_j}{dt} \right) + \nabla_{\vec{u}_j} \cdot \left(z_N \frac{d\vec{u}_j}{dt} \right) + \frac{\partial}{\partial\varphi_j} \left(z_N \frac{d\varphi_j}{dt} \right) = 0,$$

where now

$$\frac{d\vec{u}_j}{dt} = \frac{1}{m} \left(\sum_i^* f_{ij} \vec{s}_{ij} + \vec{g}_j \right),$$

where $\vec{g}_j$ depends also on the N^* neighbors of the j particle, but has no simple resolution into two-particle form. Integration as on p. 13 of Ref. I-2 gives

$$\frac{dz_1}{dt} + \vec{u}_1 \cdot \nabla_{\vec{r}_1} z_1 + \int d\vec{r}_2 \, d\vec{u}_2 \, d\varphi_2 \, \nabla_{\vec{u}} \cdot \left[\frac{z_2}{m} (\vec{s}_{21} f_{21}) \right]$$

$$+ \nabla_{\vec{u}_1} \cdot \left[\int d\vec{r}_2 \cdots d\vec{r}_{N^*+1} \, d\vec{u}_2 \cdots d\vec{u}_{N^*+1} \, d\varphi_2 \cdots d\varphi_{N^*+1} \, \frac{z_{N^*+1}}{m} \vec{g}_1 \right]$$

$$+ \frac{1}{(N-1)!} \frac{\partial}{\partial\varphi_1} \int z_N \frac{d\varphi_1}{dt} \, d\vec{r}_2 \cdots d\varphi_N = 0.$$

The first three expressions are unchanged and the last is irrelevant for the present discussion, so it is only the fourth term with which we concern ourselves, i.e., we must suggest a form for z_{N^*+1} which upon insertion of mean values for $\vec{u}$ and φ allows us to perform angular interactions on the term in brackets.

We have only to prescribe a form for z_{N^*+1} in the region where $\vec{g}_1$ is nonzero and, in fact, we assume

$$z_{N^*+1}\left(\vec{r}_1,\cdots,\vec{r}_{N^*+1},\vec{u}_1,\cdots,\vec{u}_{N^*+1},\varphi_1,\cdots,\varphi_{N^*+1},t\right)$$

$$= z_1\sigma\left[\frac{\rho_1+\cdots+\rho_{N^*+1}}{N^*+1},\ \frac{\varphi_1+\cdots+\varphi_{N^*+1}}{N^*+1},\ r_{12},\cdots,r_{1(N^*+1)}\right]$$

$$\times\ \rho(\vec{r}_2,T)\cdots\rho(\vec{r}_{N^*+1},t)\prod_{k=2}^{N^*+1}\delta\left\{\vec{u}_k-[\vec{u}_1+(\vec{r}_k-\vec{r}_1\cdot\nabla)\vec{u}_1]\right\}$$

$$\times\ \delta[\varphi_k-(\varphi_1+\vec{r}_k-\vec{r}_1\cdot\nabla\varphi_1)]$$

in this region. As before

$$z_1 = \rho\delta(\vec{u}-\bar{\vec{u}})\ \delta(\varphi-\bar{\varphi}).$$

If $\vec{P}'$ is the term in brackets above, this means that

$$\vec{P}' = \frac{1}{m}\int d\vec{r}_2\cdots d\vec{r}_{N^*+1}\prod_{k=2}^{N^*+1}\rho(\vec{r}_k)\sigma\left[\frac{\rho_1+\cdots+\rho_{N^*+1}}{N^*+1},\varphi\right.$$

$$\left.+\frac{1}{N^*+1}\sum_{k=2}^{N^*+1}(\vec{r}_k-\vec{r}_1)\cdot\nabla\varphi,r_{12},\cdots,r_{1(N^*+1)}\right]\vec{g}_1.$$

With the usual first-order expansions for ρ, σ, and $\vec{g}_1$, where

$$\vec{g}_1 = G\left[r_{12},\cdots,r_{1(N^*+1)},\frac{\varphi_1+\cdots+\varphi_{N^*+1}}{N^*+1}\right]\nabla\cdot\vec{u}\left(\frac{r_1+\cdots+r_{N^*+1}}{N^*+1}\right)\sum_{k=2}^{N^*+1}\vec{r}_k-\vec{r}_1$$

$$+\ H\left[r_{12},\cdots,r_{1(N^*+1)},\frac{\varphi_1+\cdots+\varphi_{N^*+1}}{N^*+1}\right]\frac{\partial\vec{u}}{\partial x_1}\left(\frac{r_1+\cdots+r_{N^*+1}}{N^*+1}\right)\cdot\sum_{k=2}^{N^*+1}\vec{r}_k-\vec{r}_1$$

$$+\ \left[\sum_{k=2}^{N^*+1}(\vec{r}_k-\vec{r}_1)\cdot\nabla\right]\vec{u}\left(\frac{r_1+\cdots+r_{N^*+1}}{N^*+1}\right),$$

it is straightforward that

$$\rho\vec{P}' = \frac{\partial}{\partial x_k}\left[\rho^{N^*+1}\eta\left(\frac{\partial u_k}{\partial k_i} + \frac{\partial u_i}{\partial k_k}\right) + \rho^{N^*+1}\zeta\,\delta_{ik}\,\frac{\partial u_j}{\partial x_j}\right],$$

where

$$\eta = \frac{1}{3m}\,\frac{N^*}{N^*+1}\,(4\pi)^{N^*}\left[\int_0^\infty \cdots \int_0^\infty \sigma H r_{12}^2\, dr_{12}\cdots dr_{1(N^*+1)}\right],$$

and

$$\zeta = \frac{1}{3m}\,\frac{N^*}{N^*+1}\,(4\pi)^{N^*}\left[\int_0^\infty \cdots \int_0^\infty \sigma G r_{12}^2\, dr_{12}\cdots dr_{1(N^*+1)}\right].$$

This is an expression of the form we were looking for.

APPENDIX D

HEAT TRANSFER TERMS IN THE PAF MODEL

It is desired that heat conduction be incorporated into the PAF model. This is done by allowing for heat flux as well as work flux terms in Eq. (4) of Ref. I-2. Here we now write

$$\frac{dJ_j}{dt} = -\frac{1}{2} \sum_i^* f_{ij} \frac{dr_{ij}}{dt} + \frac{1}{2} \sum_i^* \vec{g}_{ij} \cdot (\vec{u}_i - \vec{u}_j) + \sum_i^* H(J_i, J_j),$$

where H will be specified later. Among other requirements H must, of course, satisfy $H(J_i, J_j) = -H(J_j, J_i)$, so it is indeed a flux between particles.

In the previous discussion, the variable φ has usually been left unspecified. We now identify φ with internal energy. Therefore, the last expression in Eq. (6), Ref. I-2, becomes

$$\frac{\partial}{\partial J_1} \left\{ z_2 \left[-\frac{1}{2} f_{21} \frac{dr_{21}}{dt} + \vec{g}_{21} \cdot (\vec{u}_2 - \vec{u}_1) + H(J_2, J_1) \right] \right\}$$

and so instead of Eq. (15), Ref. I-2, we write

$$Q = \frac{1}{2} \int d\vec{r}_2 \, d\vec{u}_2 \, dJ_2 \left[f_{21} \vec{s}_{21} \cdot (\vec{u}_2 - \vec{u}_1) + \vec{g}_{21} \cdot (\vec{u}_2 - \vec{u}_1) + H(J_2, J_1) \right] \rho\sigma$$

$$\times \, \delta(\vec{u}_2 - \vec{u}_1 - \vec{\alpha}_{12}) \, \delta(J_2 - J_1 - \beta_{12}),$$

or

$$\bar{Q} = \frac{1}{2} \int d\vec{r}_2 \rho\sigma \left[f(r_{12}, \bar{J} + \frac{1}{2}\beta_{12}) \vec{s}_{21} \cdot \vec{\alpha}_{12} + \vec{g}(r_{12}, \vec{s}_{21}, \bar{J} + \frac{1}{2}\beta_{12}, \vec{\alpha}_{12}) \cdot \vec{\alpha}_{12} \right.$$

$$\left. + H(\bar{J} + \beta_{12}, \bar{J}) \right],$$

where

$$\vec{\alpha}_{12} = \left[\left(\vec{r}_2 - \vec{r}_1 \right) \cdot \nabla \right] \vec{u} + \frac{1}{2} \left[\left(\vec{r}_2 - \vec{r}_1 \right) \cdot \nabla \right]^2 \vec{u},$$

and

$$\beta_{12} = \left(\vec{r}_2 - \vec{r}_1 \right) \cdot \nabla \vec{J}.$$

We make the usual first-order expansions and observe that the term

$$\frac{1}{2} \int d\vec{r}_2 \, \rho\sigma f \vec{s}_{21} \cdot \vec{\alpha}_{12} \quad \text{becomes}$$

$$\frac{-2\pi\rho}{3} \left(\int_0^\infty r^3 \sigma f \right) \frac{\partial \bar{u}_k}{\partial x_k} .$$

For the $\vec{g} \cdot \vec{\alpha}$ term we calculate separately for all the expressions considered as candidates for $\vec{g}_{21}$:

(1) $A(r_{12}, \bar{\varphi} + \frac{1}{2}\beta_{12}) \vec{\alpha}_{12}$ gives $\frac{2\pi\rho}{3} \left(\int_0^\infty \sigma A r^4 \, dr \right)^2 \left(\frac{\partial \bar{u}_k}{\partial x_j} \right)^2 .$

-127-

(2) $B(r_{12}, \bar{\varphi} + \frac{1}{2} \beta_{12})(\vec{s}_{21} \cdot \vec{\alpha}_{12})\vec{s}_{21}$ gives

$$\frac{2\pi\rho}{15}\left(\int_0^\infty B_r^4 \sigma \, dr\right)\left[\frac{\partial \bar{u}_k}{\partial x_j}\left(\frac{\partial \bar{u}_k}{\partial x_j} + \frac{\partial \bar{u}_j}{\partial x_k} + \delta_{jk}\frac{\partial \bar{u}_\ell}{\partial x_\ell}\right)\right].$$

(3) $C(r_{12}, \bar{\varphi} + \frac{1}{2}\beta_{12}) \, \nabla \cdot \vec{u}\left(\frac{\vec{r}_1 + \vec{r}_2}{2}\right)\left(\vec{r}_2 - \vec{r}_1\right)$ gives

$$\frac{2\pi\rho}{3}\left(\int_0^\infty C\sigma r^4 \, dr\right)\frac{\partial \bar{u}_j}{\partial x_j}\frac{\partial \bar{u}_k}{\partial x_k} = \frac{2\pi\rho}{3}\left(\int_0^\infty C\sigma r^4 \, dr\right)\frac{\partial \bar{u}_k}{\partial x_j}\left(\delta_{jk}\frac{\partial \bar{u}_\ell}{\partial x_\ell}\right).$$

(4) $D(r_{12}, \bar{\varphi} + \frac{1}{2}\beta_{12})\left\{(\vec{r}_2 - \vec{r}_1)\cdot\frac{\partial \vec{u}}{\partial x_i}\hat{i} + \left[(\vec{r}_2 - \vec{r}_1)\cdot\nabla\right]\vec{u}\right\}$ gives

$$\frac{2\pi\rho}{3}\left(\int_0^\infty d\sigma r^4 \, dr\right)\frac{\partial \bar{u}_k}{\partial x_j}\left(\frac{\partial \bar{u}_k}{\partial x_j} + \frac{\partial \bar{u}_j}{\partial x_k}\right).$$

(5) Similar results would hold if the generalized $\vec{g}$ force, with terms in

$$\nabla \cdot \vec{u}\left(\frac{\vec{r}_1 + \cdots + \vec{r}_{N^*+1}}{N^* + 1}\right),$$

were used, since the calculations are analogous.

Hence, if we use a combination of these forces for $\vec{g}_{21}$ such that

$$(\rho\vec{P})_i = -(\nabla p_i) + \frac{\partial}{\partial x_k}\sigma_{ik},$$

then what we have here is just the expression

$$-\frac{m}{\rho}p\frac{\partial u_k}{\partial x_k} + \frac{\partial u_k}{\partial x_j}\sigma_{jk}.$$

From p. 123, Eq. (14) of Ref. I-11,

$$\rho \frac{dI}{dt} = p_{ij} \frac{\partial u_j}{\partial x_j} + \frac{\partial}{\partial x_j} \left(\kappa \frac{\partial T}{\partial x_j} \right) ,$$

where I is specific internal energy. From Eq. (19) of Ref. I-2,

$$\frac{\partial \rho \overline{J}}{\partial t} + \nabla \cdot (\overrightarrow{\rho u} \overline{J}) = \rho \frac{d \overline{J}}{dt} = \rho \overline{Q} = m p_{ij} \frac{\partial \overline{u}_i}{\partial x_j} + \int dr_2 \, \rho \sigma H(\overline{J} + \beta_{12}, \overline{J}),$$

since

$$p_{ij} = -p \, \delta_{ij} + \sigma_{ij}.$$

Therefore, as J = mI, we can associate the expression

$$\frac{\rho}{m} \int dr_2 \, \rho \sigma H$$

with

$$\frac{\partial}{\partial x_i} \left(\kappa \frac{\partial T}{\partial x_i} \right) = \nabla \cdot (\kappa \overrightarrow{\nabla T}) .$$

In fact, since temperature is a function of internal energy, we take

$$H(J_i, J_j) = \gamma [T_j(J_j) - T_i(J_i)] = \gamma (\overrightarrow{r}_2 - \overrightarrow{r}_1) \cdot \nabla T(\overrightarrow{r}_1)$$

$$+ \frac{1}{2} \gamma [(\overrightarrow{r}_2 - \overrightarrow{r}_1) \cdot \nabla]^2 \, T(\overrightarrow{r}_1),$$

so that after the usual calculation we find that

$$\frac{\rho}{m} \int d\overrightarrow{r}_2 \, \rho \sigma H(\overline{J}_2, \overline{J}_1) = \frac{\partial}{\partial x_k} \left[\frac{2\rho^2}{3m} \left(\int_0^\infty \gamma r^4 \sigma \, dr \right) \frac{\partial T}{\partial x_k} (\overrightarrow{r}_1) \right]$$

and we can take

$$\kappa = \frac{2\rho^2}{3m} \left(\int_0^\infty \gamma r^4 \sigma \, dr \right).$$

It has also been suggested that the variable φ be interpreted as entropy, so it is of interest to note that heat conduction terms can also be incorporated into PAF under this interpretation. Here we add a flux term $H(J_j, J_i)$ to Eq. (5), Ref. I-2, so that

$$\frac{d\varphi_j}{dt} = \frac{1}{2mT_j} \sum_i^* \left\{ \left[\vec{g}_{ij} \cdot (\vec{u}_i - \vec{u}_j) \right] + H(J_i, J_j) \right\} ,$$

and again we take $H(J_i, J_j) = (\text{const})(T_i - T_j)$, which gives the result

$$\rho \bar{Q} = \frac{1}{T} \left[\sigma_{ik} \frac{\partial \bar{u}_i}{\partial x_k} + \frac{\partial}{\partial x_k} \left(\kappa \frac{\partial T}{\partial x_k} \right) \right] ,$$

where

$$\kappa = \frac{\text{const}}{2mT_j} \frac{2\rho^2}{3} \int_0^\infty \sigma r^4 \, dr .$$

Equation (49.4) in Ref. I-14 gives

$$\rho T \left(\frac{\partial s}{\partial t} + \vec{v} \cdot \nabla s \right) = \frac{\partial v_i}{\partial x_k} \sigma_{ik} + \nabla \cdot (\kappa \nabla T) .$$

Since we have

$$\frac{\partial \rho \bar{\varphi}}{\partial t} + \nabla \cdot \rho \vec{u} \, \bar{\varphi} = \rho \left(\frac{\partial \bar{\varphi}}{\partial t} + \vec{u} \cdot \nabla \bar{\varphi} \right) = \rho \bar{Q} ,$$

these equations are in agreement. Unfortunately use of this procedure requires knowledge of the temperature as a function of position. Except for a polytropic gas in which $T \propto I$, this may be unknown.

APPENDIX E

MASS REARRANGEMENT IN CYLINDRICAL COORDINATES

The initial particle configuration in cylindrical coordinates is generally arranged in such a way that particle mass is proportional to radius throughout a region of constant mass density. Subsequent circulation of particles through the mesh, however, can convect massive particles towards the axis and light ones away from it, with a resulting loss of resolution or creation of instability, respectively. One effective method for relieving the instability difficulty, described in the text, involves destruction of low-mass particles which have moved far from the axis. Another method would do just the opposite; through a mass rearrangement, the mass of any particle could be changed every cycle, so as to continue the proportionality of mass to radius. Thus, for example, we could add to the procedure the interparticle mass flux calculation, whereby

$$\frac{m_j^{n+1} - m_j^n}{\delta t} = \sum_1^* K_{ij},$$

where, for mass conservation, we would require $K_{ij} \equiv -K_{ji}$. A reasonable

choice for K_{ij} seems to be

$$K_{ij} = \xi \left(\frac{r_i + r_j}{\delta t} \right) \left(\frac{m_i}{r_i} - \frac{m_j}{r_j} \right) ,$$

and it can be shown that a necessary condition for stability is that $0 < \xi < 1/2.$

Now it is necessary that such an interparticle mass flux <u>not</u> result in any <u>net</u> macroscopic flux of mass, momentum, or energy. This means, then, that the particle coordinates must change in order that subset centers of mass remain fixed. It can be shown that the only way to accomplish this is through the simultaneous solution of the following for the new coordinates, $\vec{r}_j{}'$, in terms of those before mass redistribution, $\vec{r}_j$:

$$\vec{r}_j{}' = \frac{m_j^n \vec{r}_j}{m_j^n - \delta t \sum_i^{*p} K_{ji}} - \sum_i^{*p} \frac{\vec{r}_i{}' K_{ji} \, \delta t}{m_j - \delta t \sum_\ell^{*p} K_{j\ell}} ,$$

where the p modifies the sum to include only those terms for which $K_{ji} > 0.$ (This equation is derived by insisting that all the mass associated with a given particle have the same center of mass after the redistribution.) This inhomogeneous summation equation can be solved by successive substitution of the first term on the right into the second. In many cases, a single substitution probably will suffice.

Finally, we must redistribute energy and momentum, and the appropriate equations are

$$m_j^{n+1} \vec{u}_j' = \sum_i^{*p} \vec{u}_i K_{ij} \, \delta t + \left(m_j - \sum_i^{*p} K_{ji} \, \delta t \right) \vec{u}_j,$$

$$m_j^{n+1} E_j' = \sum_i^{*p} E_i K_{ij} \, \delta t + \left(m_j - \sum_i^{*p} K_{ji} \, \delta t \right) E_j.$$

REFERENCES

(PART I)

I-1. F. H. Harlow and B. D. Meixner, "The Particle-and-Force Computing Method for Fluid Dynamics," Los Alamos Scientific Laboratory Report LAMS-2567 (June 1961).

I-2. F. H. Harlow, "Theory of Correspondence between Fluid Dynamics and Particle-and-Force Models," Los Alamos Scientific Laboratory Report LA-2806 (November 1962).

I-3. J. E. Fromm, "Lagrangian Difference Approximations for Fluid Dynamics," Los Alamos Scientific Laboratory Report LA-2535 (March 1961).

I-4. H. G. Kolsky, "A Method for the Numerical Solution of Transient Hydrodynamic Shock Problems in Two Space Dimensions," Los Alamos Scientific Laboratory Report LA-1867 (March 1955).

I-5. H. J. Longley, "Methods of Differencing in Eulerian Hydrodynamics," Los Alamos Scientific Laboratory Report LAMS-2379 (February 1959).

I-6. M. Rich, "A Method for Eulerian Fluid Dynamics," Los Alamos Scientific Laboratory Report LAMS-2826 (December 1962).

I-7. F. H. Harlow, "Two-Dimensional Hydrodynamic Calculations," Los Alamos Scientific Laboratory Report LA-2301 (April 1959).

I-8. F. H. Harlow, "The Particle-in-Cell Method for Numerical Solution of Problems in Fluid Dynamics," in Proc. of Symp. in Appl. Math., American Mathematical Society, Vol. XV, pp. 269-288 (1963).

I-9. J. Von Neumann and R. D. Richtmyer, "A Method for the Numerical Calculation of Hydrodynamic Shocks," J. Appl. Phys. 21, 232 (1950).

I-10. R. Landshoff, "A Numerical Method for Treating Fluid Flow in the Presence of Shocks," Los Alamos Scientific Laboratory Report LA-1930 (January 1955).

I-11.   F. H. Harlow, "Dynamics of Compressible Fluids," Los Alamos
        Scientific Laboratory Report LA-2412 (April 1960).

I-12.   W. Griffith, "Shock-Tube Studies of Transonic Flow over Wedge
        Profiles," J. Aeron. Sci. 19, 249 (1952).

I-13.   B. W. Marschner, "An Investigation of Detached Shock Waves,"
        Master's Thesis, California Institute of Technology (1948).

I-14.   L. D. Landau and E. M. Lifshitz, Fluid Mechanics, Addison-
        Wesley Publishing Co., Inc. (1955).

PART II

SOME BASIC PROPERTIES OF PARTICLE DYNAMICS

INTRODUCTION

The results of a pioneering study by Pasta and Ulam [II-1] indicated that it should be possible to develop a useful technique for high-speed computer solutions of problems of fluid dynamics in which fluid elements are replaced by discrete interacting particles. Their work did not, however, clarify the nature of the correspondence between the model and a true fluid. There was, for example, no indication of how the interactions should be chosen in order that the model possess the equation-of-state properties of the fluid, and in addition there was no provision made for including the dissipation necessary to remove reversibility. Later work [II-2, II-3], however, has demonstrated that these objections can be overcome. Thus it has been shown by a statistical analysis that it is possible to establish the relationship between the interparticle force function and an equation of state for the fluid. Also, it was shown that the addition of an internal variable for each particle and inclusion of a dissipative term in the force function can satisfactorily remove the reversibility. Part I of this report shows the most recent

status of the method resulting from these generalizations.

We have found, nevertheless, that considerable information which is pertinent to such a generalized model can be obtained from some simple additional numerical experiments using the original Pasta-Ulam procedure. The results of these experiments are of considerable aid in the interpretation of the earlier work and also show how to resolve some ambiguities in the development of a workable generalized model for solving nonsteady fluid dynamics problems in several space dimensions, using high speed computers. It is, therefore, the primary purpose of this Part to present these results and their interpretations.

An additional result of these simple numerical experiments has been to demonstrate a somewhat different type of problem to which this sort of calculation can be successfully applied. Apparently it is possible with very few particles to be able to make meaningful statistical analyses of the properties of true molecular assemblages with a high degree of accuracy. Some preliminary discussions of this interpretation are also included, and we shall soon present elsewhere the detailed results of an extensive investigation.

CHAPTER 1

THE NUMERICAL EXPERIMENTS

We have examined in detail the dynamics of a one-dimensional set of N particles, interacting in pairs, and confined to move between rigid walls (accomplished by holding the first and last particles identically at rest). As in the Pasta-Ulam calculations, the force between particles was repulsive and inversely proportional to their spatial separation. The initial conditions for all examples were such that the particles were uniformly spaced with separation s, and all but the end ones were moving to the right (positive x direction) with the same velocity, U.

The equations which govern all details of subsequent motion are

$$\frac{du_j}{dt} = \frac{c^2}{x_j - x_{j-1}} - \frac{c^2}{x_{j+1} - x_j} \, , \qquad \text{(II-1)}$$

$$\frac{dx_j}{dt} = u_j . \qquad \text{(II-2)}$$

These describe the time rates of changes of velocity, u_j, and position, x_j, of particle #j. The constant parameter, c^2, is the ratio of the force constant to the particle mass, the latter being the same for all particles.

To derive an energy integral of the differential equations, multiply Eq. (II-1) by u_j and sum over all particles. After some manipulation, the result becomes

$$\sum_{j=1}^{N} \frac{1}{2} u_j^2 - \sum_{j=1}^{N-1} c^2 \ln \left(\frac{x_{j+1} - x_j}{s} \right) = E. \qquad (II-3)$$

Use has been made of the fact that particles #1 and #N are held identically at rest, so that x_1 and x_N are constants. The first sum represents kinetic energy, while the second is potential energy. In the latter, the incorporation of s shows a choice of integration constant making the potential energy vanish when the particles are in their initial spacing. E is the (constant) total energy. (All energies are specific, that is, measured per unit mass.) The energy considerations are of importance for several purposes, particularly for judging accuracy of the computer solutions and for deriving the fluid-dynamic properties of the particle system.

For the computer solution of the particle dynamics, the time derivatives are replaced by finite difference approximations:

$$\frac{du_j}{dt} \rightarrow \frac{u_j^{n+1} - u_j^n}{\delta t},$$

$$\frac{dx_j}{dt} \rightarrow \frac{x_j^{n+1} - x_j^n}{\delta t},$$

in which the index n counts cycles of elapsed time, each of duration δt.

Thus, Eqs. (II-1) and (II-2) become

$$u_j^{n+1} = u_j^n + c^2 \, \delta t \left(\frac{1}{x_j^n - x_{j-1}^n} - \frac{1}{x_{j+1}^n - x_j^n} \right), \qquad \text{(II-4)}$$

$$x_j^{n+1} = x_j^n + u_j^{n+1} \, \delta t. \qquad \text{(II-5)}$$

In this way, then, evolution of the configuration through a time cycle is computed by substitution of available data into Eqs. (II-4) and (II-5) for each particle. Note that the use of the newly computed velocity in Eq. (II-5) implies that substitution into Eq. (II-4) comes first; the reason for this particular ordering is that it contributes significantly to the difference equation stability. (See, for example, Ref. II-2, pp. 18-20, for a demonstration of the stability argument.)

Whereas the original differential equations of motion are identically conservative of energy, the finite difference approximations are not. This is an important difference from the situation in Part I, where the addition of an internal variable resulted in complete conservation. It can be shown that in Part II the discrepancy per cycle is proportional to $(\delta t)^2$, so that the cumulative discrepancy over a prescribed elapsed time is proportional to δt and can therefore be made as small as desired. Experimentation has shown further that when the overall relative discrepancy in energy has been reduced to a certain smallness, then any additional decrease in the value of δt will make a negligible change in any of the calculated results, indicating that the solution is as accurate as desired. In all calculations used in this study, the value of δt was

indeed sufficiently small that the solutions, in effect, are those of the differential equations.

The details of the calculations are more particularly defined by specifying the units of distance and time. (The units of mass do not enter, all quantities such as energy and force being measured per unit mass.) In all cases, the unit of distance was chosen to be the initial particle spacing, $s \equiv 1.0$. Thus, with N particles, including those at the walls, the region of allowed motion was of length $(N - 1)s$, and contained $(N - 2)$ moving particles. The units of time are completely specified by the numerical value of c, which has the dimensions of velocity. For all problems, $c^2 = 1000$. The only variables from problem to problem were N (which was either 27 or 52) and U (which was given various positive values in the interval $5 \leq U \leq 30$).

A typical example of the results obtained is given in Fig. II-1, in which $N = 27$, $U = 25$. The lines show the positions of all 25 interior particles as functions of time. It should be emphasized that the jaggedness of the lines in some parts has resulted from straight-line connection of datum points obtained from the computer at sampling times which were many cycles apart. Data plotted from every time cycle would show completely smooth particle trajectories, but were not obtained because of the extra computer time required. It should also be noted that the periodicity of amplitude oscillation for the particles in the right-hand compression region also is an illusion resulting from the slight difference in phase between the true oscillations and the data
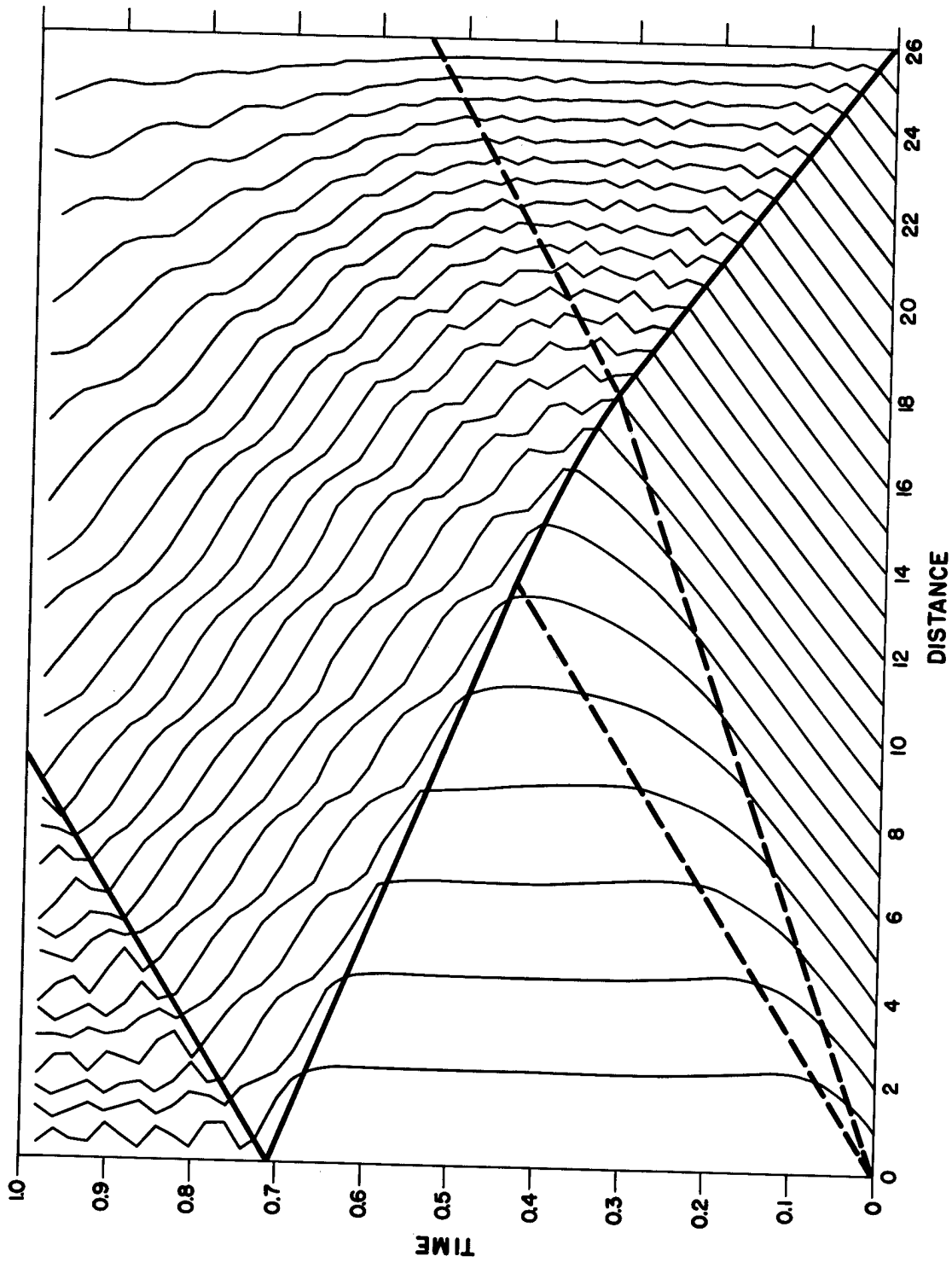
Fig. II-1. Particle positions as functions of time for the calculation with N = 27, U = 25. Heavy solid lines give observed shock position; heavy dashed lines give theoretical rarefaction bounds.

sampling period. (Samples taken in _perfect_ phase with the true oscilla-
tions would have obscured their actual amplitude, which is a quantity of
primary interest for the study.) A detailed interpretation of the many
features of these and similar results forms the main body of this part
of the report.

Figure II-2 shows, for the same calculation illustrated in Fig. II-1,
the histories of total kinetic and potential energy. Conservation of
total energy can be seen to be almost perfect. The almost exact inter-
change of kinetic and potential energies at later times is a feature to
be noted; with dissipative forces, the kinetic energy would, instead, be
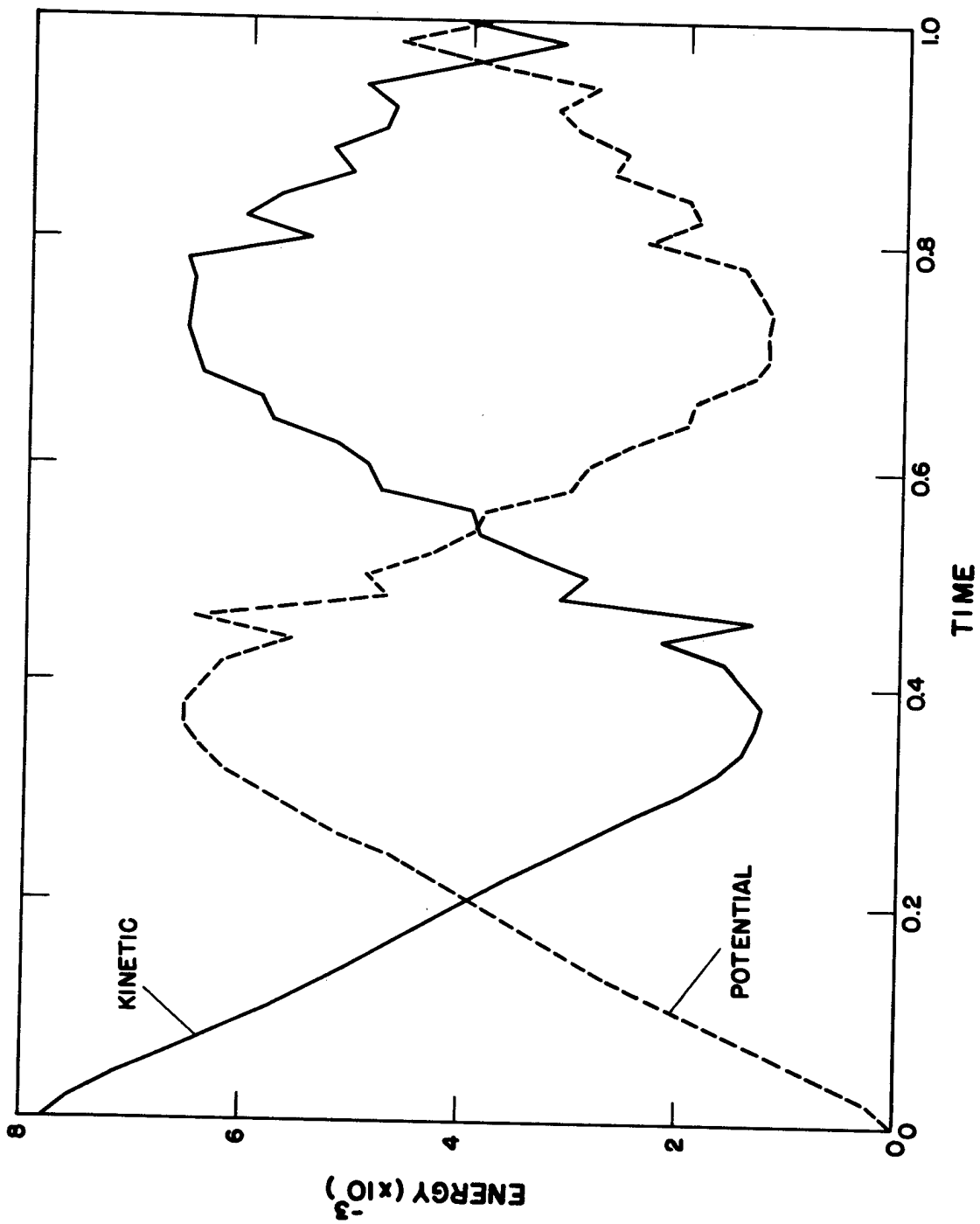expected to be less.

Fig. II-2. Kinetic and potential energies as functions of time for the calculation illustrated in Fig. II-1.

CHAPTER 2

MICROSCOPIC INTERPRETATION

Our principal purpose in performing the study was to elucidate the fluid-dynamics representation of particle-and-force models; nevertheless it is helpful to discuss first the results related to molecular dynamics interpretations. Several of the results will then be useful in the fluid-model discussion in Chapter 3 following.

There are, of course, several respects in which the one-dimensional particle array differs from a true molecular assemblage. The primary difference is the constraint to one-dimensionality itself; another significant difference is the enormous discrepancy between the number of molecules in a macroscopic material sample ($\sim 10^{20}$) and the number of particles in a calculation ($\sim 10^2$). The first of these differences precluded the possibility of representing a physically realistic problem in these preliminary calculations; the second introduces a considerably closer study of fluctuations than is usually encountered in the kinetic theory of gases. The restriction to one-dimensionality nevertheless leaves a number of features worth discussing, but any further studies intended to match

true molecular systems must have the restriction removed. Concerning the restriction to few particles, there already exist extensive data from some studies by Alder and Wainwright [II-4] which show that in at least one class of problem it is possible to obtain results of considerable accuracy with several hundred particles at most. Their investigations, however, appear to have been restricted to studies of equilibrium properties (or the approach to equilibrium) for particles interacting through short-range forces only, and for which wall effects have been minimized. Our interest, however, is in extending this type of calculation to include somewhat longer force ranges in studies of processes far from equilibrium. In addition, the effects of walls in studies of shear stress, heat conduction, shock generation, etc., are of primary concern, and it has been one of our purposes in this and other studies in progress to see which phenomena could still be investigated with the limited numbers of particles manageable by present computers.

Usually the primary objective in theoretical studies of molecular dynamics is to determine the manner in which microscopic phenomena manifest themselves in macroscopic properties. What, for example, are the relationships between velocity fluctuations and interparticle potential on the one hand to temperature, pressure, and entropy on the other? What are the microscopic processes that contribute to viscosity, heat conduction, and shock structure? There are, of course, many satisfactory answers to these questions for the relatively simple circumstances in which intermolecular forces are weak and departures from equilibrium are

small. Beyond these conditions lie the regions where perturbation theories no longer apply and the mathematical difficulties seemingly become insurmountable. These, then, are the circumstances for which detailed computer solutions of molecular dynamics problems could serve two useful purposes. First, they could explain or predict directly the physical properties of materials subjected to extreme environments. Second, they could supply the theoretician with exact and detailed data for comparisons with his analysis, for circumstances which are difficult to measure experimentally.

The present numerical studies certainly satisfy the conditions of being far from the circumstances in which simple perturbation methods can be used for theoretical investigation. For one thing, the intermolecular forces are strong, as is demonstrated by the fact that at times the potential energy of the system significantly exceeds the kinetic energy (see Fig. II-2). For another, the processes are strongly time-dependent, involving, in fact, one of the extremes of time-dependent, nonequilibrium processes — a strong shock. Thus, we must, for the present, be restricted only to discussions of interpretation of the results, entering into analysis for predictions only in heuristic fashion.

Consider, for example, the shock transition occurring as the particles "pile up" against the right-hand wall (see Fig. II-1). The calculations show several important features, all consistent with the true properties of a fluid in such circumstances. Especially evident is the well-defined shock itself, which, in its leftward propagation, maintains a

sharp transition between two regions whose properties are separately quite uniform. The region behind the shock (to the right of it) has properties of particular significance. First, there is a mean compression among the particles; second, the mean velocity of the particles has dropped to zero. Thus the kinetic energy of mean motion has vanished, and in its place is the potential energy acquired by the compression. Most significant of all, however, are the residual fluctuations in the compressed region, and it is the meaning of these which is worth investigating in detail.

First, however, note the contrast with the expansion region occurring at the left side where the particles are moving away from the wall. Again there are two regions, each with considerable uniformity, but the transition is not at all sharp, and, in addition, the stagnant region has no fluctuations.

The detailed explanation of these phenomena in terms of fluid-dynamics interpretations is reserved for Chapter 3; for the present discussion we are guided by the fact that the entropy of a fluid increases across a shock but remains constant across a rarefaction, together with the information that the _magnitude_ of entropy change across a shock can be predicted from the laws of thermodynamics and the conservation laws of mass, momentum, and energy only, and is independent of any detailed fluid properties other than those which describe the states on the two sides of the shock. It therefore becomes reasonable to inquire whether a detailed association can be made between fluctuations and entropy, and there are several ways in which such an association can be investigated. Consider first the following intuitive argument based upon simple physical

considerations. It has been shown that the differential equations governing the particle motions are completely conservative of energy. If, then, there were no fluctuations behind the shock, all of the kinetic energy would have been converted to potential, and a subsequent slow expansion would allow complete recovery of the initial conditions, in violation of the irreversibility of entropy production through a shock. Thus, the shock transition, which results in vanishing kinetic energy of mean motion, must result in a residual kinetic energy of "random" motion with consequent lowering of the recoverable potential energy. Then a subsequent expansion (such as is shown in Fig. II-1 when the left-end rarefaction interacts with the shock) will return the system to a state which differs from that at initial time. This is well shown by the retention of the fluctuations in Fig. II-1 at $t \approx 0.7$ when the re-expansion has returned the system nearly to its initial compression; the kinetic energy retained in those fluctuations is that which cannot be recovered, in accord with the second law of thermodynamics.

Yet to be explained, however, is the question of how the particles "know" just how much fluctuation to create when the shock goes by. As is stated before, this cannot depend upon the detailed nature of the inter-molecular forces except insofar as they contribute to the pressure states on the two sides of the shock, i.e., to the time averages of the inter-particle forces at only two mean states. This implies that any type of detailed variations in intermolecular force which does not change the two crucial average forces must result in the same magnitude of shocked-region

fluctuations. Only the detailed structure of the shock transition itself can vary.

Actually, it is possible to proceed somewhat further in the explanation of these phenomena through a consideration of several simple quantitative arguments. We have seen that the equation of motion for particle #j can be written in the form

$$\frac{d^2 x_j}{dt^2} = F(x_j - x_{j-1}) - F(x_{j+1} - x_j),$$

in which F is a force function which is repulsive when positive. As a model of the behavior of a particle during shock passage, consider the motion of #j when the motions of its neighbors are prescribed to follow the _means_ expected for them in the transition, i.e.,

$$x_{j\pm1} = (j \pm 1)s + Ut, \qquad \text{for } t < t_{j\pm1}$$
$$= (j \pm 1)s + Ut_{j\pm1}, \quad \text{for } t > t_{j\pm1},$$

in which $t_{j\pm1}$ is the time at which the shock intersects particle #j ± 1. We now define $\epsilon(t)$ to represent the deviation of the position of particle #j from the mean position between its two neighbors:

$$\epsilon(t) \equiv \frac{1}{2}(x_{j+1} + x_{j-1}) - x_j,$$

so that ϵ has initial conditions (at $t = t_{j+1}$) of the form $\epsilon = 0$, $d\epsilon/dt = 1/2\, U$. Then, except at the two singular times,

$$\frac{d^2 \epsilon}{dt^2} = F\left[\frac{1}{2} (x_{j+1} - x_{j-1}) + \epsilon\right] - F\left[\frac{1}{2} (x_{j+1} - x_{j-1}) - \epsilon\right],$$

which, for sufficiently small values of ϵ, can be approximated by

$$\frac{d^2 \epsilon}{dt^2} = 2\epsilon \ DF\left(\frac{x_{j+1} - x_{j-1}}{2}\right) \equiv -\zeta^2 \epsilon.$$

Here D symbolizes derivative with respect to argument. The condition that ζ^2 is a slowly varying function of time can reasonably be assumed in consistency with the smallness of ϵ. [Both require, for validity, that $U(t_{j-1} - t_{j+1}) \ll s$; i.e., that the shock be weak.] With slow variations of ζ^2, the equation can be solved with sufficiently accurate approximation to give

$$\epsilon(t) = \frac{U}{2\zeta} \sin \zeta(t - t_{j+1}),$$

or, for $t > t_{j-1}$,

$$\epsilon(t) = \frac{U}{2\zeta_1} \sin \zeta_1 t, \tag{II-6}$$

where we have, without loss of generality, chosen $t_{j+1} = 0$. The quantity ζ_1 is given by

$$\zeta_1^2 \equiv -2 \ DF\left(\frac{s}{\eta}\right), \tag{II-7}$$

where η is the shock compression, available theoretically from the considerations of Chapter 3. Applied to the force function at hand,

$$F(\zeta) \equiv \frac{c^2}{\zeta} \ ,$$

we get

$$\zeta_1^2 = \frac{2c^2 \eta^2}{s^2} \ ,$$

and

$$\epsilon(t) = \frac{sU}{2\eta c \sqrt{2}} \sin\left(\frac{c\eta t \sqrt{2}}{s}\right) . \tag{II-8}$$

Thus the results of this simple analysis are in agreement with the fact that the amplitude of oscillations behind the shock should be independent of the details of the force function. Furthermore, when applied to the numerical calculations, the result is in good agreement. The observed amplitude for the calculation shown in Fig. II-1, for example, is about 0.15. For that problem, $U = 25$, $\eta = 2.0$, $c = 31.62$, and the amplitude calculated from Eq. (II-8) is 0.14.

From Eq. (II-6) we see that the fluctuation velocity after shock passage is given by

$$u_j = \frac{d\epsilon}{dt} = \frac{U}{2} \cos \zeta_1 t, \tag{II-9}$$

so that the magnitude of the velocity amplitude is independent of the force function altogether. Thus the time average of $1/2(u_j)^2$, the specific kinetic energy of the fluctuations behind the shock, is

$$< \frac{1}{2} (u_j)^2 > = \frac{1}{16} U^2, \tag{II-10}$$

which is one-eighth of the specific kinetic energy in front of the shock.

Again this result can be compared with those of the calculation shown in Fig. II-1, although the comparison cannot be exact, since there is no time at which only shocked particles contribute kinetic energy. The nearest time might be t = 0.4, at which time nineteen particles have been shocked and the others are nearly at rest. Equation (II-8) would then predict a total specific kinetic energy

$$\frac{19}{16} U^2 = 742.$$

Reference to Fig. II-2, however, shows the kinetic energy to be somewhat higher than this, and the reason for the discrepancy can be seen in Fig. II-1, which shows that particles #8 to 11 have already acquired extra backwards motion from the rarefaction, thereby increasing their kinetic energies.

Exploiting even further the results of our simple model, we may derive an expression for the entropy of the assemblage by use of the H theorem of Boltzmann, which states that the entropy is given by

$$nS = -k \iint \Psi \ln \Psi \, du \, dx,$$

where S is the specific entropy of n particles in a region of length L, Ψ is the total one-particle distribution function for the system, and the integrations extend over all possible positions and velocities. Neglecting deviations near walls, Ψ is essentially independent of position in a region of uniformity; it represents the probability density for finding any particle with specified values of position and velocity,

and has the normalization property

$$\iint \Psi \, du \, dx = n.$$

Let u' be the amplitude of velocity fluctuations. Then we may write

$$\Psi \equiv \frac{n}{Lu'} \cdot Q \left(\frac{u}{u'} \right),$$

in which Q is independent of n and L, and depends upon u' only through the ratio u/u'. Insertion of this into the Boltzmann formula leads to the result

$$S = k \left(\ln \frac{u'}{\eta} + \text{constant} \right).$$

This, now, can be put into a more useful form through combination with Eqs. (II-8) and (II-9), leading finally to

$$S = S_o + k \ln \left(\frac{\epsilon'}{s} \right), \tag{II-11}$$

in which ϵ' is the amplitude of oscillation and S_o is a constant. We have therefore verified the correspondence between entropy and oscillations, showing, in fact, that the former is a function only of the amplitude of the latter, as expected.

The interpretation up to this point is "microscopic," because it is based upon the dynamics of the individual particles. Having shown on this basis that the microscopic properties of the fluctuations are related to a gross property (entropy), it will now be possible to proceed with the macroscopic interpretation in Chapter 3. In this

interpretation, fluctuation effects are treated as if a dissipative force had been added to convert fluctuation energy into the heat of macroscopic elements, as would be the case in any realistic general use as a fluid-dynamics model.

There are several additional features that could be studied from a molecular-dynamics viewpoint. Some of these have been presented by Blackman [II-5] and Butler [II-6], and an extensive report by Gentry, Harlow, and Martin [II-7] will soon be published.

CHAPTER 3

MACROSCOPIC INTERPRETATION

The investigation presented in Chapter 2 reveals that a number of
the computed particle dynamics features are related to true molecular
assemblages, and suggests that the statistical properties of nonequilibrium
processes could be studied with considerable accuracy through molecular
trajectory calculations. Such calculations can also be given a different
interpretation, in which each particle represents a macroscopic element
of fluid containing an extremely large number of molecules. In reality,
each element should have an internal degree of freedom representing its
heat energy. For adiabatic motions, this could be identified with the
interparticle potential energy, while for more general motions, we may
identify the kinetic energy of fluctuations as the additional dissipative
heat.

In the formulation of a practical method, an internal variable is
introduced for each particle (see Part I). Then the potential energy is
fed into this internal variable through work done by the nondissipative
force function, while a fictitious dissipative force function is intro-
duced to convert the fluctuation energy into additional heat.

This dissipative force must be velocity-dependent, so that its effects are irreversible and result in removal of the fluctuations in velocity (see Ref. II-3). Even without the introduction of this more convenient representation of heat energy, it is still possible to give a full, satisfactory interpretation of the present results in terms of fluid-dynamics concepts, thereby establishing the basis for development of a practical computing method.

One of the basic properties characterizing a fluid is its possession of an equation of state. This means that the dynamics of a fluid depend upon only a few _average_ properties, rather than upon the detailed motions of all its molecules. Specifically, we mean by equation of state a unique relationship among density, heat energy, and pressure. If such can be found for the numerical calculations described in Chapter 2, and if its use with fluid-dynamics theory gives results in agreement with the macroscopic dynamics observed from the computer, then our demonstration of a fluid-dynamics interpretation will be complete. This will be accomplished in this chapter.

First, we require an interpretation for density, which has been implied through the introduction of the compression, η, in Chapter 2. Working again with specific quantities, the density, ρ, is defined as the reciprocal particle spacing. (The meaning could be made precise through calculation of moments of a Liouville equation. For our present heuristic purposes, the looser definition will be sufficient.)

Second, we need an expression for heat (internal) energy.

This comes from Eq. (II-3), in which we substitute $u_j = u + \delta u$ for the velocity, δu being the fluctuation. Then the local energy per unit mass is, on the average,

$$E = c^2 \ln \frac{\rho}{\rho_o} + \frac{1}{2} u^2 + \frac{1}{2} (\delta u)^2.$$

Now the term $u^2/2$ represents the local kinetic energy of mean motion; all the rest must be interpreted as heat energy. Combining the results of Eqs. (II-8) and (II-10), we find that the expression for fluctuation kinetic energy can be written $c^2 A^2/2$, in which $A \equiv \epsilon'\eta/2$. (Thus A is the ratio of fluctuation amplitude to local particle spacing.) The required expression for specific internal energy, I, is thus

$$I = c^2 \ln \frac{\rho}{\rho_o} + \frac{1}{2} c^2 A^2. \tag{II-12}$$

Finally, an expression for pressure is required. This can be derived directly from the virial theorem in the case of our particular interparticle force function. The details are given by Butler [II-6], who shows that

$$p = c^2 \rho (1 + A^2). \tag{II-13}$$

[A straightforward derivation using the technique of Ref. II-3 yields the first part of Eq. (II-13), in confirmation of the validity of that technique. Derivation of the second part could likewise be accomplished if a proper dissipative force function were chosen; indeed the analysis in that case actually would serve as a guide for the choice.]

These results now can be combined to give the required equation of state

$$p = c^2\rho + 2\rho I - 2c^2\rho \ln \frac{\rho}{\rho_0} . \qquad (\text{II-14})$$

(Note the factor 2 in the second term, confirming agreement with the statistical-mechanical equation for a polytropic gas with one degree of freedom.) The applicability of this result can be tested in a number of ways. We first investigate whether or not the thermodynamic derivation of an expression for entropy agrees with the statistical result of Chapter 2. The starting point is the equation

$$\frac{\partial S}{\partial \rho} = - \frac{\rho}{\rho^2} \frac{\partial S}{\partial I} ,$$

in which S is a function of ρ and I. With Eq. (II-14), this becomes a partial differential equation whose solution is

$$S = \text{function of} \left(\ln \frac{A}{\eta} \right) .$$

The function here is arbitrary, but a choice can be made to give complete agreement with the statistical result, Eq. (II-11). This constitutes the first confirmation of the fluid-dynamics interpretation.

For further investigation we need an expression for the sound speed in the fluid, which in general is given by

$$w = \left(\frac{\partial p}{\partial \rho} \right)_{S=\text{const}}$$

A short calculation then gives for this case

$$w = c \sqrt{1 + 3A^2} . \qquad (\text{II-15})$$

Consider now the rarefaction at the left in the calculation shown in Fig. II-1. The envelope of the rarefaction is formed of two sound signals, each moving relative to the fluid with speed $w = c$. These calculated bounds are shown in Fig. II-1 by the straight lines passing obliquely through $X = 0$, and it can be seen that agreement with the actual bounds is excellent. In addition, the right-hand bound can be followed after interaction with the shock. According to the theory of Chapter 2, $A = U/(2c\sqrt{2})$, so that Eq. (II-15) gives $w = 35.1$ behind the shock.

Figure II-1 shows the continuation with this sound speed beyond the shock, and again excellent agreement is apparent.

One additional comparison can be made for the rarefaction region. Application of the theory of characteristics to the solution of the rarefaction problem shows that

$$u - c \ln \frac{\rho}{\rho_o}$$

is a constant through the rarefaction. For the example shown in Fig. II-1, this gives the result for density in the rarefaction region:

$$\rho = \rho_o \exp\left(-\frac{25}{31.62}\right) = 0.453 \ \rho_o.$$

Thus the mean distance between particles after rarefaction passage should be 2.21, again in excellent agreement with the observed separation.

The dynamics of the shock itself, in particular the variation of shock propagation velocity with initial material velocity, is the first comparison that gives any indication of significant discrepancy between

the computer results and those of the simple heuristic model used for analysis.

The shock-dynamics relationships are derived from four basic statements: the three Rankine-Hugoniot conservation principles and the equation of state. The first three are rigorously correct, so that any discrepancy in the final comparison must bear directly on the adequacy of the equation of state. This raises two important questions, which strike deeply into the validity of particle-and-force models for fluid dynamics: Are the particle dynamics completely capable of representation by an equation of state, insofar as macroscopic studies are concerned? Or is it possible to put the burden of discrepancy completely onto the approximations involved in deriving the particular equation of state for these studies? These questions cannot at present be answered completely, although it seems now that the answer to the first is: The dynamics are _almost_ capable of such a representation; the discrepancy is small in many circumstances of interest. But such an answer prompts several new questions, and in order to answer them, comparisons are still being made between particle-dynamics calculations and a variety of fluid dynamics situations for which solutions are known. Incidentally, it is easily shown that these further investigations, to which a heat variable and dissipative force are added, must be carried out in at least two space dimensions, where enforced ordering among particles no longer occurs, and interpenetrations must be anticipated. Dissipative addition in one dimension converts the particle dynamics calculations to familiar

Lagrangian computing methods which are <u>known</u> to work properly in a wide variety of applications.

We shall consider two expressions for the shock speed as a function of initial material speed. The first is derived using the conservation laws and the full equation of state. The other is a fictitious form, for comparison, in which there are forced to be no fluctuations after shock passage. For this we use the equations of state in which A = 0; that is, $p = c^2 \rho$. We shall see that the computer results lie between these two, suggesting that the fluctuations predicted by the heuristic analysis are somewhat too strong.

The actual derivations, which follow standard technique, need not be presented here. For the full equation of state, the algebraic solution must be performed numerically; for the fictitious case, a simple closed solution can be found. The results are presented in Fig. II-3, together with the results from numerous computer calculations in which the initial particle speeds were varied. In all cases, shock velocity is relative to material ahead, and thus approaches c = 31.62 as the material velocity becomes small. The results themselves give no hint as to whether the burden of discrepancy should be placed on the capability of interpretation or upon the heuristic model used for that purpose. It is therefore encouraging that the shocks shown in Part I are in good agreement with their expected behaviors.

Other features in Fig. II-1 have been calculated, but the results add no new extensions to the conclusions beyond those which can be
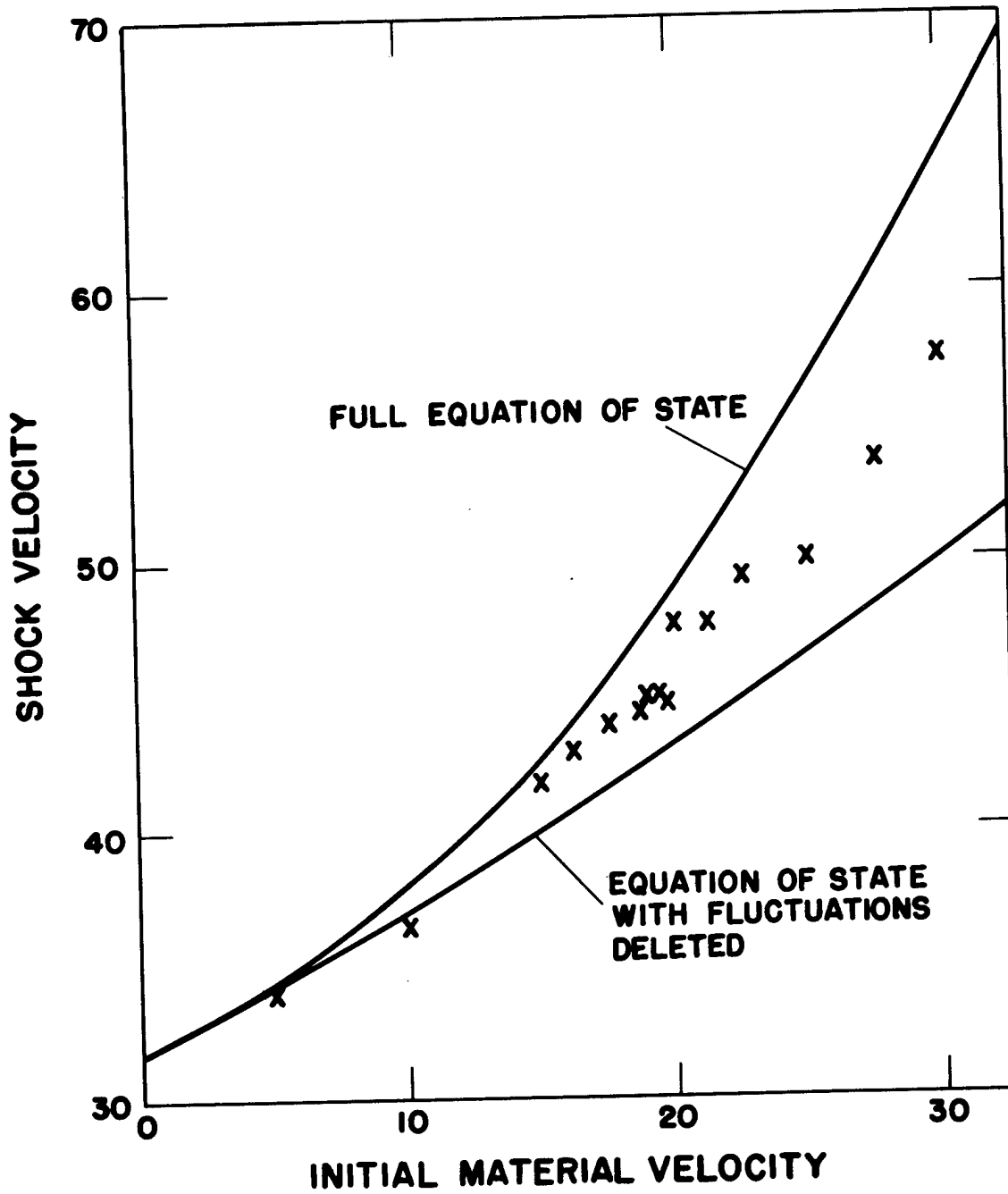
Fig. II-3.   Shock speed as function of material speed. Computer
results are shown by x; solid lines are theoretical.

observed visually. Thus, for example, it can be seen that the second shock in the upper left-hand corner results in a further strengthening of the oscillations, as expected, but quantitative prediction yields only that same qualitative result.

Thus we come to a restatement of the principal conclusions from Part II of this report:

1. The Pasta-Ulam calculations showed fluid-dynamics properties, even though they lacked the two desirable features of correspondence and dissipation, because of the close relationship between fluctuations and entropy and because of the capability of equation-of-state representation even with fluctuations.

2. The improvements to be expected from the addition of dissipative forces and from the proper use of force functions can result in a useful fluid-dynamics method, even though the correspondence cannot be "instantaneous" but must rely on statistical properties. The results of Part I further strengthen this conclusion.

3. The statistical properties of true molecular assemblages are likely to be amenable to computer studies with few particles, even for strongly nonequilibrium processes involving important wall interactions.

REFERENCES

(PART II)

II-1. J. R. Pasta and S. Ulam, "Heuristic Numerical Work in Some Problems of Hydrodynamics," Math. Tables and Other Aids to Comp. 13, No. 65 (1959).

II-2. F. H. Harlow and B. D. Meixner, "The Particle-and-Force Computing Method for Fluid Dynamics," Los Alamos Scientific Laboratory Report LAMS-2567 (June 1961).

II-3. F. H. Harlow, "Theory of Correspondence between Fluid Dynamics and Particle-and-Force Models," Los Alamos Scientific Laboratory Report LA-2806 (November 1962).

II-4. B. J. Alder and T. Wainwright, "Molecular Dynamics by Electronic Computers," Proceedings of the International Symposium on Transport Processes in Statistical Mechanics," Interscience Publishers Inc., New York, 1958.

II-5. S. S. Blackman, "A Theoretical and 'Experimental' Investigation of One-Dimensional Molecular Distribution Functions," unpublished Master's Thesis, University of New Mexico, 1963. (LADC-5771.)

II-6. T. D. Butler, "Force-on-the-Wall Calculations for One-Dimensional Dense Gases with Intermolecular Potentials," unpublished Master's Thesis, University of New Mexico, 1964. (LADC-6438.)

II-7. R. A. Gentry, F. H. Harlow, and R. E. Martin, "Computer Experiments for Molecular Dynamics Problems," Methods in Computational Physics, Vol. 4, Academic Press, New York, in press.